

# The Effects of Nuclear Radiation on Aging Reinforced Concrete Structures in Nuclear Power Plants

by

Somayeh Sadat Mirhosseini

A thesis  
presented to the University of Waterloo  
in fulfillment of the  
thesis requirement for the degree of  
Master of Applied Science  
in  
Civil Engineering

Waterloo, Ontario, Canada, 2010

© Somayeh Sadat Mirhosseini 2010

I hereby declare that I am the sole author of this thesis. This is a true copy of the thesis, including any required final revisions, as accepted by my examiners.

I understand that my thesis may be made electronically available to the public.

## Abstract

In this thesis we look at one of the aging mechanisms that may have affected current aged Nuclear Power Plants (NPPs). Irradiation as an age-related degradation mechanism is studied for Reinforced Concrete (RC) in NPPs. This problem can be important for aged reactor buildings, radwaste buildings, spent nuclear fuel, research reactors, or accelerators that experience high levels of radiation close to existing thresholds. Mechanical properties of concrete are the most important parameters affected by radiation in NPPs. Compressive strength of concrete is reduced between 80 and 35 % for radiation fluences between  $2 \times 10^{19}$  and  $2 \times 10^{21}$  n/cm<sup>2</sup>. Tensile strength reduction is more significant than compressive strength. It is reduced between 20 and 80 % for a radiation fluence equal to  $5 \times 10^{19}$ . We chose three radiation levels  $2 \times 10^{19}$ ,  $2 \times 10^{20}$ ,  $2 \times 10^{20}$  based on experimental results as the critical levels of radiation that RC structures in NPPs may be exposed to.

Structures susceptible to the problem are mostly RC walls; so the RC panel is chosen as an appropriate representative scale element for the analysis. The effect of radiation on mechanical properties of concrete is considered to analyze degraded scale elements. Material properties, geometry, and loading scenarios of scale elements are selected to be close to actual quantities in existing nuclear power plant. Elements are analyzed under six types of loading combination of shear and axial loading conditions. A nonlinear finite element program, Membrane-2000, based on the Modified Compression Field Theory (MCFT) is used to solve scale elements numerically. Element behaviors are studied considering the factors influence ultimate strength capacity, failure mode, and structural ductility index of members. The results show that ultimate shear capacity of the elements subjected to combinations of shear and tension loading are reduced significantly for highly reinforced elements ( $1.35 < \rho < 1.88$ ) in  $2 \times 10^{21}$  n/cm<sup>2</sup> radiation. RC panels under shear-biaxial and uniaxial compression also show significant strength capacity reduction in radiation levels  $2 \times 10^{20}$  n/cm<sup>2</sup> and  $2 \times 10^{21}$  n/cm<sup>2</sup>, respectively. Failure modes of the elements change from yielding of steel to shear failure by increasing level of degradation for the elements with reinforcement ratio between 0.9 and 1.88. Ductility of the RC panels is reduced significantly in the critical levels of radiation. Ductility of the elements became less than the allowable ductility value by increasing level of radiation.

## Acknowledgments

First and foremost I offer my sincerest gratitude to my supervisors, Dr Mahesh D. Pandey and Maria Anna Polak, who have supported me through my thesis with their patience and knowledge whilst allowing me the room to work in my own way. I attribute the level of my Masters degree to their encouragement and effort and without them this thesis, too, would not have been completed or written.

I am indebted to my many of my friends to support me with their academic comments and suggestions that guided me through the research.

I gratefully acknowledge Dr Evan Bentz from U of T who provided me great supports for his software. I would also like to thank Dr. Dan J. Naus from Oak Ridge National Laboratory (ORNL) for his advice and precious times spending to answer my questions.

Many thanks go in particular to Rania Al-Hammoud, Rizwan Azam, Dritan Topuzi, Jian Deng, and Xufang Zhang. I am much indebted to them for their valuable advice and precious times to listen to my concerns about this thesis and gave their critical comments about them.

I would like to show my gratitude to my officemates during the one year being in University of Waterloo. I thank Oxana Skiba, Jian Deng, Anup Kumar Sahoo, and Mathew Ming Ma for providing an excellent environment to do this research.

I would also like to convey thanks to the Faculty of Civil and Environmental Engineering for providing the financial means and facilities.

I wish to express my love and gratitude to my beloved families; for their understanding and endless love, through the duration of my studies.

Finally, I would like to thank everybody who was important to the successful realization of this thesis, as well as expressing my apology that I could not mention personally one by one.



## Dedication

This is dedicated to my parents who thought me that the best kind of knowledge to have is that which is learned for its own sake. It is also dedicated to my loving husband who supported me all the time.

# Contents

List of Tables	x
List of Figures	xiii
<b>1 Introduction</b>	<b>1</b>
<b>2 Literature Review</b>	<b>5</b>
2.1 Concrete Structural Components in Nuclear Power Plants . . . . .	5
2.1.1 Containment Structures . . . . .	11
2.1.2 Safety Related Structures . . . . .	11
2.2 Reinforced Concrete Containment Design Requirements (ASME <i>III</i> div 2)	17
2.2.1 Load Applied . . . . .	17
2.2.2 Design Criteria . . . . .	19
2.3 Nuclear Safety Structures Related Design Requirements (ACI-349) . . . . .	22
2.3.1 Material Properties . . . . .	22
2.3.2 Strength and Serviceability Requirements . . . . .	26
2.3.3 Shear Design . . . . .	29
2.4 Aging Phenomena . . . . .	32
2.4.1 Aging Research Study . . . . .	32
2.4.2 Age-Related Concrete Degradation in NPPs . . . . .	37
2.5 Radiation Degradation in NPPs . . . . .	40
2.5.1 Background of Radiation . . . . .	40
2.5.2 Radiation Effects on Reinforced Concrete Structures . . . . .	43
2.5.3 Radiation Limit . . . . .	48

<b>3</b>	<b>Analytical Procedure</b>	<b>51</b>
3.1	Membrane Elements Studied in This Study . . . . .	51
3.1.1	Geometry Properties . . . . .	52
3.1.2	Material Properties . . . . .	53
3.1.3	Degradation Factors . . . . .	55
3.1.4	Loading Scenarios . . . . .	55
3.2	Analytical Method Used in This Study . . . . .	57
3.2.1	The Modified Compression Field Theory(MCFT) . . . . .	59
3.2.2	Membrane-2000 . . . . .	68
3.3	Discussion on the Selection of Membrane Elements . . . . .	79
3.3.1	RC Panels from Containment . . . . .	79
3.3.2	RC Panels from Safety Class Structures in NPP . . . . .	80
3.3.3	Element Details . . . . .	85
3.3.4	Loading Scenarios for RC Panels . . . . .	91
3.3.5	Element Definition . . . . .	96
<b>4</b>	<b>Analysis of Results</b>	<b>97</b>
4.1	Load-Deformation Curve . . . . .	97
4.2	Ultimate strength Capacity Reduction . . . . .	100
4.2.1	Elements Subjected to Tension . . . . .	101
4.2.2	Elements Not Subjected to Tension . . . . .	104
4.3	Failure Mode Changes . . . . .	107
4.4	Ductility Index Reduction . . . . .	108
<b>5</b>	<b>Conclusion and Further Research Recommendations</b>	<b>113</b>
5.1	Conclusion . . . . .	113
5.2	Further Research Recommendations . . . . .	115
	<b>Appendices</b>	<b>117</b>
<b>A</b>	<b>Ultimate strength Capacity and Ductility Reduction</b>	<b>118</b>

<b>B Element Responses and Analysis</b>	<b>125</b>
<b>References</b>	<b>136</b>

# List of Tables

2.1	Typical safety-related concrete structures at BWR plants[49] . . . . .	9
2.2	Typical safety-related concrete structures at PWR plants[49] . . . . .	10
2.3	Load categories (ASME <i>III</i> division 2) . . . . .	18
2.4	Load combinations and load factors (ASME section III division 2) (continues)	20
2.5	Load combinations and load factors (ASME section III division 2) . . . . .	21
2.6	Typical shielding concrete types and their elements density(continues)[31] .	23
2.7	Typical shielding concrete types and their elements density[31] . . . . .	24
2.8	Absorption and scattering cross section used in shielding concrete[35] . . .	25
2.9	Typical Mechanical and thermal properties of representative concretes after curing[10] . . . . .	26
2.10	Load combinations and load factors (ACI-349) . . . . .	28
2.11	Strength reduction factor for safety-related reinforced concrete members in NPPs (data obtained from ACI-349) . . . . .	29
2.12	Deterioration factors on physical process in concrete and their effects[48] .	37
2.13	Deterioration factors on chemical process in concrete and their effects[48] .	38
2.14	Effect of neutron irradiation on compressive strength of concrete . . . . .	45
3.1	Steel distribution of the elements R1, R2, R3, and R4 . . . . .	54
3.2	Material properties of the elements R1, R2, R3, and R4 . . . . .	54
3.3	Degradation levels assumed in this study based on the critical radiation levels in NPPs . . . . .	56
3.4	Loading conditions that are studied in this research . . . . .	58
3.5	Element R1 details . . . . .	69

3.6	Peak strain for varieties of $f'_c$ [16]	72
3.7	Compression softening models available in Membrane-2000	74
3.8	Tension stiffening models available in Membrane-2000	75
3.9	Standard reinforcing steel available in Membrane-2000	76
3.10	Reinforcing steel layout	77
3.11	RC panels details	80
3.12	Reinforced concrete wall design forces and reinforcement in ABWR design(continues)[21]	86
3.13	Reinforced concrete wall design forces and reinforcement in ABWR design[21]	87
3.14	Reinforcement ratios and loading ratios of RC walls in ABWR	88
3.15	ABWR details of shear walls exposed to high energy line break[21]	90
3.16	ABWR details of non-shear walls exposed to high energy line break[21]	90
3.17	Shear-axial load ratios of experiments and existing NPPs	95
3.18	Element's name based on the variables of the element properties	96
4.1	Different elements analyzed in this study with respect to the variables considered in the analysis	98
4.2	Ultimate strength capacity reduction of elements R1, R2, R3, and R4 in different levels of degradation when shear loading increases	102
4.3	Ultimate strength capacity reduction of elements R1, R2, R3, and R4 in different levels of degradation when shear loading increases	106
4.4	Slope of the line between different reinforcement ratios	108
4.5	Ductility index of elements R1, R2, R3, and R4 in different levels of degradation when shear loading increases	112

# List of Figures

2.1	ABWR plan [21] . . . . .	6
2.2	Containment structures division in NPPs . . . . .	7
2.3	Wall and dome reinforcing elements for hemispherical dome containment [52]	8
2.4	Reactor building section (ABWR) [21] . . . . .	12
2.5	Reactor building internal structures [21] . . . . .	13
2.6	PWR dry containment arrangement [52] . . . . .	14
2.7	A thin-walled concrete cask surrounded with a reinforced concrete over-pack [41] . . . . .	15
2.8	A metallic thick-walled cask [41] . . . . .	16
2.9	Distribution of structures and passive components over component category [51] . . . . .	34
2.10	Distribution comparison of SPC degradation occurrences over components [51]	35
2.11	Distribution comparison of SPC degradation occurrences over aging mechanism [51] . . . . .	36
2.12	Radioactive decay[66] . . . . .	42
2.13	Effect of neutron radiation on concrete compressive strength relative to non-irradiated and unheated control specimen results[27] . . . . .	46
2.14	Effect of neutron radiation on concrete tensile strength relative to non-irradiated and unheated control specimen results[27] . . . . .	46
2.15	Aggregate cracking due to ASR [1] . . . . .	47
2.16	Gel generated around aggregates [1] . . . . .	48
3.1	General form of the RC panels are analyzed in this study . . . . .	52
3.2	Specimens series R details . . . . .	53

3.3	Degradation levels 1, 2, and 3 are assumed for the degradation factors of compressive strength in the analysis of the RC panels . . . . .	56
3.4	Degradation levels 1, 2, and 3 are assumed for the degradation factors of tensile strength in the analysis of the RC panels . . . . .	57
3.5	Structures include membrane elements[63] . . . . .	60
3.6	Reinforced concrete panel with complete loading scenario[16] . . . . .	60
3.7	Constitutive equations of the MCFT[63] . . . . .	61
3.8	Average strain in a cracked membrane element[63] . . . . .	61
3.9	Equilibrium conditions in $x$ direction [63] . . . . .	63
3.10	Stress and strain condition for the modified compression field theory for membrane elements [63] . . . . .	64
3.11	Empirical stress-strain relationship[63] . . . . .	65
3.12	Comparison of local stresses at a crack with calculated average stresses[63] . . . . .	67
3.13	Quick define window in Membrane-2000 . . . . .	69
3.14	Membrane section built by quick define . . . . .	70
3.15	Material properties can be defined in Membrane-2000 . . . . .	71
3.16	Concrete properties can be defined in Membrane-2000 . . . . .	72
3.17	Reinforcing steel properties of the element R1 can be defined in Membrane-2000 . . . . .	75
3.18	Reinforcing steel layout details of the element R1 . . . . .	76
3.19	Load definition in Membrane-2000 . . . . .	78
3.20	Reinforcement ratios of existing containment[12] . . . . .	80
3.21	ASME manual example of RC containment[52] . . . . .	81
3.22	Inside and outside of primary containment (ABWR)[21] . . . . .	83
3.23	Radiation zones in primary containment vessel (ABWR)[21] . . . . .	84
3.24	Distribution of concrete compressive strength over thickness of biological shield of ORNL-Graphite reactor[27] . . . . .	89
3.25	Membrane element with in plane loading[60] . . . . .	92
3.26	Membrane element with out of plane loading [60] . . . . .	92
3.27	Combined pressurization and tangential shear[54] . . . . .	93



3.28	Location of elements under biaxial compression in vessels [65] . . . . .	94
3.29	Relationship of axial load and shear load in actual reactor buildings[26] . .	95
4.1	Typical load deformation diagram for a membrane element . . . . .	99
4.2	Comparison of element R3 ( $\rho = 3\%$ ) under shear and biaxial tension loading in different levels of degradation . . . . .	100
4.3	Effect of reinforcement ratio and shear-biaxial tension loading ratio in dif- ferent levels of radiation (normalized) . . . . .	103
4.4	Ultimate shear stress changes with reinforcement ratio and compressive strength[62] . . . . .	104
4.5	Ultimate shear stress changes with reinforcement ratio and compressive strength for the elements under biaxial tension loading with loading 1:1:2 .	105
4.6	Shear strength variation when reinforcement increases in $x$ and $y$ directions[63]	107
4.7	Failure mode changes when reinforcement ratio increases in different levels of degradation . . . . .	109
4.8	Ductility index for elements with different reinforcement ratio as degradation level and $\frac{v_{xy}}{f_x}$ increases . . . . .	111
A.1	Effect of reinforcement ratio and shear-biaxial tension-compression loading ratio in different levels of radiation (normalized) . . . . .	119
A.2	Effect of reinforcement ratio and shear-uniaxial tension loading ratio in dif- ferent levels of radiation (normalized) . . . . .	120
A.3	Effect of reinforcement ratio and shear-uniaxial compression loading ratio in different levels of radiation (normalized) . . . . .	121
A.4	Effect of reinforcement ratio and shear-biaxial compression loading ratio in different levels of radiation (normalized) . . . . .	122
A.5	Ductility reduction of the elements subjected to shear-biaxial tension-compression loading when radiation increases . . . . .	123
A.6	Ductility reduction of the elements subjected to shear-uniaxial tension load- ing when radiation increases . . . . .	124

# Chapter 1

## Introduction

The starting point of this research was reviewing aging degradation in Nuclear Power Plants (NPPs). Aging phenomena is under consideration for all structures in all of the world. However it is under specific attention for NPPs during the last two decades since all plants built in 1950s, 1960s and 1970s are in their second operating life time. Nuclear energy becomes one of the most important sources of energy during last half century. However, there are lots of awareness by failure in NPPs during their history and the most significant one was Chernobyl accident in 1986. The number of occurrences of accident for NPPs shows that there are always uncertainties during construction and operation life time of a NPP. Degradation mechanisms in composite material like Reinforced Concrete (RC) is one the most important of these uncertainties. It provides an open research area corresponding to analyze systems and components in NPPs beyond their design consideration. Elasto-plastic analysis is one of the strong tools to have realistic prediction of these structures behavior.

Designers may be reluctant to analyze NPPs building beyond elastic range. They believe that design specifications provided by codes limit RC structures to elastic range for design load combinations. So, plastic and permanent displacement in most cases are not occurred. However, there are applications of failure mechanism analysis in NPPs where structures should be analyzed beyond elastic range [44]. Some of these applications are:

1. The assessment of realistic safety margins,
2. The impact assessment of increased seismic input, and
3. The fragility analysis for RC buildings.

This thesis investigates one of the aging mechanisms that may be applicable for current aged NPPs. This problem is applied on the aged reactor buildings, radwaste building,

Spent Nuclear Fuel, research reactor, or accelerators that experience high levels of radiation close to existing thresholds. As it will be mentioned in Section 2.5.3, difficulty of having experiments from aged NPPs and also variables which are not controlled for experiments done in this area provide no general agreement on the following questions:

1. What is the level of radiation that damage concrete?
2. What is the level of degradation caused by radiation?
3. Will RC structures experience critical levels of deterioration caused by radiation?

Reviewing experiments in the literature brought us questions looking further. Here are questions tried to be answered in this study:

1. Is radiation a serious problem for concrete structures in NPPs?
2. What will be the level of radiation that damages concrete?
3. Will RC structures in NPPs experience this level of radiation?
4. What types of RC structures could experience irradiation?
5. What are geometry and material properties of such structures?
6. How these structures behave under different levels of irradiation?
7. What are the most affected mechanical properties of the RC elements?

Reviewing large numbers of references on the radiation deterioration for RC structures in NPPs show that different nuclear design codes chose their threshold based on the more reliable researches conducted by Hilsdorf in 1978 and Kaplan in 1989 [37, 27]. Critical levels of radiation that may deteriorate concrete in NPPs were found from the experimental results available in literature. RC structures that are susceptible to high levels of radiation and possibility of being exposed to those critical radiation levels is reviewed in literature. Biological shields, primary containment structures, and nuclear fuel storages were found applicable to radiation damage.

NPPs like most concrete structures are threatened by deterioration. Degradation may mostly occur as a result of construction fault, which can usually be fixed in the constructing process. However, there are varieties of deterioration mechanisms due to aging affects. The most important concrete deterioration mechanisms in NPPs are sulphate attack, alkali-aggregate reactions, frost attack, leaching, radiation, elevated temperature, salt crystallization and fatigue attack.

Irradiation is studied in details to have better understanding of the degradation mechanism. Radiation is a product of nuclear fission in a reactor core. The main purpose of the reactions in the reactor core is producing heat. Heat energy will be transferred to electricity in transformers for industry, or public use. Neutron, gamma, and beta are other products of the reaction in the reactor core. Neutron is one of the most important particles that are considered in shielding requirements. Neutron fluence dimension is  $n/cm^2$ . It is the result of multiplication of constant radiation flux ( $n/cm^2/s$ ) and time (second). Neutron fluences are divided into three categories based on their kinetic energy:

1. Slow or thermal neutron (kinetic energy  $< 0.5eV$ )
2. Intermediate or epidermal neutron ( $0.5 < \text{kinetic energy} < 5000eV$ )
3. Fast neutron (kinetic energy  $> 500,000eV$ )

Mechanical properties of concrete are the most important parameters affected by radiation in NPPs. Compressive strength of concrete is reduced between 80 and 35 % for radiation fluences between  $2 \times 10^{19}$  and  $2 \times 10^{21}n/cm^2$  respectively. Tensile strength reduction is more significant than compressive strength. It is reduced between 20 and 80 % for a radiation fluence equal to  $5 \times 10^{19}n/cm^2$ .

Concrete strength reduction, which is a serious problem for RC structures, has been studied by researchers for few centuries. There are different factors that affect concrete strength and are considered in design process by entering strength reduction factor in codes [18]. However, it is important to have a better understanding of strength reduction sources and their uncertainty during long period of time. It is possible that codes are expected to be properly conservative but some unexpected factors influence building resistance and reduce safety margins considerably. Hence, it is always necessary to study behavior of deteriorated components. Even design methods used by codes seem to be conservative enough. This issue is more sensitive for structures such as NPPs, whose failure may affect several generations of human and nature.

Strength reduction does not considerably affect flexure capacity of a RC member. However, it affects significantly shear capacity of the member. Hence, shear capacity of degraded scale elements is reviewed in this study. RC structures, which are exposed to high levels of neutron particles, in NPPs are reviewed to select an appropriate scale element. These structures are mostly RC walls, so a RC panel is the best scale element to analyze.

Selection of material and geometry properties of the scale elements is one of the most important parts of the thesis since it makes all values close to existing NPPs values. Loading scenarios that elements experience is another important issue that are selected based on critical situations and values exist in NPPs. RC panels are analyzed under six types of loading:

1. Pure shear (P)
2. Shear-biaxial tension (BT)
3. Shear-biaxial tension compression (BTC)
4. Shear-biaxial compression (BC)
5. Shear-uniaxial tension (UT)
6. Shear-uniaxial compression (UC)

The Modified Compression Field Theory (MCFT) is chosen as one of the best theories to predict shear capacity of complex RC structures [63]. The scale elements are analyzed by Membrane-2000, a nonlinear Finite Element (FE) software based on the MCFT. Factors influencing undegraded shear capacity of the elements is studied to have appropriate results comparisons. Finally, ultimate strength capacity reduction, changing of failure mode, and ductility index reduction is studied for undegraded and degraded elements.

# Chapter 2

## Literature Review

### 2.1 Concrete Structural Components in Nuclear Power Plants

Structural systems in NPPs are divided into three categories: concrete shear wall structures, steel framed structures, and concrete slabs. The most commonly used structures in NPPs are shear walls in containment and internal structures. ACI-349, and ASME Boiler and Pressure Vessel committee define requirements for all concrete structure design for NPPs. Concrete containment design is based on ASME section *III* division 2. RC safety-related structures and other structures, which are not included in ASME section *III* division 2, are designed based on ACI-349.

Structures over nuclear reactors are built to protect the environment from radiation exposure and thermal effect of radioactive process and also to protect reactor and auxiliary systems from severe accidental loads. Figure 2.1 shows Advanced Boiler Water Reactor building as an example plan for NPPs.

Containment can be steel, reinforced, or prestressed concrete. The chart shown in Figure 2.2 gives general division of containment types.

Concrete is widely used in NPPs structures in PWRs and BWRs. However, use of concrete is not restricted to these two kinds of reactor. It has also been used for research reactors, particle accelerators, and high level radioactive research laboratories for weapon, medical, academic, and commercial purposes [37]. Structural design of concrete elements is mostly based on statistical and dynamical loads in severe accidents or natural phenomena such as tornado, earthquake, and tsunami.

Importance of containment becomes more clear when one considers probable accidents in NPPs. Three Mile Island accident, occurred on March 28, 1979, is one of the most im-

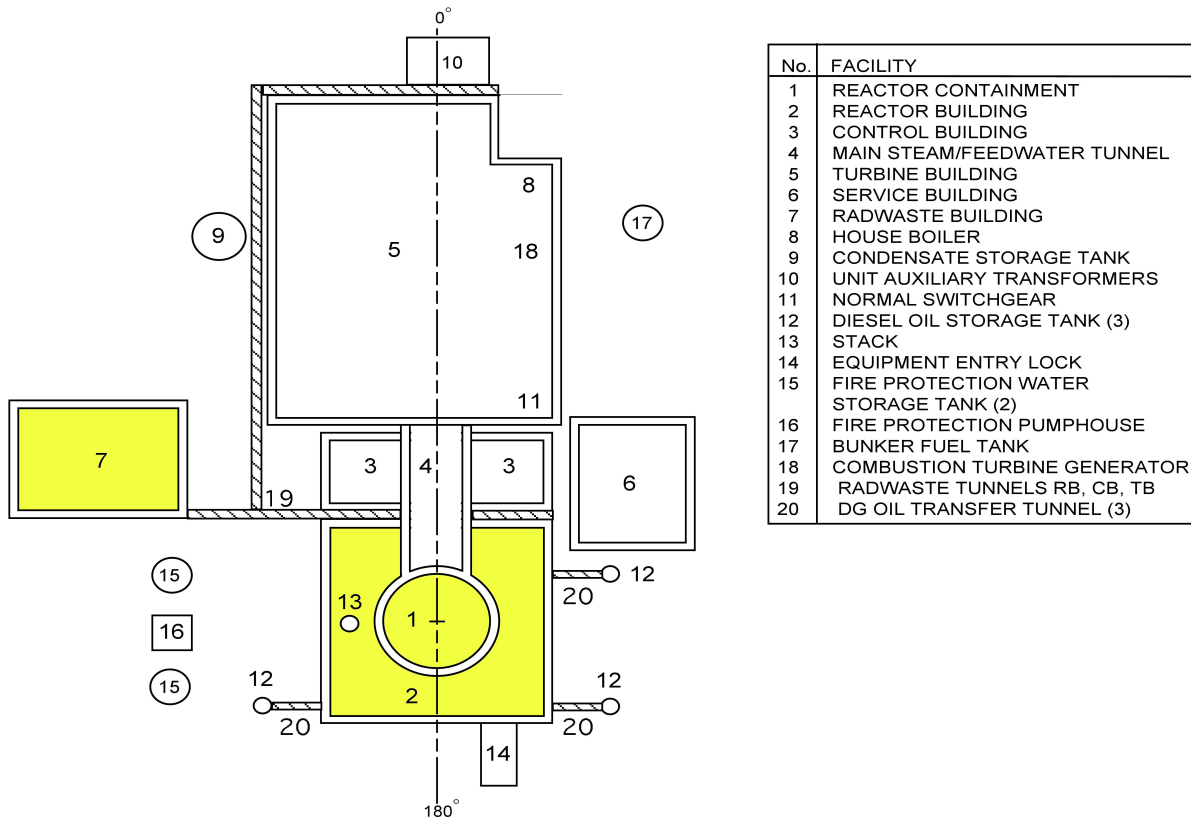


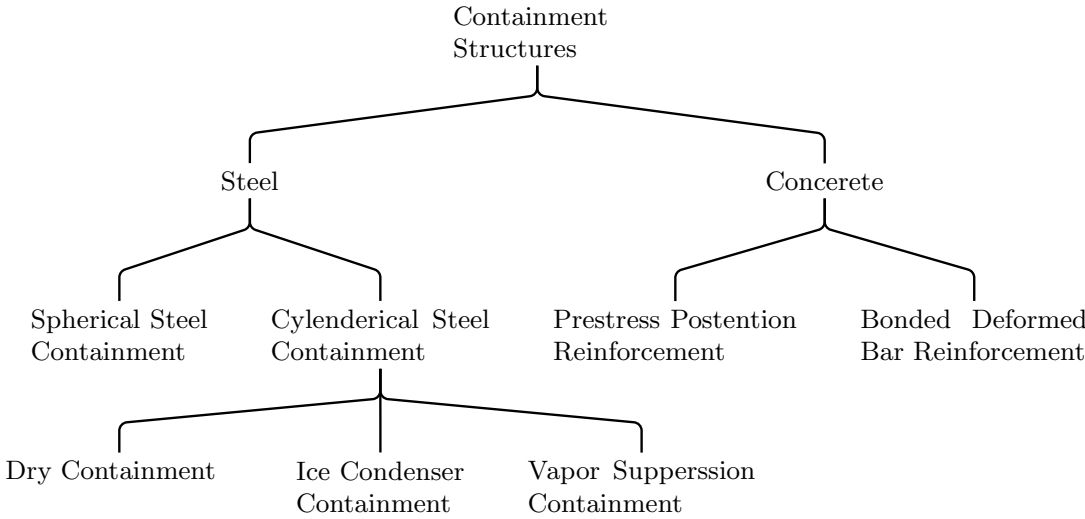
Figure 2.1: ABWR plan [21]

portant nuclear accidents in the United State during last century. The accident showed the importance of containment corresponding to hydrogen bubbles and high neutron exposure [2].

Structural and shielding performances are considered in the design of reinforced or prestressed concrete components in NPPs. Based on the level of radiation that each element is exposed to, an appropriate concrete mix design is chosen for the structures. For instance, the layout of a PWR dry containment is shown in Figure 2.3. It can be seen from the figure that primary and secondary shielding walls are the closest structures to the reactor (the radiation source) in the NPP. Consequently, they are exposed to a higher level of radiation compare to the primary and secondary containments.

Safety-related concrete structures in NPPs consist of containment and internal structures. Typically safety-related concrete structures at BWRs and PWRs are tabulated in Tables 2.1 and 2.2, respectively.

Figure 2.2: Containment structures division in NPPs





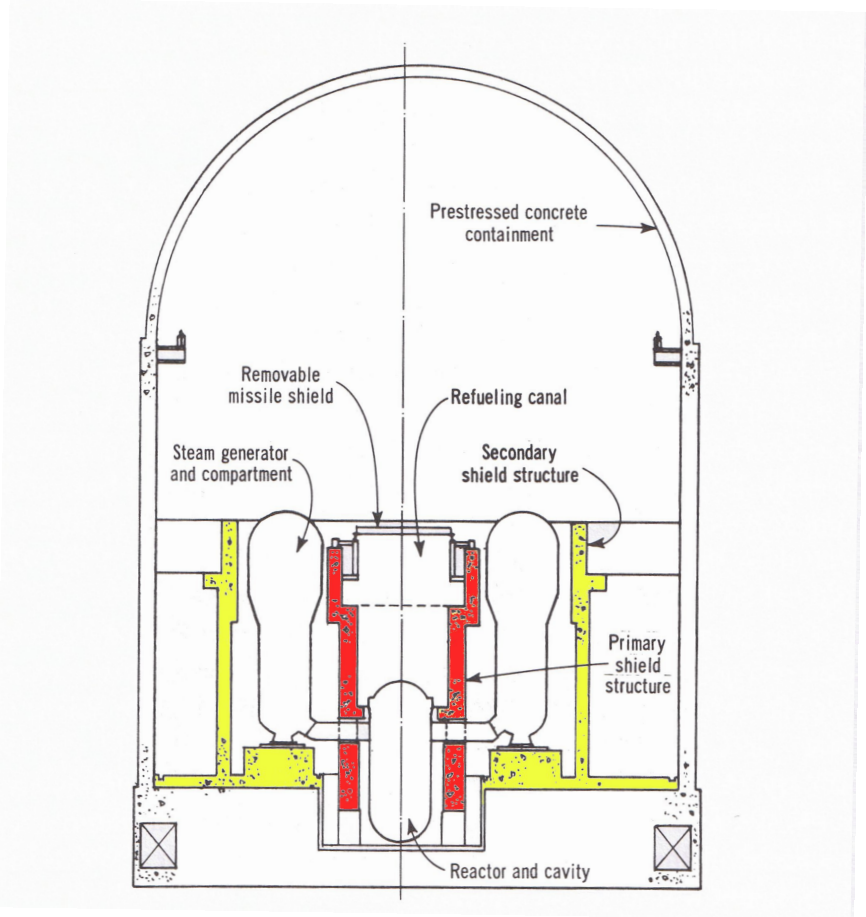


Figure 2.3: Wall and dome reinforcing elements for hemispherical dome containment [52]

Table 2.1: Typical safety-related concrete structures at BWR plants[49]

Structures	Components
Primary Containment	Basement Foundation, Drywell Pedestal, Vertical Walls (Mark I), Steel Liner , Suppression Chamber (Mark I) , Chamber Steel Liner (Mark I) , Vertical Walls (Mark II) , Vertical walls (Truncated Cone-Mark II), Concrete Dome (Mark III) , Polar Crane Support (Mark III)
Containment Internal Structures	Basement Foundation , Reactor Pedestal/Support Structure, Biological (Reactor) Shield Wall, Floor Slabs, Walls, Columns, Diaphragm Floor (Mark II), NSSS Equipment Pedestal/Supports, Upper and Fuel Pool Slabs (Mark III), Drywell Wall (Mark III), Weir/Vent Wall (Mark III), Crane Support Structure (Mark III)
Secondary Containment/Reactor Building	Basement Foundation , Walls, Slabs, Columns, Equipment Supports/Pedestals, Sacrificial Shield Wall (Metal Containment), Spent/New Fuel Pool Walls/Slabs, Drywell Foundation (Mark I)
Other Structures	Foundations, Walls, Slabs, Cable Duct, Pipe Tunnels, Stacks, Concrete Intake Piping, Cooling Tower Basins, Dams, Intake Crib Structures, Embankments , Tanks , Water Wells

Table 2.2: Typical safety-related concrete structures at PWR plants[49]

Structures	Components
Primary Containment	Basement Foundation, Tendon Access Galleries, Vertical Walls (and Buttresses) , Ring Girder (Prestressed Concrete Containment) , Dome , Basement Foundation
Containment Structures                      Internal	Bottom Floor (metal Containment) , Floor Slabs, Wall, Columns, NSSS Equipment Pedestal/Supports, Primary Shield Wall (Reactor Cavity), Reactor Coolant Vault Walls, Beams, Crane Support Structures, Ice Condenser Divider Wall and Slab, Refueling Pool and Canal Walls
Secondary Containment/Reactor Building	Foundation, Walls, Slabs
Other Structures	Foundations , Walls, Slabs, Cable Duct , Pipe Tunnels, Stacks , Concrete Intake Piping , Hyperbolic Cooling Tower , Dams , Intake Crib Structures, Embankments , Tanks , Water Wells

### 2.1.1 Containment Structures

Containment protects the surrounding environment of a reactor from radioactive release. Earlier containment structures were dependent on the type of Nuclear Steam Supply System (NSSS) [52]. Nowadays, containment structures do not that much depend on type of reactors because of developing of new efficient materials. Old NPPs are mostly under consideration because of aging phenomena. So, focus of this part is on typical containment structures that are at the end of their operation life or at the beginning of their renewal license. Concrete containment is attached to a liner that provides leak tightness. Exposed surface of carbon steel liner is protected from degradation mechanism like abrasion by a thin layer of concrete. There are two types of containment; primary or secondary containment, which are different for BWR and PWR NPPs.

Primary containment for both BWR and PWR are attached to a liner that provides leak tightness. Exposed surface of carbon steel liner is protected from abrasion by a thin layer of concrete. The difference between the primary of BWR and PWR is in their geometry and design. PWR containment consists a vertical cylindrical wall and an ellipsoidal, hemispherical, or torispherical dome.

Secondary containment is either steel containment or concrete containment. In the cases of concrete, secondary containment is called enclosure buildings. It provides a relatively air-tight space around the primary containment for having a slight negative pressure when radioactive substances release. Enclosure buildings usually are a thin free-standing RC shell with a dome.

Steel containment pressure vessel is relatively thin and needs to be protected from external missiles or environmental extreme loads. It also provides a radiation shield for environment. Secondary containment makes an air space around the containment vessels and this air space can be maintained at a slight vacuum and the resulting in-leakage is filtered.

### 2.1.2 Safety Related Structures

Containment internal structures are classified on high safety class between concrete structures in NPPs. Internal structures have higher sensitivity in their design since their failure can produce huge disaster for whole structure. They should also provide radiation shielding during plant operation and control radiation exposure in case of a loss-of-coolant accident (LOCA). Section of Reactor Building (RB) for an Advanced Boiler Water Reactor (ABWR) is shown in Figure 2.4.

Internal Structures and components are listed in Figure 2.5 where concrete structures that are more related for this thesis are highlighted. Shielding structures and Spent Nuclear Fuel (SNF) storages are the most important structures exposed to high levels of radiation.

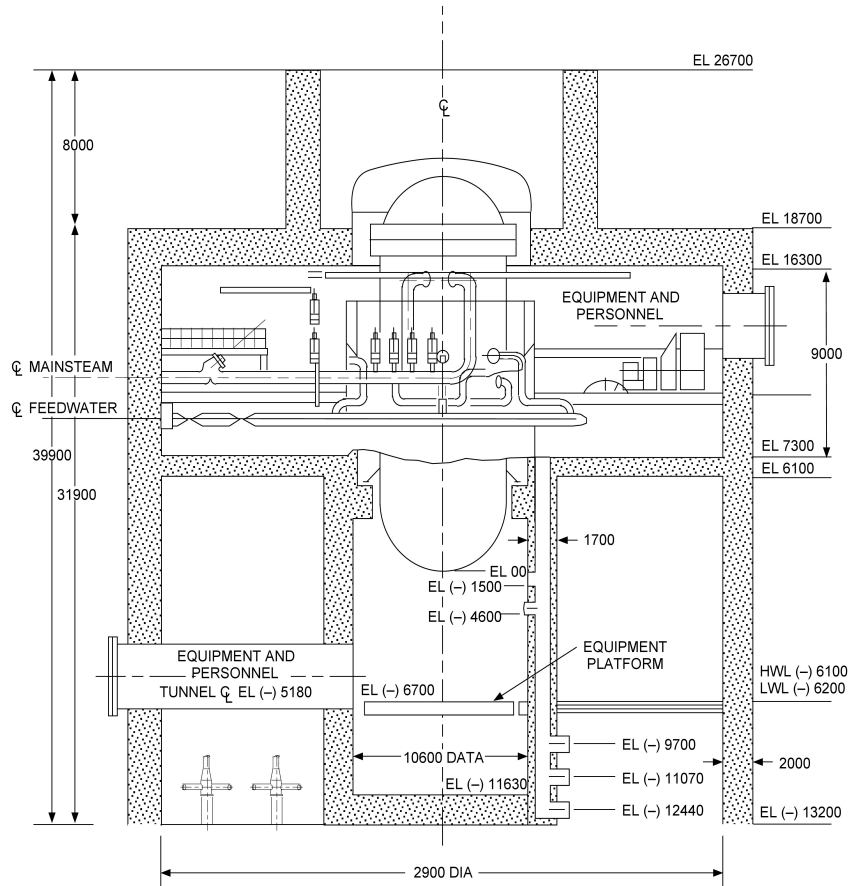


Figure 2.4: Reactor building section (ABWR) [21]

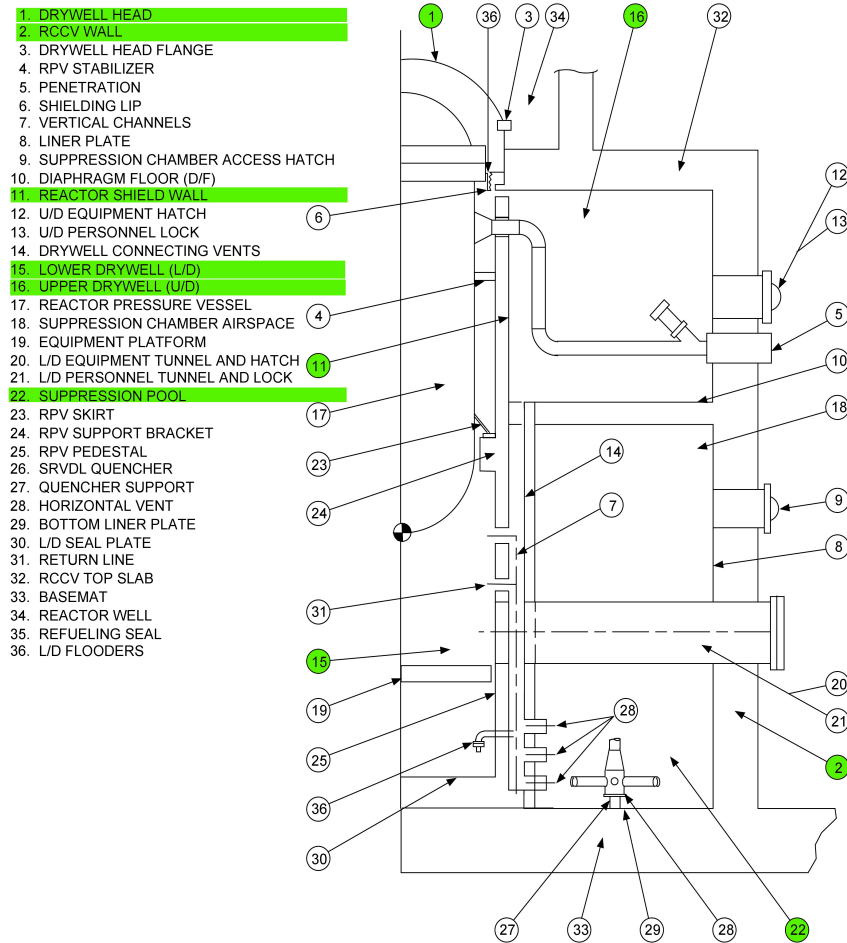


Figure 2.5: Reactor building internal structures [21]

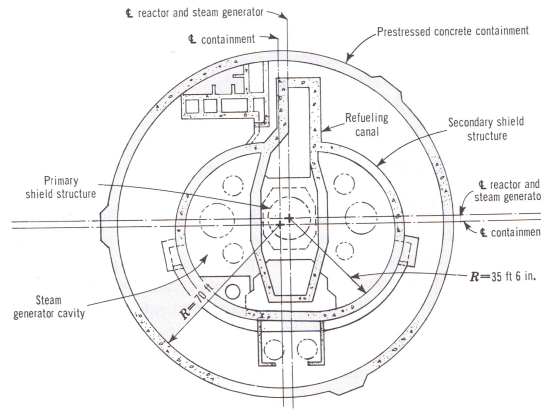


Figure 2.6: PWR dry containment arrangement [52]

## Shielding Structures

Shielding structures are also in safety class *I* in NPPs. Shielding concrete requirements should be considered during shielding structure design procedure. Type and intensity of radiation source should be determined (e.g. photons or neutrons). These sources are dependent on the reactor type and its design. Maximum allowable level of exposure on external surface is another factor required for basic containment design. Maximum permissible radiation doses can be obtained from the International Commission on Radiological Protection (ICRP) recommendations. Reduction factor (attenuation factor) is important to calculate appropriate wall thickness for the structure. Concrete proportioning is also directly related to this factor. Aggregate and cement paste of concrete used for containment should govern these requirements [37]. There are two types of shielding structures; Primary and Secondary shields are shown in Figure 2.6.

For PWRs, primary shield is the closest concrete structure around the reactor vessel and is called biological shield. Structural system of primary shield is usually shear wall and it connects foundation slab to the operation floor. Secondary shield or reactor coolant component wall protects the reactor coolant systems from radiation and other sources of external (disasters) or internal (LOCA) damage. Internal structures are different in their details for dry and ice condenser PWRs [52]. However shear walls are mostly focused in this thesis. Mostly common walls in the Containment Internal structures are primary and secondary shields.

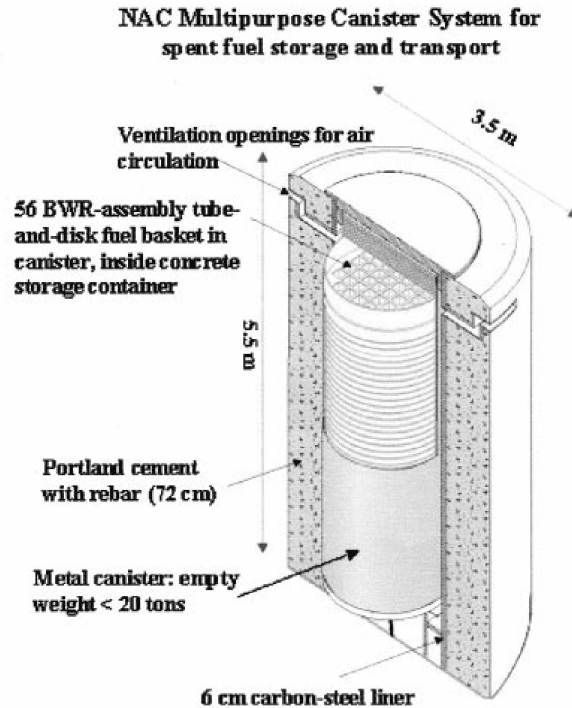


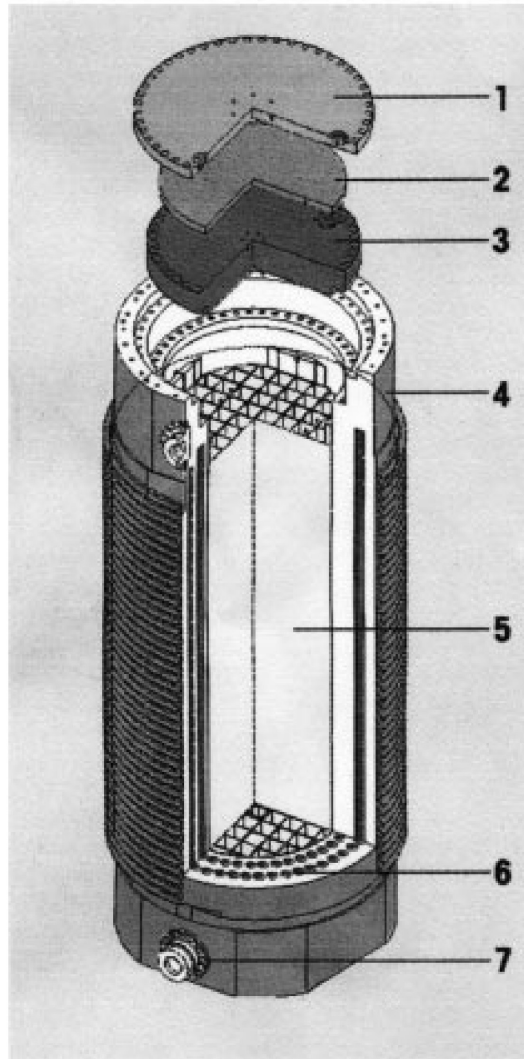
Figure 2.7: A thin-walled concrete cask surrounded with a reinforced concrete overpack [41]

## Spent Nuclear Fuel Storages

Spent Nuclear Fuel (SNF) storages are the structures that store the SNF removed from reactor core. There are two types of SNF storages: wet and dry storages. SNF is stored in the wet storages inside cooling water pools designed with RC walls and steel liners inside reactor buildings. SNF remains in wet storages for 5 years for the radioactive activity decay, then it will be transferred to dry storages off-site.

Dry storages can be vault, silos, or cask storage. Vault and silos are RC building and cylinder respectively. Cask storages are made from metal (ductile cast iron), reinforced concrete, or combination of both. Usually, there are two types of cask: thick-walled cask and thin-walled cask surrounded by a RC overpack. As can be seen from Figure 2.8, radiation protection is provided by the metallic thick wall in thick-walled cask. In the case of the cask with overpack concrete walls, air circulation between the cask and overpack protect the environment from radiation (see Figure 2.7)





### **Castor V/52**

- 1 Secondary lid**
- 2 Neutron moderator plate**
- 3 Primary lid**
- 4 Cask body with cooling fins**
- 5 Fuel assembly basket**
- 6 Neutron moderator Rods**
- 7 Trunnion**

Figure 2.8: A metallic thick-walled cask [41]

## 2.2 Reinforced Concrete Containment Design Requirements (ASME *III* div 2)

### 2.2.1 Load Applied

Secondary and primary containment structures are the last protection layers of nuclear facilities and are very important for providing leak tightness of NPPs. Consequently, in addition to normal and severe load conditions in the design of conventional structures, extreme and abnormal load conditions are also considered for nuclear structure design. One of the most challenging part of the design is considering all possible loading condition for these buildings. Load categories are defined according to different stages from inside of the building to surrounding of the structure. They are numerated below:

1. Normal or service load
2. Severe environmental load
3. Extreme environmental load
4. Abnormal loads

Normal or service load category includes those that are applied during normal operation plant and shutdown. According to ASME Boiler and Pressure Design Code section *III* division 2, dead-load  $D$ , live-load  $L$ , thermal effect  $T_o$ , pipe reaction  $R_o$ , and operating pressure  $P_o$  can be in the first two categories of loading. Operating basis earthquake and design wind load are included in severe environmental load category.

Extreme environmental conditions are defined for safe shutdown earthquake  $E_{ss}$  and tornado wind pressure  $W_t$  load conditions. Last category is abnormal loads in which concern is huge loads caused by postulated high-energy pipe break accidents like equipment pressure  $P_a$ , thermal load  $T_a$ , pipe reactions  $R_a$ , reaction load of broken pipes  $R_r$ , jet impingement load  $R_{rj}$ , and missile impact equivalent static load  $R_{rm}$  [52]. Summarizing of these four load categories can be found in Table 2.3

Load combinations use in the design of a RC containment is discussed in section *III* division 2 of the ASME Boiler and Pressure Vessel Code. As shown in Tables 2.4 and 2.5 (Table 2.5 and 2.5 should be summed for the load combinations), there are fifteen cases that are divided into service and factored load combinations. Service load combinations are considered for test, construction and normal conditions. Factored load combinations are divided into five categories with different combinations of severe, extreme, and abnormal environmental loading. Load combinations that are usually governing the design of

Table 2.3: Load categories (ASME III division 2)

categories	Load level	Load source <sup>a</sup>
Service	Normal	$D L F G T_o R_o P_\nu$
	Construction	$D L F T_o$
	test	$D L F P_t T_t$
Factored	Severe environmental	$W E_o$
	Extreme environmental	$E_{ss} W_t$
	Abnormal	$H_a P_a T_a R_a R_{rr} R_{rj} R_{rm}$

<sup>a</sup>  $D$ : Dead,  $L$ : Live,  $F$ : Fluid,  $G$ : high energy divides relief load,  $T_o$ : Operating thermal load,  $R_o$ : Pipe reaction in operating conditions,  $P_\nu$ : Pressure variation,  $P_t$ : Pressure during test,  $T_t$ : Thermal load during test,  $P_a$ : Pressure by a postulated pipe break,  $T_t$ : Thermal load during test,  $W$ : Operating basis wind load,  $E_o$ : Operating basis earthquake,  $E_{ss}$ : Safe shut down earthquake,  $W_t$ : Tornado,  $H_a$ : Internal flooding,  $P_a$ : Pressure by a postulated pipe break,  $T_a$ : Thermal load during design basis accident,  $R_a$ : Pipe reaction in a postulated pipe break,  $R_{rr}$ : Pipe reaction during design basis accident,  $R_{rj}$ : Jet impingement load during design basis accident,  $R_{rm}$ : Missile load during design basis accident

RC containments are number 3, 8, 11, and 15 of normal, abnormal, abnormal-severe environmental, and abnormal-extreme environmental loading conditions respectively. Load combinations number 3, 8, and 11 govern design of the shell and number 11 and 15 govern design of the basement [3].

### 2.2.2 Design Criteria

Containment design procedure includes following steps:

1. Preliminary analysis
2. Finite element analysis
3. Final design
4. Special consideration
5. Final check and design report

Generally stresses in a structure are divided into three categories; primary, secondary, and high peak stresses. However, the place of typical stresses included in these categories are different for different buildings. For example, thermal stresses are in the secondary category for typical building while they are in the primary stresses group for buildings like NPPs that are more subjected to thermal sources. Structures are designed for primary stresses and are checked for secondary and peak stresses.

Primary stresses can not be controlled because they are related to external load sources like snow, wind, and earthquake. They should satisfy equilibrium conditions to have stability.

Secondary stresses are produced by self-constraint of the body and then they can be controlled by defining a specific strain pattern. So, there is no need for these stresses to satisfy external and internal equilibrium laws. Thermal joints in buildings are some examples of predefined strain pattern for secondary stresses.

Peak stresses are potential sources of failure, but they do not cause significant deflection or degradation in short period of time. The most well known failure caused by peak stress is fatigue failure. Stress concentration is the source of these stresses and it might be due to local discontinuity and thermal stresses.

Table 2.4: Load combinations and load factors (ASME section III division 2) (continues)

Load condition	No.	D	L	F	$P_t$	G	$P_a$	$T_t$	$T_o$	$T_a$
Test	1	1	1	1	1	-	-	1	-	-
Construction	2	1	1	1	-	-	-	-	1	-
Normal	3	1	1	1	-	1	-	-	1	-
Severe Environmental	4	1	1.3	1	-	1	-	-	1	-
	5	1	1.3	1	-	1	-	-	1	-
Extreme Environmental	6	1	1	1	-	1	-	-	1	-
	7	1	1	1	-	1	-	-	1	-
Abnormal Environmental	8	1	1	1	-	1	1.5	-	-	1
	9	1	1	1	-	1	1	-	-	1
	10	1	1	1	-	1.25	1.25	-	-	1
Abnormal-Severe Environmental	11	1	1	1	-	1	1.25	-	-	1
	12	1	1	1	-	1	1.25	-	-	1
	13	1	1	1	-	1	-	-	1	-
	14	1	1	1	-	1	-	-	1	-
Abnormal-Extreme Environmental	15	1	1	1	-	1	1	-	-	1

<sup>a</sup> D: Dead, L: Live, F: Fluid,  $P_t$ : Pressure during test, G: high energy divides relief load,  $P_a$ : Pressure by a postulated pipe break,  $T_t$ : Thermal load during test,  $T_o$ : Operating thermal load,  $T_a$ : Thermal load during design basis accident

Table 2.5: Load combinations and load factors (ASME section III division 2)

Load condition	No.	$E_o$	$E_{ss}$	W	$W_t$	$R_o$	$R_a$	$R_r$	$P_\nu$	$H_a$
Test	1	-	-	-	-	-	-	-	-	-
Construction	2	-	-	1	-	-	-	-	-	-
Normal	3	-	-	-	-	1	-	-	1	-
Severe Environmental	4	1.5	-	-	-	1	-	-	1	-
	5	-	-	1.5	-	1	-	-	1	-
Extreme Environmental	6	-	1	-	-	1	-	-	1	-
	7	-	-	-	1	1	-	-	1	-
Abnormal Environmental	8	-	-	-	-	-	1	-	-	-
	9	-	-	-	-	-	1.25	-	-	-
	10	-	-	-	-	-	1	-	-	-
Abnormal-Severe Environmental	11	1.25	-	-	-	-	1	-	-	-
	12	-	-	1.25	-	-	1	-	-	-
	13	1	-	-	-	-	-	-	-	-
	14	-	-	1	-	-	-	-	-	1
Abnormal-Extreme Environmental	15	-	1	-	-	-	1	1	-	-

<sup>a</sup>  $E_o$ : Operating basis earthquake,  $E_{ss}$ : Safe shut down earthquake, W: Operating basis wind load,  $W_t$ : Tornado,  $R_o$ :Pipe reaction in operating conditions,  $R_a$ :Pipe reaction in a postulated pipe break,  $R_r$ :Load during design basis accident,  $P_\nu$ : Pressure variation,  $H_a$ :Internal flooding

## 2.3 Nuclear Safety Structures Related Design Requirements (ACI-349)

RC structures that are not covered by ASME Boiler and Pressure Vessel codes are designed based on ACI-349 code. These structures are in the safety related category of NPP components because they protect nuclear safety class components or systems. Aging phenomena in NPPs and importance of safety related structures are mentioned in Section 2.4. The renewal of expired licenses of NPPs is necessary. Safety-related structures are one of the most important issues for renewing license of a NPP.

As mentioned in Section 2.1, RC shields and some parts of containment internal structures that are close to high radioactive sources are parts of the safety related structures. These structures are mostly RC wall types [52]. So, focus is on the parts of the code that are related to design and analysis of walls, which are illustrated in Chapter fourteen of the code. RC panels that are analyzed in this research are all subjected to shear with or without axial loading. Shear capacity of the panels is analyzed and the results for not degraded and degraded elements are compared. This thesis will specifically concentrate on designing of the structural component subjected to shear that is illustrated in Chapter 11 of ACI-349 code.

Material properties, design, and analysis requirements of RC panels from shields are defined according to ACI-349 and are explained with details in the following sections.

### 2.3.1 Material Properties

Generally, codes start by definition of material properties of the structures. Since the panels are RC, reinforcement and concrete are the only materials we need to explain here.

#### Concrete

Concrete includes cement, aggregate, water, and admixture. Concrete mix design for shields has some extra consideration than other structures designed based on ACI-349. For example, aggregates should be based on the “Specification for Aggregates for Radiation-Shielding Concrete” (ASTM C 637). American National Standard Institute publishes an standard for concrete radiation shields in NPPs; ANSI/ANS-6.4, titled as the nuclear analysis and design of concrete radiation shielding for NPPs. The standard focuses on the appropriate properties of the concrete for attenuation of fast neutron particles which will be explained in Section 2.5.

Concrete mixture for shields can contain 13% cement, 7% water (including water in the aggregate) and 80% aggregate [10]. Different types of concrete are available for shielding.

Table 2.6: Typical shielding concrete types and their elements density(continues)[31]

Concrete Type <sup>a</sup>	Density ( $gcm^2$ )	Element <sup>b</sup> Partial Density							
		<i>H</i>	<i>O</i>	<i>Si</i>	<i>Ca</i>	<i>C</i>	<i>Na</i>	<i>Mg</i>	<i>Al</i>
Ordinary	2.3	0.013	1.165	0.737	0.194		0.04	0.006	0.107
Magnetite	3.53	0.011	1.168	0.091	0.251			0.033	0.083
Barytes	3.35	0.012	1.043	0.035	0.168			0.004	0.014
Magnetite and Steel	4.64	0.011	0.638	0.073	0.258			0.017	0.048
Limonite and Steel	4.54	0.031	0.708	0.067	0.261			0.007	0.029
Serpentine	2.1	0.035	1.126	0.460	0.150	0.002	0.009	0.297	0.042

<sup>a</sup> Magnetite ( $FeO.Fe_2O_3$ ), Barytes ( $BaSO_4$ ), Limonite (a hydrated  $FeO_3$  ore plus steel punchings), and Serpentine ( $3MgO.2SiO_2.2H_2O$ ) are as aggregate .

<sup>b</sup> H: Hydrogen, O: Oxygen, Si: Silicon, Ca: Calcium, C:Carbon , Na: Sodium, Mg: magnesium, Al: Aluminum.

As shown in Tables 2.6 and 2.7, the concrete types are recognized mostly by their differences in aggregates.

Specification for radiation shields is mainly because of absorption and scattering factors. Absorption is an important characteristic of the materials used in shielding structures in NPPs. Materials with high absorptivity are used as radiation protection in NPPs. Absorptivity is the ability of the material to catch neutrons particles. The process will release energy in form of gamma-ray energy. As seen in Table 2.8, minerals such as Boron-10 are very good choices to be added to the normal concrete to increase this ability because they absorb high range of neutron particles and release low amount of gamma-ray energy.

Scattering is another desirable property of the material used in shielding structure. Materials that are more probable to scatter neutron particles are better in protecting environment from radiation effect. Boron is also responsible for thermal neutron absorbing of concrete shields [10]. As can be seen in Table 2.8, hydrogen has a high ability for this purpose.

Different concrete mixture produces different mechanical and thermal properties shown in Table 2.9. Since irradiation affects compressive and tensile strength of concrete,  $f'_c$  and



Table 2.7: Typical shielding concrete types and their elements density[31]

Concrete Type <sup>a</sup>	Density ( $gcm^2$ )	Element <sup>b</sup> Partial Density							
		<i>S</i>	<i>K</i>	<i>Fe</i>	<i>Ti</i>	<i>Cr</i>	<i>Mn</i>	<i>V</i>	<i>Ba</i>
Ordinary	2.3	0.003	0.045	0.029					
Magnetite	3.53	0.005		1.676	0.192	0.006	0.007	0.011	
Barytes	3.35	0.361	0.159						1.551
Magnetite and Steel	4.64			3.512	0.074			0.003	
Limonite and Steel	4.54		0.004	3.421				0.004	
Serpentine	2.1		0.009	0.068		0.002			

<sup>a</sup> Magnetite ( $FeO.Fe_2O_3$ ), Barytes ( $BaSO_4$ ), Limonite (a hydrated  $FeO_3$  ore plus steel punchings), and Serpentine ( $3MgO.2SiO_2.2H_2O$ ) are as aggregate .

<sup>b</sup> S:Sulfur, K:Potassium, Fe:Iron, Ti: Titanium, Cr: Chromium, Mn: Manganese, V:Vanadium, Ba:Barium

Table 2.8: Absorption and scattering cross section used in shielding concrete[35]

Element	Absorption Cross Section (barns <sup>a</sup> )	Scattering Cross Section (barns)
Hydrogen ( <i>H</i> )	0.3	99.0
Oxygen( <i>O</i> )	0.0	4.2
Boron ( <i>B</i> )	755.0	4.0
Silicon ( <i>Si</i> )	0.2	1.7
Iron ( <i>Fe</i> )	2.5	11.0
Barium ( <i>Ba</i> )	1.2	8.0
Aluminum ( <i>Al</i> )	0.2	1.4
Calcium ( <i>Ca</i> )	0.4	3.2
Sodium ( <i>Na</i> )	0.5	0.4
Sulfur ( <i>S</i> )	0.5	1.1

<sup>a</sup> Barns is a unit of area equals to  $10^{-28}m^2$ .

Table 2.9: Typical Mechanical and thermal properties of representative concretes after curing[10]

Property	Concrete type			
	Ordinary	Barytes <sup>a</sup>	Limonite and steel <sup>a</sup>	Serpentine <sup>a</sup>
Density ( $gcm^{-3}$ )	2.2-2.4	3.5	4.3-4.5	2.1-2.2
Specific heat( $Jg^{-1}K^{-1}$ )	0.65	0.52	0.7	-
Thermal conductivity( $WM^{-1}K^{-1}$ )	0.88	1.6	2.8-3.6	0.9
Coefficient of thermal expansion ( $10^{-6}K^{-1}$ )	14	-	7	32
Tensile strength (Mpa)	2-3	2	-	-
Compressive strength (Mpa)	38	25-29	38	13-16

<sup>a</sup> Barytes ( $BaSO_4$ ), Limonite (a hydrated  $FeO_3$ ) plus steel punchings, and Serpentine ( $3MgO.2SiO_2.2H_2O$ ) are as aggregate .

$f_t$  are two important properties of these types of concrete in this study.

## Reinforcement

Reinforcement in safety class structures of NPPs should be based on ACI-349. There is no regularity or requirements considering shielding structures in ACI-349. The only limitation regarding mechanical properties of reinforcing steel is to limit the sizes of cracks for massive concrete sections by limiting yields strength of reinforcement  $f_y$ . Yielding strength of the panels is limited to maximum 415 MPa for deformed reinforcements. Young modulus of reinforcing steel  $E_s$  is equal to 199948 MPa.

There is only one concern pointed in ACI-349R-01 (Commentary on code Requirements for nuclear safety related concrete structures) regarding to irradiation and reinforcement: epoxy coating for reinforcement used in the environment with high temperature and radiation should be analyzed for the long-term durability of structures.

### 2.3.2 Strength and Serviceability Requirements

ACI-349 has the same strength design method as ACI-318. Minimum strength value of structural systems and their components should be equal to maximum value of load com-

binations applied to the structures. RC structures in NPPs should be analyzed by finite element methods of analysis for the critical sections such as opening, base connection, cylinder, and roof or dome connection.

American code uses Load and Resistance Factor Design (LRFD) for designing non-prestressed concrete structures and prestressed concrete structures. Chapter 9 of ACI-349 presents general design consideration for safety related structures in NPPs. It starts first with defining of the load categories and combinations. Then, the design strength reduction factor is specified for members subjected to flexure, axial, shear, and torsion loads or combination of them.

### Load Categories

Load categories for shielding concrete structures are almost the same as concrete containment. Loads are divided into normal, severe environmental, extreme environmental, and abnormal load. As shown in Table 2.3, normal loads include D (dead), L (live), F (fluid), H (soil),  $T_o$  (temperature in operating conditions) loads. Concrete containment structures have  $R_o$  (pipe reaction in operating conditions) and  $P_v$  (external pressure variation) instead of H. Severe and extreme environmental load categories are quite similar. Abnormal load category in containment has  $H_a$  (internal flooding) extra to what concrete shields have.

### Load Combinations

ACI-349 considers eleven load combinations for design. Table 2.3 is provided compared to the ASME sec III division 2 load combination. There are some significant differences between load combinations corresponding to different applications of these structures. A significant difference is higher factors for D, L, F, and  $H_a$  loads for shielding concrete design than containment structures design.  $P_t$ , G, and  $P_v$  are completely eliminated for shielding structures and  $R_o$  has more effect than  $R_a$  on the shielding design. ACI-349 does not have clear categories like ASME for load combinations, however, there are some subsections that illustrate load applications. Load categories are explained based on the load definition; for example,  $W_t$  in load combination 5 shows extreme environmental condition. Abnormal categories (6,7 and 8) can be easily found by having missile load  $R_a$  ( $Y_r$ ,  $Y_j$ ,  $Y_m$ ).

### Strength Reduction Factor

Strength reduction factor  $\phi$  in ACI-349 is divided into 5 groups tabulated in Table 2.11.

The panels analyzed are subjected to shear and axial loads. Hence, the strength reduction factor, which is suggested by ACI-349 is 0.85.

Table 2.10: Load combinations and load factors (ACI-349)

Load Combination	Load Types <sup>a</sup>																	
	D	L	F	P <sub>t</sub>	G	P <sub>a</sub>	T <sub>t</sub>	T <sub>o</sub>	T <sub>a</sub>	E <sub>o</sub>	E <sub>ss</sub>	W	W <sub>t</sub>	R <sub>o</sub>	R <sub>a</sub>	R <sub>r</sub>	P <sub>v</sub>	H <sub>a</sub>
1	1.4	1.7	1.4	-	-	-	-	-	-	-	-	-	-	1.7	-	-	-	1.7
2	1.4	1.7	1.4	-	-	-	-	-	1.7	-	-	-	-	1.7	-	-	-	1.7
3	1.4	1.7	1.4	-	-	-	-	-	-	-	-	1.7	-	1.7	-	-	-	1.7
4	1.0	1.0	1.0	-	-	-	-	1.0	-	-	1.0	-	-	1.0	-	-	-	1.0
5	1.0	1.0	1.0	-	-	-	-	1.0	-	-	-	-	1.0	1.0	-	-	-	1.0
6	1.0	1.0	1.0	-	-	1.25	-	-	1.0	-	-	-	-	-	1.0	-	-	1.0
7	1.0	1.0	1.0	-	-	1.15	-	-	1.0	1.5	-	-	-	-	1.0	1.0	-	1.0
8	1.0	1.0	1.0	-	-	1.0	-	-	1.0	-	1.0	-	-	-	1.0	1.0	-	1.0
9	1.05	1.3	1.05	-	-	-	-	-	1.05	-	-	-	-	1.3	-	-	-	1.3
10	1.05	1.3	1.05	-	-	-	-	1.05	-	1.3	-	-	-	1.3	-	-	-	1.3
11	1.05	1.3	1.05	-	-	-	-	1.05	-	-	-	1.3	-	1.3	-	-	-	1.3

<sup>a</sup> D: Dead, L: Live, F: Fluid, P<sub>t</sub>: Pressure during test, G: high energy divides relief load, P<sub>a</sub>: Pressure by a postulated pipe break, T<sub>t</sub>: Thermal load during test, T<sub>o</sub>: Operating thermal load, T<sub>a</sub>: Thermal load during design basis accident, E<sub>o</sub>: Operating basis earthquake, E<sub>ss</sub>: Safe shut down earthquake, W: Operating basis wind load, W<sub>t</sub>: Tornado, R<sub>o</sub>: Pipe reaction in operating conditions, R<sub>a</sub>: Pipe reaction in a postulated pipe break, R<sub>r</sub>: Load during design basis accident, P<sub>v</sub>: Pressure variation, H<sub>a</sub>: Internal flooding

Table 2.11: Strength reduction factor for safety-related reinforced concrete members in NPPs (data obtained from ACI-349)

Reinforced Concrete Members	Strength Reduction Factor $\phi$
Flexure without Axial Load	0.9
Axial Tension - Axial Tension and Flexure	0.9
Axial Compression - Axial Compression and Flexure	0.75
Other Reinforced Member	0.7
General Shear and Torsion	0.85
Shear in Joist	0.6
Shear Joist (Critical Loads)	0.85
Bearing on Concrete	0.7

### 2.3.3 Shear Design

Concrete structures in NPPs are designed based on elastic behavior of material in service loads. Safety related structures and their structural components are subjected to the shear are designed based on the chapter 11 of ACI-349. General shear design of RC members is covered by Sections 11.1, 11.3, and 11.5 of ACI-349. There are some specifications for structures like deep flexural members, bracket and corbels, walls, transfer of moments to columns, slabs, and footings. In this section, general shear design of RC structures in NPPs is reviewed firstly. Then, shear design of walls is explained since the elements studied in this thesis are mostly from RC walls in NPPs. Interior walls can be shields, or fuel storage that are subjected to high levels of radiation after 40 years.

#### General Shear Design Requirements of RC structures

Shear design starts with verifying Equations (2.1) and (2.2) for factored shear force  $V_u$  and reduced nominal shear strength  $V_n$ . All RC sections subjected to the shear forces should satisfy Equation (2.1).

$$\phi V_n \geq V_u \quad (2.1)$$

where

$$V_n = V_c + V_s \quad (2.2)$$

where  $\phi$  is the shear strength reduction factor equal to 0.85 (Table 2.11).

Nominal shear strength of the panels are provided by concrete  $V_c$  and shear reinforcements  $V_s$ . The concrete shear strength for RC structures are different for members subjected to shear and flexure, axial compression and tension.  $V_c$  is calculated generally with Equation (2.3) for members subjected to shear and flexure, axial compression, and significant axial tension, respectively.

$$V_c = \begin{cases} 2\sqrt{f'_c}b_wd & \text{Shear and flexure} \\ 2\left(1 + \frac{N_u}{2000A_g}\right)\sqrt{f'_c}b_wd & \text{Shear and axial compression} \\ 0 & \text{Shear and significant axial tension} \end{cases} \quad (2.3)$$

where,  $f'_c$ : concrete compressive strength,  $b_w$ : web width,  $d$ : distance from extreme compression point to centroid of the tension reinforcement,  $N_u$ : axial load (positive sign for compression and negative sign for tension), and  $A_g$ : maximum aggregate size.

Equations (2.4) is an alternative for computing  $V_c$  when more information is available:

$$V_c = \begin{cases} \left(1.9\sqrt{f'_c} + 2500\rho_w\frac{V_u d}{M_u}\right)b_wd & \text{Shear and flexure} \\ 3.5\sqrt{f'_c}b_wd\sqrt{1 + \frac{N_u}{500A_g}} & \text{Shear and axial compression} \\ 2\left(1 + \frac{N_u}{500A_g}\right)\sqrt{f'_c}b_wd & \text{Shear and significant axial tension} \end{cases} \quad (2.4)$$

where,  $V_u$ : factored shear force at section,  $\rho_w$ :  $\frac{A_s}{b_wd}$ , and  $M_u$ : factored moment at section.

It is important to notice that all units are in the US customary system ( $f'_c$  and  $\frac{N_u}{A_g}$  in psi). Another important point is that the sign of tension and compression is opposite of our sign in Membrane-2000 analysis (for ACI-349, tension is negative).

Shear reinforcement should be provided when  $V_u$  is greater than  $\phi V_c$  in a section. Value of  $V_s$  varies based on shear reinforcement type. However, it should not exceed

$8\sqrt{f'_c b_w d}$ . For the shear reinforcement perpendicular to axis of members and inclined stirrup, Equation (2.5) is used. For calculating value of  $V_s$  for a single bar, or a single group of parallel bars, all bent up at the same distance from the support and different distance from the support Equation (2.5) is used.  $V_s$  obtained from Equation (2.5) should be less than  $8\sqrt{f'_c b_w d}$  and it should be less than  $3\sqrt{f'_c b_w d}$  when obtained from equation used for single, or group of bars.

$$V_s = \begin{cases} \frac{A_v f_y d}{s} & \text{Perpendicular reinforcement} \\ \frac{A_v f_y (\sin \alpha + \cos \alpha) d}{s} & \text{Inclined stirrup} \\ A_v f_y \sin \alpha & \text{single bar, group of bars, and stirrup} \end{cases} \quad (2.5)$$

where,  $A_v$ : area of shear reinforcement,  $in^2$ ,  $f_y$ : yield strength of non prestressed steel,  $psi$ ,  $S$ , shear reinforcement space,  $in$ ,  $\alpha$ : angle between stirrup and longitudinal axis of member.

### Special Provision in Shear Design for Walls

Shear design for radial (out of plane) and tangential (in plane) shear force is different in ACI-349. Radial shear force is perpendicular to the face of walls and tangential shear force is horizontal in plane of walls. General shear design explained above is applicable for panels with punching shear force. The RC panels that are analyzed are membrane elements with combination of biaxial load and tangential shear.

Design of walls for in plane shear strength is also based on Equations (2.1) and (2.2). However,  $V_n$  should satisfy Equation (2.6) for walls subjected to axial compression and tension respectively.

$$V_c \lesssim \begin{cases} 2\sqrt{f'_c} h d & \text{Shear and axial compression} \\ 2\left(1 + \frac{N_u}{500A_g}\right) \sqrt{f'_c} b_w d & \text{Shear and axial tension} \end{cases} \quad (2.6)$$

If more information is available,  $V_c$  can be computed as the minimum value of Equation (2.7)(when  $\frac{M_u}{V_u} - \frac{l_w}{2}$  is negative, equation includes moment is not applicable)



$$V_c = \begin{cases} 3.3\sqrt{f'_c}hd + \frac{N_u d}{4l_w} \\ (.6\sqrt{f'_c} + \frac{l_w(1.25\sqrt{f'_c} + .2\frac{N_u}{l_w h})}{\frac{M_u}{V_u} - \frac{l_w}{2}})hd \end{cases} \quad (2.7)$$

where,  $l_w$ : horizontal length of wall and  $h$  is overall thickness of member, *in*.

The shear strength can be provided by horizontal shear reinforcing steel. Horizontal shear reinforcement is obtained by  $\rho_h$  and can be used to find  $V_s$  from Equation (2.8).

$$V_s = \frac{A_v f_y d}{s_2} \quad (2.8)$$

Where,  $s_2$  is spacing of shear or torsion reinforcement in direction perpendicular to longitudinal reinforcement, *in*.

The vertical shear reinforcement ratio ( $\rho_n$ ) should satisfy Equation (2.9).

$$\max(0.0025, (0.0025 + 0.5(2.5 - \frac{h_w}{l_w})(\rho_h - .0025))) \lesssim \rho_n \lesssim \rho_h \quad (2.9)$$

where  $h_w$  is total height of wall from base to top, *in*.

## 2.4 Aging Phenomena

Over 16 percent of world's electricity and 20 percent of US electricity is provided by NPPs (World Nuclear Association, April 2009). Most of over 100 reactors in US build in 1950s pass their operation life time. Replacement of all components of NPPs is not economically feasible. The US Nuclear Regulatory Commission (NRC) paid attention to aging phenomena in NPPs during last two decades.

### 2.4.1 Aging Research Study

Oak Ridge National Laboratory (ORNL), Idaho National Laboratory (INL), Brookhaven National Laboratory (BNL) and Electric Power Research Institute (EPRI) are the most well known laboratories that were joined with NRC in these research areas. Nuclear Regularities (NUREG) 6424, 6679 and 6715 are some of the results of these accompanies that hundreds of publications described the results of those programs. Some of these programs are numerated below:

## 1. NEC Programs

- (a) NPP Aging (NPAR) [39]
- (b) Structural Aging (SAG) [49]
- (c) NPP Generic Aging Lessons Learned (GALL) [57]
- (d) Assessment of In-service Conditions of Safety-Related NP Structures [4]

## 2. Industry Programs

- (a) Numeric Industry Reports (IRs)
- (b) NEI - Industry Guideline for monitoring the effectiveness of maintenance at NPPs [24]
- (c) American Concrete Institute Codes and Standard

## 3. Technical Information

- (a) Summary of Japanese literature [55]
- (b) Organization of economic co-operation and development (OECD) - Nuclear Energy Agency (NEA)

## **Current Research**

Need of sufficient statistical information about age-related degradation mechanisms in NPPs is more clear to perform License Renewal Applications (LRA). The most recent project that is going on in US about "Development of Seismic Capability Evaluation Technology for Degraded Structures and Components" in NPPs is a joined project between Korean Atomic Energy Research Institute (KAERI) and BNL. The project started from 2007 and continues for 5 years till 2012 in 5 tasks. The goal of the project is studying the effects of aging on the seismic risk evaluation system.

Components with higher priorities are reviewed in the first year. As seen from Figure 2.9 piping system, exchanger, and Reactor Pressure Vessels (RPV) have higher number of degradation occurrences in U.S. NPPs. However, Figure 2.9 is a general distribution and there is no information about years or comparison between the results of different researches. For more information Figure 2.10 is shown. Difference between the bar charts may be due to differences in the methods for degradation definition or detection and also some preferences for their researches.

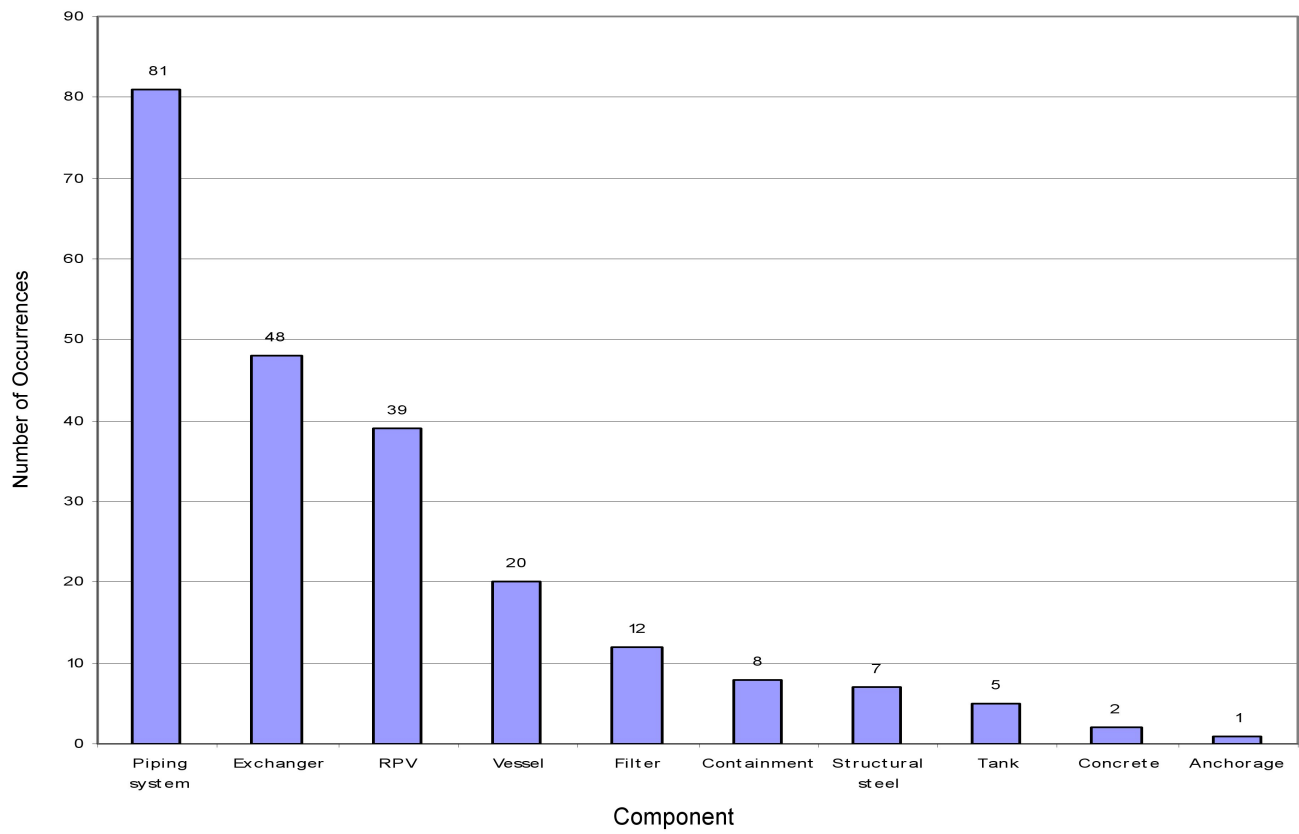


Figure 2.9: Distribution of structures and passive components over component category [51]

### Degradation Occurrences by Components

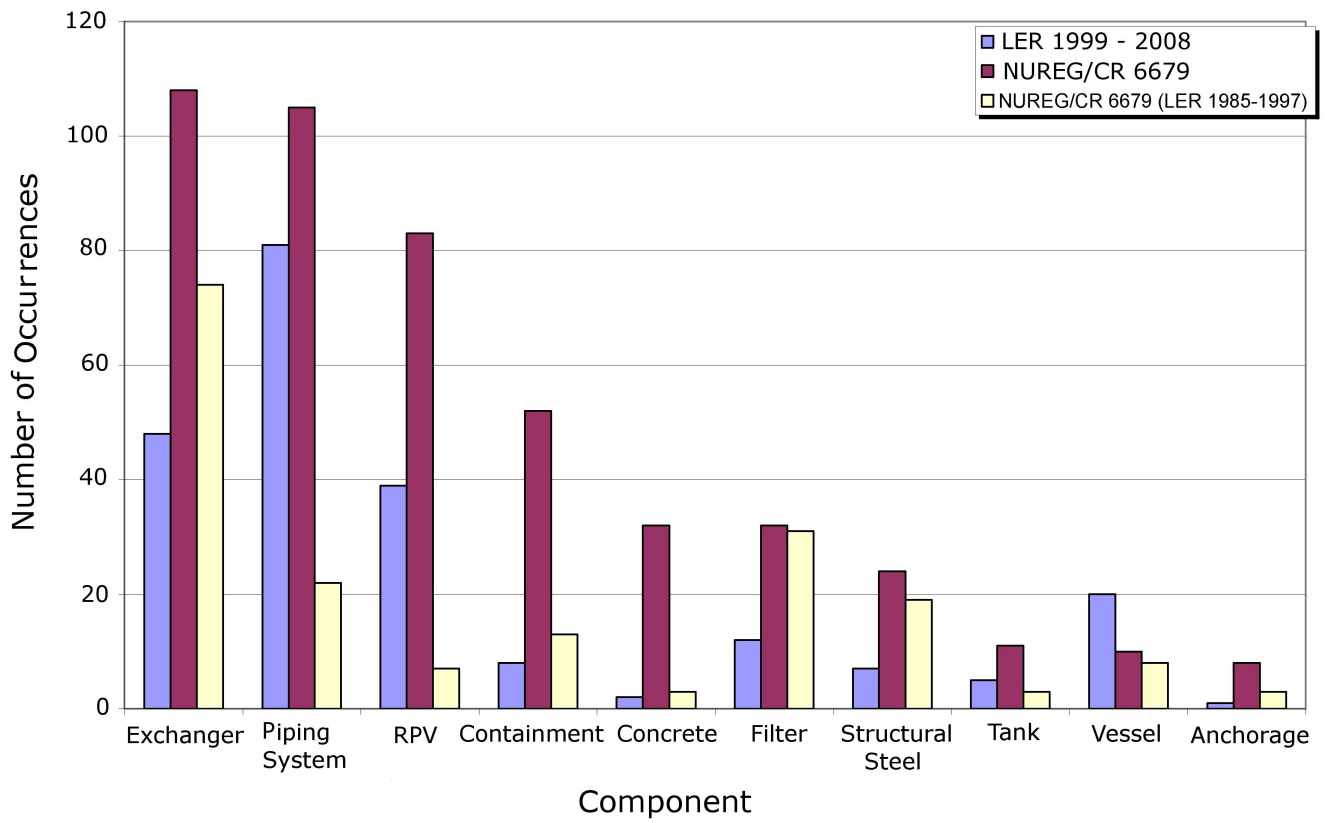


Figure 2.10: Distribution comparison of SPC degradation occurrences over components [51]

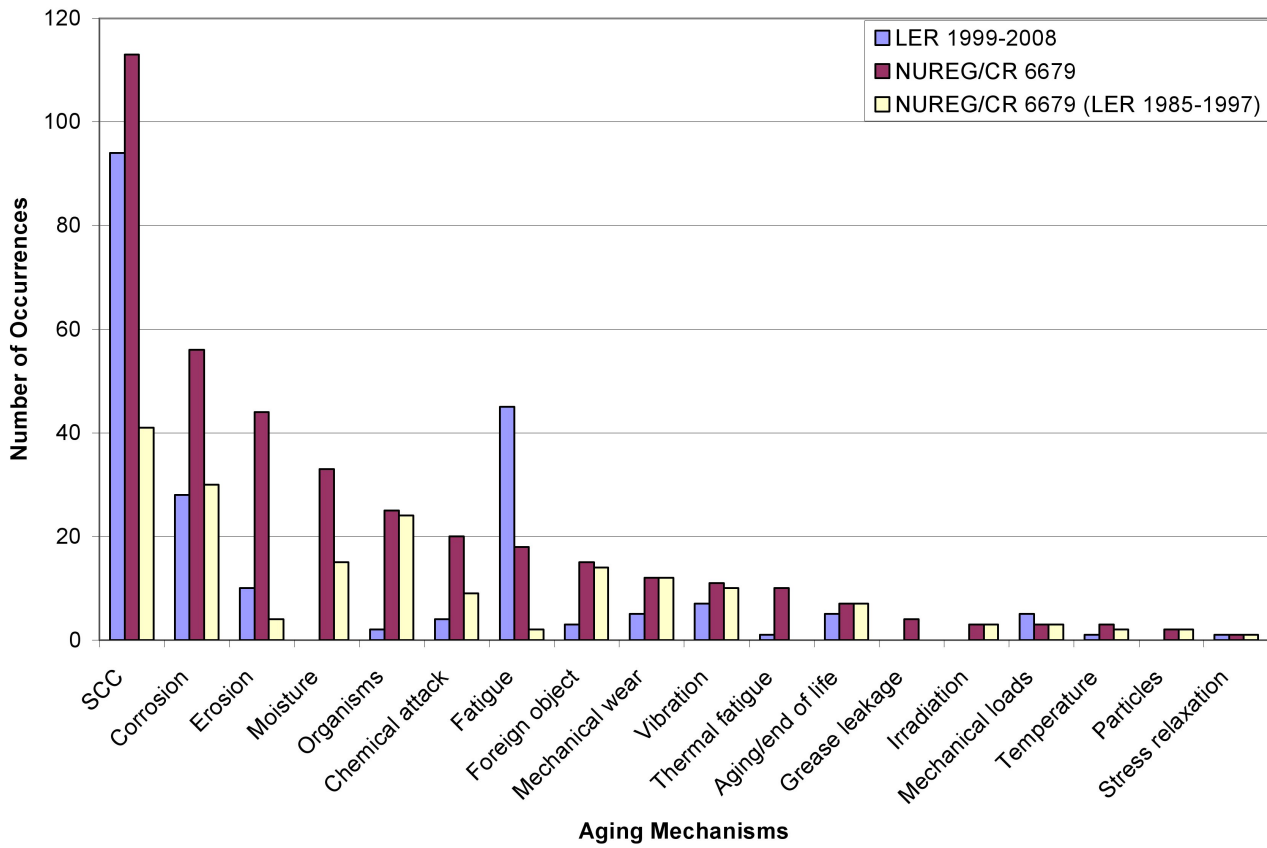


Figure 2.11: Distribution comparison of SPC degradation occurrences over aging mechanism [51]

Table 2.12: Deterioration factors on physical process in concrete and their effects[48]

Deterioration factors on physical process	Primary manifestation
Cracking	reduced durability
Salt crystallization	cracking, loss material
Freezing and thawing	Cracking, scaling, disintegration
Abrasion, erosion, cavitation	section loss
Thermal exposure, thermal cycling	Cracking, spalling, strength loss
Irradiation	Volume change, cracking
Fatigue, vibration	cracking
Settlement	Cracking, spalling, misalignment

## 2.4.2 Age-Related Concrete Degradation in NPPs

Concrete is one of the most useful material for construction. Brittle behavior of concrete is improved during the time by combining it by adding ductile material like reinforcing steel. Mixing steel and concrete as an efficient combination for structures ,however, made a susceptible mixed material for different degradation mechanisms. Degradation of RC structures may occur in cement paste, aggregate or embedded steel. Possibility of different deterioration mechanisms depend on wide varieties of internal and external variables. Degradation mechanisms are categorized in two groups: degradation on physical and chemical process. Degradation categories are available in Tables 2.12 and 2.13.

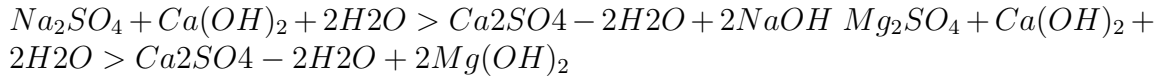
NPPs like most concrete structures are threatened by deterioration. Degradation may mostly occur as a result of the construction fault. So, they usually be fixed in the constructing process. There is also a variety of deterioration due to aging affects. These failures may increase at the end of service life and make large damages to the structures and consequently human societies. Degradation may occurs in concrete part or reinforcing steel. Some of the most concrete deterioration mechanisms in NPPs are briefly illustrated with respect to the order of occurrence and their possibility of occurrence as follow:

**Sulphate attack:** As shown in chemical equation bellow, as a result of reaction of high sulfate content in soil and ground water with free calcium hydroxide, gypsum ( $Ca_2SO_4$ ) is produced. Then gypsum combines with the hydrated calcium aluminate and creates ettringite. The reactions cause expansion then volume of concrete changes and

Table 2.13: Deterioration factors on chemical process in concrete and their effects[48]

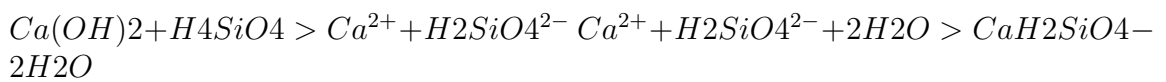
Deterioration factors on chemical process	Primary manifestation
Efflorescence, leaching	Increased porosity
Sulfate attack	Volume change, cracking
Delayed ettringite formation	Volume change, cracking
Acids, bases	Disintegration, spalling, leaching
Alkali-aggregate reactions	Disintegration, cracking
Aggressive water	Disintegration, loss material
Phosphate	Surface deposits
Biological attack	Increased porosity, erosion

cracking occurs.



Possibility of sulfate attack in NPPs is a local problem in the united state and it is mostly for elements exposed to soils and water that contain sulphate. A common example for this deterioration factor is pipes which have sewage sulphate-bearing water [36].

**Alkali-Aggregate Reactions (AAR):** AAR is an internal reaction in concrete. As seen from the equations below, AAR begins with producing of the alkali silicate gel with combination of Alkali and siliceous aggregate. At the Second step,  $Ca^{2+}$  combines with the gel and hard calcium silicate hydrate is produced. Then entered alkali solution transform siliceous minerals into bulky alkali silicate gel. This process produce expansive forces in aggregate. Finally, accumulation of these pressures causes micro-structure cracks in concrete and accelerating of these cracks make one of the most considerable deterioration of concrete.



**Frost attack:** Freeze/thaw cycles cause frost attack in concrete structures. Concrete consists of some specific amount of water. Frozen water produces volume change in concrete, so crack occurs because of concrete expansion. The resistance of concrete in freezing environment is provided by air bobbles entered in concrete. Concrete components of NPPs that are exposed to freezing weather are susceptible to the frost damage.

**Leaching:** Leaching involves the degradation of concrete by the dissolution of the soluble constituents of a material. Acidic waters cause leaching in the concrete elements. Consequently Leaching decreases by increasing the PH. Pipes that consist water are most likely components in NPPs susceptible to the leaching degradation mechanism. Coolant towers that are subjected to water are another group of structures that may degraded by leaching.

**Irradiation :** Degradation mechanism of radiation is not clear and there is no general agreement about possibility of this mechanism in NPPs. However, experimental results show significant concrete strength reduction for some certain levels of neutron radiation. NPP components that are susceptible for these deterioration process are mostly shielding structures. The radiation effect on RC in NPPs is discussed in the last chapter in details.

**Elevated Temperature:** High temperature affects the properties of concrete by changing in the thermal coefficient and the thermal gradients developed within a thick concrete element. Aggregate and hydrated cement can be affected by temperature regarding to the temperature differential and the cycling period. Generally, durability of Portland cement concretes is in the range of 0 to 400 degree centigrade(reference 2.87 Clifton). Experimental results show that both aggregate and cement paste degraded above this range. For instance, Limestone aggregate degradation speed increases sharply when temperature pass 500 degree centigrade (reference 2.88 .clifton). The compressive strength of concrete decreases when temperature increases and also modulus of elasticity will be affected also when temperature rises.

**Salt crystallization:** Salt crystallization is a slow degradation and some times needs a few decades to take place. Due to water evaporation, some dissolved soluble salts produced. Crystal propagation causes some extra internal stresses to the concrete and beyond tensile strength of concrete they cause cracking. In the case of NPPs, salt crystallization is most likely for the elements that have more probability of evaporation such as inner walls, basements, tunnels, slabs on-grade, and partly immerse columns [36].



**Fatigue:** Fatigue is a degradation mechanism that needs time to occur. Failure may not occur for some amounts of load in a single time, however, failure can take place by repeating the loading, temperature, or moisture. Propagation of micro cracks as a result of the fluctuated load application increases rate of deterioration in concrete elements. The locations that are faced with vibration in NPPs such as pipes are more susceptible to fatigue damages. Usually design codes consider design stress limit levels to make sure that this kind of failure does not occur, however, there are some possibilities of the fatigue degradation when the RC structures get old.

## 2.5 Radiation Degradation in NPPs

RC structures are used for many energy infrastructures such as NPPs. Since every structure has a particular service life, a main issue in maintaining infrastructures is determining failure of structures during their life time and proposing appropriate approach to extend serviceability of the structures for a few decades.

Deterioration is the result of concrete or reinforcing steel materials and it is investigated by analyzing the inspection data that are obtained from different testing techniques. A widely considerable issue for concrete structures is the effect of aging specially for NPPs. Generally, a structure fails when its strength and stiffness decrease to a value under its applied stress. Concrete strength is divided into two categories: compressive and tensile strength. Since concrete is brittle material, tensile strength is the weak point of concrete. Reinforcements are used to increase concrete capacity due to loading. Cracking is unavoidable in RC structures. So, prestressed concrete structures are used to reduce harmful effect of the low tensile capacity of the RC structures. However, some structures such as shielding structures are more sensitive and have higher standards compared to the normal structures.

### 2.5.1 Background of Radiation

Understanding of the radiation effect on concrete needs a brief background about radiation. Following parts of the thesis presents general information include atomic physic concepts, definition of ionization, and radiation energy sources.

The main goal of a nuclear reactor in a NPP is producing the energy in the form of heat to use for transformers and finally producing electricity. Heat energy is obtained from the reactor core by a controlled reaction of nuclear fission during transformation of a heavy nucleus into two lighter nuclei. As a result of this reaction, heat and radiation is produced. Nuclear fission can be spontaneous or man made. Reactor cores are designed to speed up the nuclear fission and manage the measure of energy and radiation that are released.

## Structure of Atoms

Any material consists of a number of atoms and characteristics of a matter depends exactly on its atomic properties. Atom consists of charged particles (positively such as protons or negatively such as electrons) or uncharged particles (neutral particles such as neutron and photon). An atom has a nucleus at the center and electrons that are located on orbitals with specific distance from the nucleus. Materials are shown with the form of their atoms like  ${}^A_Z X_N$  where A is number of electrons, Z is number of protons and N is number of neutrons. Chemical properties of a material depend on the number of its electrons and its physical and nuclear properties depend on the mass of the atom. Mass of an atom generally is described by the mass of its nucleus. Atoms are divided into stable atoms and unstable atoms.

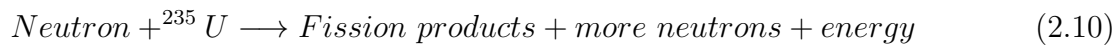
Stability of an atom depends on its mass. Scientist define the ratio of the number of neutron to the number of proton as a measure of stability. For stable atoms, this ratio is less than 20. For heavy stable elements, this ratio is around 1.5. For example, the heaviest stable element in nature is Uranium-235 ( $N/Z = 1.554$ ).

## Nuclear Reactions in Reactor Cores

Two types of nuclear reaction are considered more important for nuclear reactors. they are divided into the spontaneous disintegration of the nuclei and colliding between the nuclei and the nuclear particle. Some heavy nucleus splits by very slow speed to the other lighter nuclei. This disintegration of the nuclei is known as radioactivity. One of the most pronoun of this type of reaction is the radioactive decay.

Radioactive decay may be in a natural way that can be seen in environment too or some different forms from the controlled nuclear reaction in reactor cores. First type of radioactive decay includes three types of *alpha*, *beta*, and *gammadecay*. As can be seen from Figure 2.12, Nucleus include *alphadecay* emits a helium nucleus  $He_2^4$  and conversion of a neutron into a proton by the emission of an electron and a neutrino is *betadecay*. *gammadecay* occurs with photon emission and changing level of stability of a nucleus. Second type of radioactive decays are those which may happen because of many unstable nuclei that can not be produced normally in the nature. One of the most important examples of the nuclei including the second type of decays is  $Kr_3^{876}$ .

Nuclear collision reaction is a process of splitting a heavy weight nucleus to two lighter nuclei by projecting a particle to the heavy nucleus. As can be seen from formulated form of the process available in Equation (2.10), energy and radiation are produced during this fission.



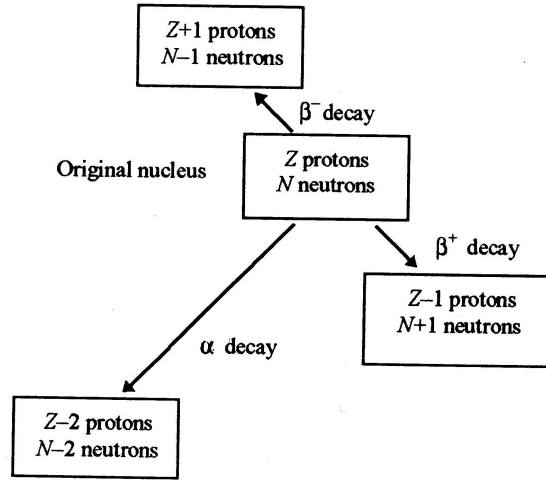
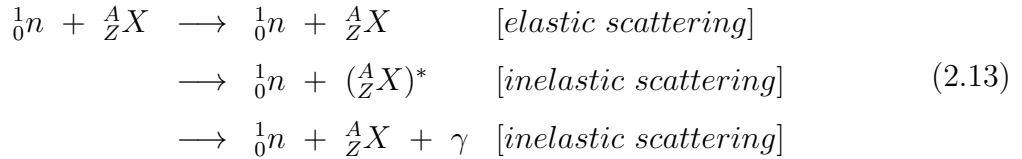
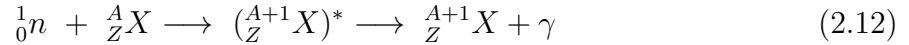


Figure 2.12: Radioactive decay[66]

Interaction between neutrons and nuclei includes the nuclear fission, radiative capture, and scattering. They are formulated in the form of Equations (2.11), (2.12), and 2.13 respectively which  $(\frac{A}{Z}X)^*$  is a nucleus in an excited state.



## Ionization

Shielding structures are used to protect the environment from radiation effects. Radiation is divided into non-ionizing radiation and ionizing radiation. However, shielding is necessary only for ionizing radiation. Applications of ionizing radiation are nuclear weapons, nuclear reactors, and radioactive substances.

Ionizing radiation will occur during radioactivity process. When an unstable atom wants to change to stable condition, it may release energy or particles. this is called radioactivity. Ionizing radiation occurs when radioactive particles change an atom or molecule by changing the number of its particles (electron, proton, neutron...) into an ion.

Ionizing radiation is divided into two categories; electromagnetic waves and nuclear particles. Electromagnetic waves consist of x-rays and gamma rays. Nuclear particles consist of alpha, beta, and neutron. Another division is directly ionizing radiation (charged particles such as electron, proton, alpha, and beta) and indirectly ionizing radiation (uncharged particles such as neutron and photon).

## Radiation Energy and Sources

Radiation energy or binding energy is the energy that is required to separate particles of the nucleus of one atom. In other words, it is the energy that will be released if the neutrons and protons are separated from each other. Electron volt is the unit of binding energy and one eV is equal to  $1.602 \times 10^{-19}$  joules.

An important particle that is considered in shielding requirements is the neutron. Neutrons are uncharged particles and do not ionize directly. However, they can produce other sort of rays that are capable of ionizing atoms. Neutrons are divided into three groups according to their kinetic energy. Thermal or slow neutron's energy level is less than 0.5 electron volt(eV). Epidermal or intermediate neutron particles have a level of energy around 5000 eV. Fast neutrons, which are the most important particles due to deterioration of concrete structures have the kinetic energy level higher than 500,000 eV [37].

There are two types of radiation regarding to time consideration: neutron flux and fluence. Neutron flux unit is  $n/cm^2/s$  and neutron fluence unit is  $n/cm^2$ . Radiation which produce age-related degradation is neutron fluence, which is multiplication of neutron flux and time. Neutron fluence can be divided into three categories:

1. Slow or thermal neutron (dose  $< 10^{10}n/cm^2$ )
2. Intermediate or epidermal neutron ( $10^{10} < \text{dose} < 10^{20}n/cm^2$ )
3. Fast neutron (dose  $> 10^{20}n/cm^2$ )

### 2.5.2 Radiation Effects on Reinforced Concrete Structures

Concrete is one of the most effective materials for control radiations released from nuclei reactions. Two important issues in protecting environment from the harmful effects of

radiation are absorption and scattering. The goal of every concrete shielding is absorbing maximum neutron particles and releasing the minimum energy. Losing energy of neutron by colliding nucleus of concrete material occurs during scattering process.

NPPs like most RC structures are threatened by deterioration due to aging affects. These failures may increase during service life and make large damages to the structures and consequently human societies. Degradation may occurs in reinforcing steel or concrete part.

Radiation may reduce fracture toughness of embedded rebar in RC structures exposed to high level of radiation. However, deterioration of reinforcing steel due to radiation is not serious compare to concrete irradiation. There is no requirements in American codes for NPPs regarding to reinforcing steel and radiation [64].

Deterioration in concrete may affect on physical or chemical process. Degradation factors on both process; physical and chemical are summarized in Tables 2.12 and 2.13 respectively. Shielding concrete deterioration is mostly due to volume changes. Concrete expansion cause cracking and cracks are harmful for the concrete due to corrosion dilemma.

## **Radiation Effect on Aggregate and Cement Paste**

Laboratory investigations on radiation effects on concrete properties mostly focus on the aggregate behavior due to high radiation exposures. Change of aggregate properties due to radiation that affects directly mechanical properties of concrete [38].

Different type of aggregates shows different change exposed to fast neutrons. For example, tensile strength of limestone aggregate decreased by 30 percent when exposed to a fast neutron fluence about  $2 \times 10^{19} \text{n/cm}^2$  and tensile strength of flint aggregate decreased by about 40 percent [38]. Aggregate with same type but from different sources showed wide differences in reaction to the fast neutron fluence. The volume change of concrete is mostly due to aggregate volume change because the micro structure of aggregate is affected by radiation. Aggregate with the same type and the same chemical composition may show different volume change because of different micro structure [23].

Radiation effect on cement paste is not significant. Volume change in cement as a result of shrinkage is related to weight loss caused by drying at elevated temperatures not due to the radiation effect [20].

## **Radiation effect on mechanical properties of concrete**

Mechanical properties such as compressive and tensile strength and modulus of elasticity are widely affected by radiation [27]. Experiments on aggregate and cores from non active reactors showed significant decreasing of mechanical properties due to fast neutron

Table 2.14: Effect of neutron irradiation on compressive strength of concrete

Neutron fluence (n/cm <sup>2</sup> )	Not irradiated unheated %	Irradiated unheated %	Not irradiated heated%	Irradiated heated %
$2 \times 10^{18}$	100	80-115	100	80-105
$2 \times 10^{19}$	100	80-110	100	75-105
$2 \times 10^{20}$	100	60-85	100	-95
$2 \times 10^{21}$	100	35-45	100	-60

fluence. However, some of these results did not separate temperature effect from radiation effect. The temperature effect is hard to distinguish from the radiation effect. Hilsdorf tried to collect experimental results and separate the effect of temperature and radiation. The comparison between the heated-irradiated and unheated-irradiated results shows that radiation effect is significant without considering the temperature effect.

Radiation fluences more than  $5 \times 10^{19}$ n/cm<sup>2</sup> reduces compressive strength of concrete significantly [27]. The effect of radiation on aggregates will change volume of the concrete as a result of the atomic movement. Increasing of concrete volume was measured for specific aggregates (e.g flints). Figures 2.13 and 2.14 show results from other investigations compared by Hilsdorf [27]. The range of compressive strength reduction shown in Figure 2.13 is available in Table 2.14. It shows significant decrease in compressive strength of concrete for neutron radiation above  $2 \times 10^{19}$ n/cm<sup>2</sup>.

In addition to compressive strength, the modulus of elasticity was also studied. Slight increasing in the modulus of elasticity is probable due to the radiation effect [37].

The radiation effect on tensile stress was studied in 1989 [37]. High nuclear fluence can reduce tensile stress and this reduction is more significant than compressive strength. One of the applications of having high neutron radiation levels is the shielding structure. As discussed before, shielding concrete has extra admixtures to increase the absorptivity and scattering of concrete. The radiation effects on tensile strength is available in Figure 2.14. It is stated that tensile reduction is much more dependent in the concrete types. Experimental Results show reduction between 0.2 and 0.82 for neutron fluence  $5 \times 10^{19}$ n/cm<sup>2</sup>.

### Radiation effect on chemical process

Chemical process of concrete is affected by radiation. Alkali Silica Reaction (ASR) is one of these chemical processes affected by radiation. Experimental results show that irradiated

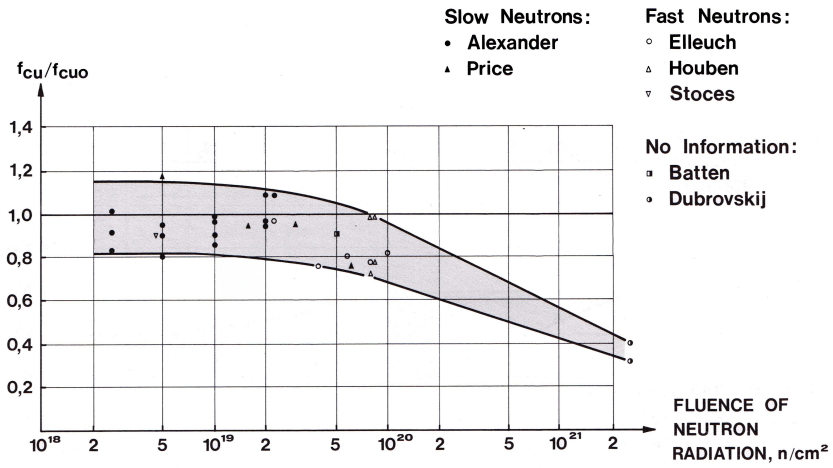


Figure 2.13: Effect of neutron radiation on concrete compressive strength relative to non-irradiated and unheated control specimen results[27]

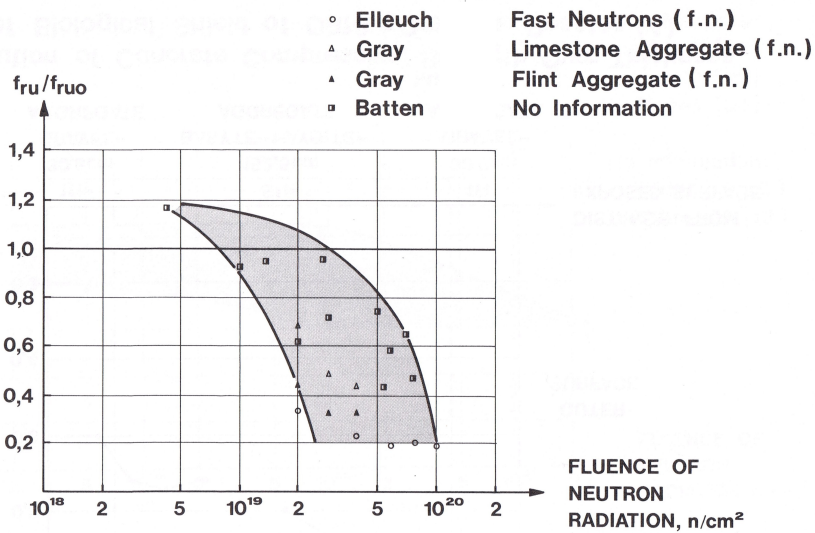


Figure 2.14: Effect of neutron radiation on concrete tensile strength relative to non-irradiated and unheated control specimen results[27]

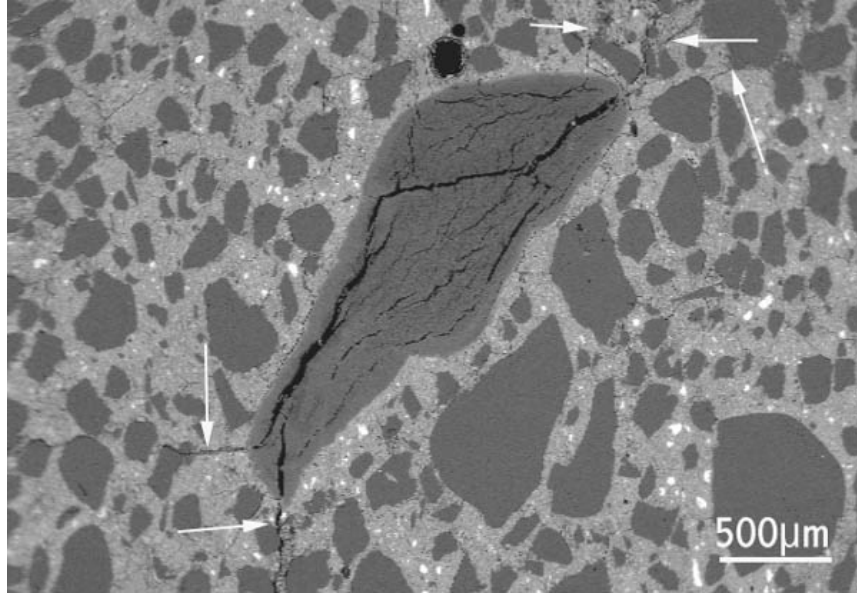
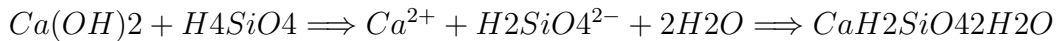


Figure 2.15: Aggregate cracking due to ASR [1]

concrete have affected by ASR harder than non-irradiated concrete [30].

Alkali Silica Reaction is one of the most known types of the chemical deterioration happened in concrete. It is a reaction between silica-rich aggregate and alkaline solution micropore in concrete. Reaction is shown as follows:



At first step, alkali combines with siliceous aggregate to produce alkali silicate gel. Then, as a result of this reaction  $Ca^{2+}$  is released and combines with the gel and hard calcium silicate hydrate is produced. Entered alkali solution transform siliceous minerals into bulky alkali silicate gel. This process produces expansive forces in aggregate. As seen from Figures 2.15 and 2.16, accumulation of these pressures causes micro-structure cracks in concrete and accelerating of these cracks make one of the most considerable deterioration of concrete.

Radiation effect on ASR becomes important in long-time period of NPPs life time. Radiation effect on mortars was reported in 1972 [22]. According to the paper, cracks propagate in specimens badly when radiation exceeds  $10^{20}n/cm^2$  at a temperature of  $125^\circ C$ . Aggregate has an important role in this process. Another important factor in the AAR reaction is chemical composition of cement paste and co-existing aggregate. However, investigations show that irradiation may affect considerably even on carefully selected aggregates [30].

According to the investigation, gamma-rays threshold for affecting concrete is dose of



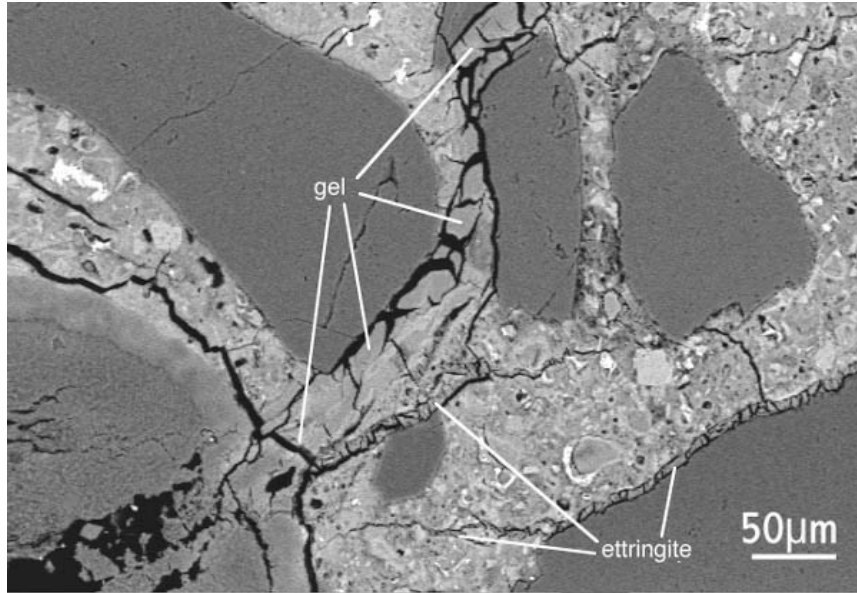


Figure 2.16: Gel generated around aggregates [1]

$10^{10}$  GY and for the fast neutron is around  $10^{19}$  n/cm<sup>2</sup> [30]. For fast neutrons (more than  $10^{19}$  n/cm<sup>2</sup>) considerable deterioration due to the aggregate expansion and the shrinkage of the cement paste is observed. The degree of deterioration depends on the aggregate selection and cement mixture. For example, the expansion at a dose of  $5 \times 10^{19}$  n/cm<sup>2</sup> is about one percent for limestone and flint, and is 0.1 percent for serpentine [30].

Unified absorbed gamma-rays during 60-year life time of a commercial NPP is around  $10^9$  Gy and it is lower than threshold, however, this amount for fast neutrons is close to the critical amount [30].

### 2.5.3 Radiation Limit

There are two concerns for establishing a radiation threshold for RC structures in NPPs. First, the level of radiation that concrete structures are exposed in NPPs during long time is not clear. Second, there is no general agreement on the specific levels of radiation that concrete will be deteriorated. We tries in this study to collect the varieties of data and choose the most reliable ones, which scientists refer to.

## Levels of Radiation for Concrete Structures in NPPs

Primary containment internal structures, biological shields, and spent nuclear fuel storages are three types of structure that may be exposed to the critical levels of radiation. RC structures in NPPs may be exposed to different types of radiation fluxes such as thermal neutron, fast neutron, and gamma radiation. The level of radiation that structures are exposed to is related to the type of reactor and concrete mixture. The radiation fluence during the long term will be achieved by multiplying of constant radiation fluxes and period of time. According to the available data, primary shields may experience neutron radiation fluence beyond  $5 \times 10^{19} \text{n/cm}^2$  [27]. Concrete reactor vessel may be exposed to the thermal neutron, fast neutron, and gamma radiation with the values  $6 \times 10^{19} \text{n/cm}^2$ , 2 to  $3 \times 10^{18} \text{n/cm}^2$  and  $10^{11} \text{rd}$  after 30 years, respectively [28]. The tests from the BEPO reactor by United Kingdom Atomic Energy Authority (UKAEA) show a constant flux around  $3 \times 10^{11} \text{n/cm}^2/\text{s}$ , which is equivalent to the fluence  $3.78 \times 10^{20} \text{n/cm}^2$  after 40 years[56].

It is probable for the closer structures to the reactor core to experience the critical fast neutron radiation levels at the end of their operating life time [30]. However, the new generations of NPPs (1990s) seem to not having the same problem. One of the most recent reactor designs which is available for public is ABWR. The neutron radiation fluence that safety related structures may experience in an ABWR is estimated as  $10^{14} \text{n/cm}^2$ [21]. By reviewing data from 1960s and 1970s decades and comparing them to ABWR design, we can point it out that the past generations of reactors have higher constant fluxes and their concrete structures may experience the critical levels of radiation after 40 years.

## Levels of Radiation That Deteriorate Concrete

The level of radiation that concrete will be damaged considerably is dependent on lots of correlated variables. One of the most challenging problem is that deterioration caused by temperature and radiation can not be easily separated. The measurement of radiation effect on concrete is also very hard because it depends on some factors such as material properties (absorption, scattering), material state of testing, neutron energy spectrum and neutron dose rate [27]. In addition to these complexity, conflicts in some papers show difficulty of not having enough information about radiation fluences, which deteriorate concrete, in NPPs [47].

At the beginning of research (1958) about the radiation effect on concrete properties, investigation of Blosser team showed that chemical properties and density of the graphite reactor shield at Oak Ridge National Laboratory had not changed between investigations done during 8 years. Only compressive strength of the reflector shield had 40 percent decrease. They came to the result that compare to temperature effect, radiation effect on

concrete is ignored [9]. This conclusion was also stated by Engineering Compendium on Radiation Shielding because of the fact that speed of increasing thermal neutron fluences is much more higher than speed of fast neutron fluence increase. For example, 30 years takes time to achieve a fluence of  $10^{21}\text{n/cm}^2$  by a constant flux density of  $10^{12}\text{n/cm}^2/\text{s}$ , however, only hours need to achieve from this flux density to the fluence that temperature increases four times [34].

The effect of radiation was not considered seriously compared to the temperature effect till the year 1978. As shown in Figures 2.13, and 2.14, the investigation that separated effect of temperature and radiation showed a radiation range between  $2 \times 10^{19}\text{n/cm}^2$  and  $2 \times 10^{21}\text{n/cm}^2$  that the mechanical properties of concrete is significantly affected by radiation directly.

The concrete deterioration due to radiation is not only for the primary containment and shields. There are limited number of experiments from fuel storage canals, radwaste building, and spent nuclear fuel that show concrete strength reduction due to radiation. For example, the tests on material of reactor fuel storage canal at Idaho National Engineering and Environmental Laboratory (INEEL) showed 50 % decrease of concrete strength for gamma irradiation of  $2^{11}\text{R/hr}$  [58].

### **Radiation Thresholds for Aging NPPs**

All disagreement in this area results to having different radiation threshold for different codes. Here are limitations set by American and European standards for radiation exposure in 1960s, 1970s and 1980s to reduce risk of the radiation degradation in shielding concrete.

1. American Society of Mechanical Engineers (ASME) pressure Vessel and Piping Code (section III, division 2) chooses threshold for neutron exposure at  $10^{21}\text{n/cm}^2(nvt)$ .
2. The British Specification for Prestressed concrete Pressure Vessels for Nuclear Reactors says that for radiation fluence less than  $5 \times 10^{19}\text{n/cm}^2$  effect of radiation on concrete properties is not considerable [32]
3. According to American National Standard Institute ANSI, compressive strength and modulus of elasticity are degraded for exposure more than  $10^{19}\text{n/cm}^2$ .

# Chapter 3

## Analytical Procedure

In order to investigate the radiation deterioration, we need to have appropriate understanding of the location of structures exposed to the critical level of radiation. These structures are usually located on the interior layers of NPPs. As it will be explained further, the primary containment is the border of radiation protection in NPPs. There are usually two types of RC walls: shell and box walls. Appropriate representative Reinforced Concrete (RC) elements chose to analyze. Geometry, material properties, and loading conditions of the elements chose based on the existing Nuclear Power Plants (NPPs). Degradation factors, which represent the critical levels of radiation, are selected based on the experimental results from literature.

### 3.1 Membrane Elements Studied in This Study

RC membrane elements are chosen to study the effects of the radiation degradation on RC structures in NPPs. RC structures in NPPs are mostly RC walls, so membrane elements are appropriate representative elements for the whole structures. The RC panels studied in this research are selected in the way that can represent actual properties of the elements in NPPs, which are exposed to high levels of radiation. Discussions on the selection of the RC panel properties are described in Section 3.3.

There are four types of RC panels: R1, R2, R3, and R4. The general form of the RC panels is shown in Figure 3.1. Details of the membrane elements are explained in the following section.

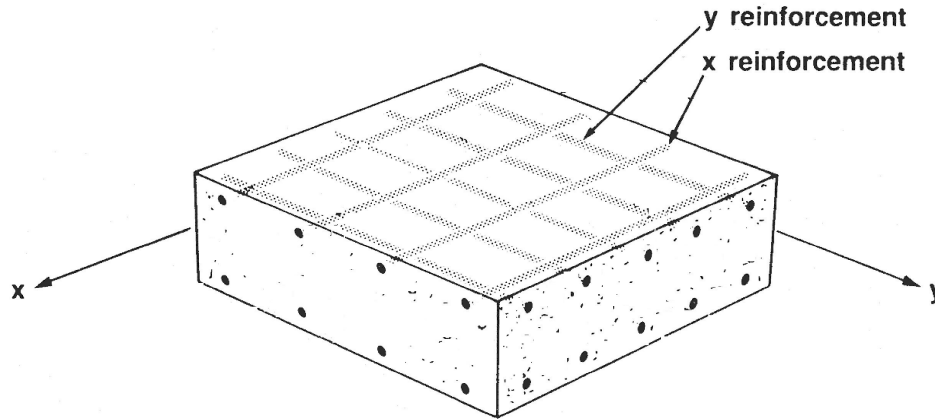


Figure 3.1: General form of the RC panels are analyzed in this study

### 3.1.1 Geometry Properties

The geometry properties of the RC panels can be divided into two categories: cross section and reinforcing steel geometry properties. For the cross sections of the elements, dimensions of the element are important. The RC panels have rectangular cross section  $l \times t$ , in which  $l$  and  $t$  are length and thickness of the elements respectively. The analysis that is done in this study is on shear stress-strain relationship of the elements. Elements have unit length since stress-strain relationships are dimension independent. Concrete thickness of the elements is the only cross section geometry property that will be asked for the numerical solution, which is explained in Section 3.2. The concrete thickness value of  $380 \text{ mm}$  is assumed for all the elements.

Geometry properties of the reinforcing steel include reinforcement ratio in  $x$  and  $y$  directions, bars diameters, and steel layout. Elements R1, R2, R3, and R4 can be distinguished by their reinforcement ratios  $\rho$ . The elements have the same amount of reinforcement ratio  $\rho$  in  $x$  and  $y$  direction. The values of  $\rho_x$  and  $\rho_y$  are equal to 0.9, 1.35, 1.88, and 3 % for the elements R1, R2, R3, and R4, respectively. Reinforcement ratios are chosen from different locations of RC walls in NPPs, which are exposed to high levels of radiation. Bar diameter is selected as JD 29 based on the actual bar diameter in RC walls in NPPs. The reinforcing steel is distributed into the two layers at bottom and top of the cross section in  $x$  and  $y$  directions. The steel distribution of the element R1 is shown in Figure 3.2 as an example. Distance of the bottom layer of steel to the top and bottom level ( $d$  and  $c$ ) of the cross section is  $x$  and  $y$  direction is kept constant for all of the elements. So, distance between the bars  $a$  will change by changing the reinforcement ratio of the elements. The details of

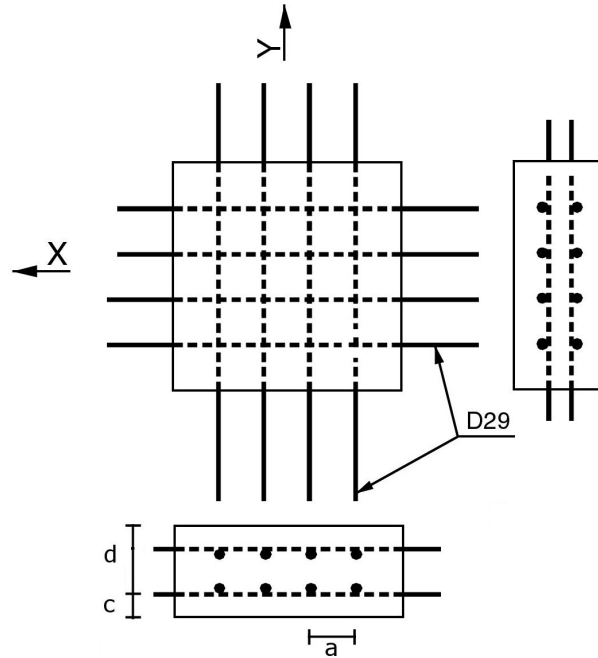


Figure 3.2: Specimens series R details

the steel distribution are available in Table 3.1 for the elements R1, R2, R3, and R4.

### 3.1.2 Material Properties

Material properties of RC panels are divided into concrete and reinforcing steel properties. As shown in Table 3.2, mechanical properties of concrete, such as compressive and tensile strength, will be entered in our analysis. Concrete compressive strength  $f'_c$  is chosen as  $27.6 \text{ MPa}$  ( $4000 \text{ PSI}$ ) for all of the elements. The value of  $f'_c$  is selected based on the data available from shielding structures in existing NPPs (Section 3.3). Tensile strength, compressive, and tensile stress-strain of concrete are chosen using the analysis method explained in Section 3.2. Reinforcing steel used for the RC panels is the standard steel ASTM A-615 grade 60. The yielding strength of the reinforcing steel is  $414 \text{ MPa}$  which satisfy the maximum yielding strength of the the code ACI-349 for safety-related RC structures in NPPs ( $415 \text{ MPa}$ ). The reinforcing steel properties such as the elastic modulus, strain hardening, rupture strain, and ultimate strain are available in Section 3.2.

Table 3.1: Steel distribution of the elements R1, R2, R3, and R4

Element	$\rho_x = \rho_y$ %	Bar Diameter <i>mm</i>	Bar Area <i>mm</i> <sup>2</sup>	$d_x^a$ <i>mm</i>	$c_x^b$ <i>mm</i>	$d_y^a$ <i>mm</i>	$c_y^b$ <i>mm</i>	$a_x^c = a_y^c$ <i>mm</i>
R1	0.9	28.6	642	284	96	252	128	375
R2	1.35	28.6	642	284	96	252	128	250
R3	1.88	28.6	642	284	96	252	128	180
R4	3	28.6	642	284	96	252	128	113

<sup>a</sup>  $d_x$  and  $d_y$  are distance of the bottom layer to the top of the cross section in  $x$  and  $y$  direction shown in Figure 3.2

<sup>b</sup>  $c_x$  and  $c_y$  are distance of the bottom layer to the bottom of the cross section in  $x$  and  $y$  direction

<sup>c</sup>  $a_x$  and  $a_y$  are distance between the reinforcing steel in  $x$  and  $y$  direction

Table 3.2: Material properties of the elements R1, R2, R3, and R4

Element	Concrete			Reinforcing Steel
	Compressive strength $f'_c$ ( <i>MPa</i> )	Tensile Strength $f_t$ ( <i>MPa</i> )	$a_g^b$ ( <i>mm</i> )	Yielding Strength $f_y$ ( <i>MPa</i> )
$R_i^a$	27.6 (4000 <i>psi</i> )	1.7 (247 <i>psi</i> )	25	414 (60,000 <i>psi</i> )

<sup>a</sup>  $R_i$  represents R1, R2, R3, and R4.

<sup>b</sup>  $a_g$  is maximum aggregate size used in the concrete mix design.

### 3.1.3 Degradation Factors

Three critical levels of radiation are assumed degradation levels 1, 2, and 3 (D1, D2, and D3). Each degradation level represents two issues: fast neutron fluence, which the RC panels are exposed to, and strength reduction values corresponding to the neutron fluences. Firstly, high levels of fast neutron radiation that concrete may experience in a NPP is studied for the each level of degradation. As explained in Section 2.5.3, fast neutron radiation fluences are achieved by concrete during long time. The neutron fluences are calculated by multiplying time to the constant fast neutron fluxes. The constant neutron fluxes mentioned in the literature varied between  $3 \times 10^{10}\text{n/cm}^2$  and  $3 \times 10^{12}\text{n/cm}^2$ . Constant fast neutron fluxes  $3 \times 10^{10}\text{n/cm}^2$  and  $3 \times 10^{11}\text{n/cm}^2$  can produce fast neutron fluences  $3.78 \times 10^{19}\text{n/cm}^2$  and  $3.78 \times 10^{21}\text{n/cm}^2$  after 40 years in the NPP, which are close to thresholds provided by American and European codes.

Second consideration for the each level of degradation is amount of deterioration that the neutron fluences will produce. Neutron fluences assumed for this study are the critical radiation levels that deteriorate concrete significantly. As shown in Table 2.14, compressive strength of concrete will be reduced by the fast neutron fluences  $2 \times 10^{19}\text{n/cm}^2$ ,  $2 \times 10^{20}\text{n/cm}^2$ , and  $2 \times 10^{20}\text{n/cm}^2$  by the average values 95, 72, and 40 %. As mentioned in Section 2.5.2, tensile strength of concrete also reduces from 20 to 80 % for the radiation level  $5 \times 10^{19}\text{n/cm}^2$ .

Table 3.3 shows that the RC panels studied in this thesis are exposed to degradation levels D1, D2, and D3 with the compressive strength reduction values equal to the average of the ranges shown in Table 2.14. Degradation levels are shown in Figures 3.3 and 3.4. Three tensile strength reduction factors are assumed for the degradation levels D1, D2, and D3 which coincide with the lower, average and upper bounds of the reduction range between 20 to 80 %. Undegraded elements are also examined to compare the results of the degraded elements.

### 3.1.4 Loading Scenarios

The RC panels analyzed in this research are under 6 different loading scenarios numerated bellow:

1. Pure shear
2. Shear plus biaxial tension
3. Shear plus biaxial compression
4. Shear plus biaxial tension-compression



Table 3.3: Degradation levels assumed in this study based on the critical radiation levels in NPPs

Degradation Level	Neutron Flux n/cm <sup>2</sup> /s	Neutron Fluence <sup>a</sup> n/cm <sup>2</sup>	Compressive Strength Reduction %	Tensile Strength Reduction %
U <sup>a</sup>	0	0	0	0
D1	$1.58 \times 10^{10}$	$2 \times 10^{19}$	0.95	0.8
D2	$1.58 \times 10^{11}$	$2 \times 10^{20}$	0.725	0.5
D3	$1.58 \times 10^{12}$	$2 \times 10^{21}$	0.4	0.2

<sup>a</sup> U represents the undegraded level

<sup>b</sup> A neutron fluence is accumulative radiation of a constant neutron flux after 40 years

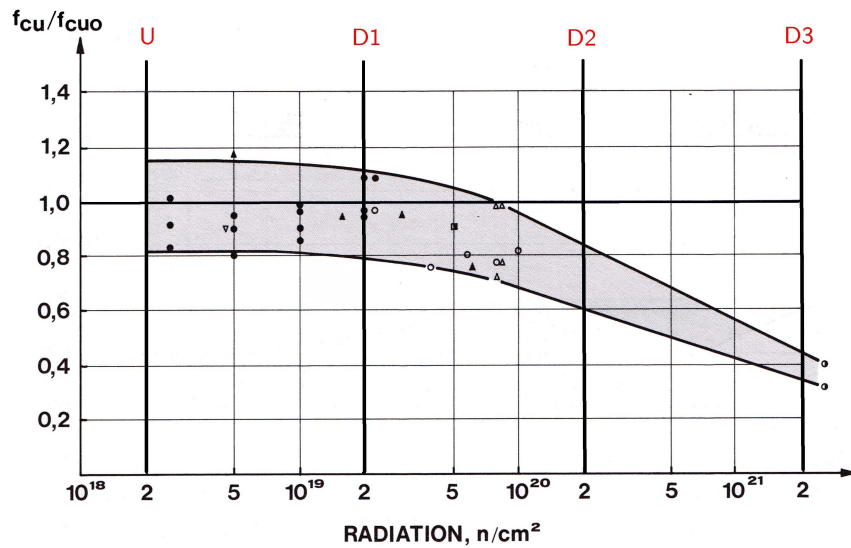


Figure 3.3: Degradation levels 1, 2, and 3 are assumed for the degradation factors of compressive strength in the analysis of the RC panels

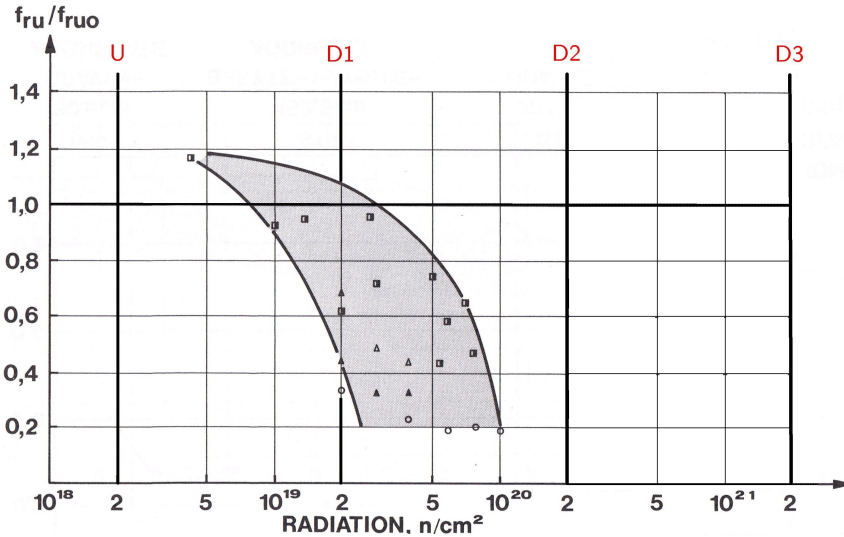


Figure 3.4: Degradation levels 1, 2, and 3 are assumed for the degradation factors of tensile strength in the analysis of the RC panels

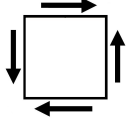
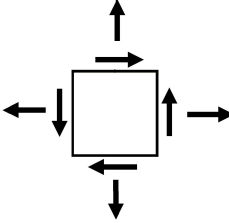
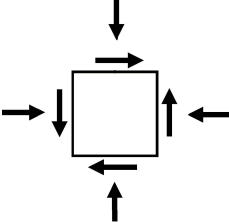
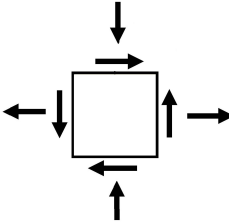
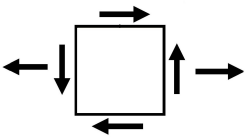
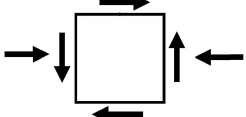
5. Shear plus uniaxial tension
6. Shear plus uniaxial compression

Loading conditions are chosen based on the most probable conditions that RC panels exposed to high levels of radiation may experience. It has been noticed that compressive strength reduction as a result of radiation degradation is a serious problem for shear capacity rather than flexural capacity of the RC members. Hence, shear strength of the RC panels are analyzed for degradation levels U, D1, D2, and D3. As it will be fully explained in Section 3.3.4, loading scenarios can be distinguished by two variables: ratio of axial loads in  $x$  and  $y$  direction  $\frac{f_x}{f_y}$  and ratio of shear to axial load  $\frac{v_{xy}}{f_x}$ . Different loading conditions and assumed loading ratios, used in this study, are shown in Table 3.4.

## 3.2 Analytical Method Used in This Study

RC structures such as offshore oil platforms, nuclear containment structures and their internal structures show a very complex behavior under extreme loading conditions. At the same time, high levels of safety should be provided for these types of structures regarding

Table 3.4: Loading conditions that are studied in this research

Loading Category	Element	$\frac{f_x}{f_y}$	$\frac{v_{xy}}{f_x}$	$f_x : f_y : v_{xy}$	Loading Pattern
Pure shear	$PRi^a - L001$	-	-	0:0:1	
Shear-biaxial tension	$BTRi - L111$	1	1	1:1:1	
	$BTRi - L112$	1	2	1:1:2	
	$BTRi - L114$	1	4	1:1:4	
Shear-biaxial tension	$BCRi - L111$	1	-1	-1:-1:1	
	$BCRi - L112$	1	-2	-1:-1:2	
	$BCRi - L114$	1	-4	-1:-1:4	
Shear-biaxial tension-compression	$BTCRi - L111$	-1	-1	1:-1:1	
	$BTCRi - L112$	-1	-2	1:-1:2	
	$BTCRi - L114$	-1	-4	1:-1:4	
Shear-uni-axial tension	$UTRi - L101$	-	1	1:0:1	
	$UTRi - L102$	-	2	1:0:2	
	$UTRi - L104$	-	4	1:0:4	
Shear-uni-axial compression	$UCRi - L101$	-	-1	-1:0:1	
	$UCRi - L102$	-	-2	-1:0:2	
	$UCRi - L104$	-	-4	-1:0:4	

<sup>a</sup>  $R_i$  represents elements R1, R2, R3, and R4.

to human and environment health. Hence, scientists have worked for more than a century to establish appropriate theories to formulate behavior of these structures. These theories are based on scale models that can be generalized to the whole structures. Membrane elements can be analyzed as a scale model for RC walls in NPPs.

Shear design and analysis of RC structures in NPPs, which are mostly wall type, is a challenging issue. Effect of irradiation is more considerable on shear design of such complex structures. So, it is important to find an appropriate theory that can properly illustrate behavior of membrane elements under specific loading conditions. As explained in the following section, the Modified Compression Field Theory (MCFT) is one of the best ones for this purpose.

Membrane-2000 is a nonlinear finite element method that uses MCFT to analyze RC panels under different loading scenarios. The procedure of the computation will be fully explained in this section. Primary element details will be completed during the analysis with Membrane-2000. Geometrical and material properties need to be defined for RC panels completely by using Membrane-2000. Different options for the element properties are also available in the following sections.

### 3.2.1 The Modified Compression Field Theory(MCFT)

The MCFT is developed in 1982 by Vecchio's experimental results of 30 RC panels under different combination of shear and normal stresses. The theory is based on the Compression Field Theory [43] [14]. The most important difference between CFT and MCFT is considering tensile potential of concrete between cracks in calculations. The theory is published in American Concrete Institute journal in 1986 by Vecchio and Mitchell [63]. The final form was completed by two small changes in 1987 [13]. MCFT is a sectional analysis that can be a rational one for the conventional flexure analysis specially for RC elements subjected to shear as well as compression and tension. The first core of the theory is developed from membrane elements which can be found in complex structures in Figure 3.5. A more complete example can be seen in Figure 3.6

MCFT is a theory that consider cracked RC members as new material with new stress-strain relationship based on the average stress and average strain. As shown in Figure 3.8, for having average stress and average strain, section should have been cracked. The most critical part of the theory is checking compatibility between average and real stresses in a cracked RC member same as all theories, MCFT has its own constitutive equations that satisfy equilibrium and compatibility conditions shown in Figure 3.7. Constitutive modeling of MCFT needs theoretical relationships based on Mohr's circle for stress and strain separately. Experimental work should also be conducted for finding empirical equations that complete the model by giving the stress-strain relationship.

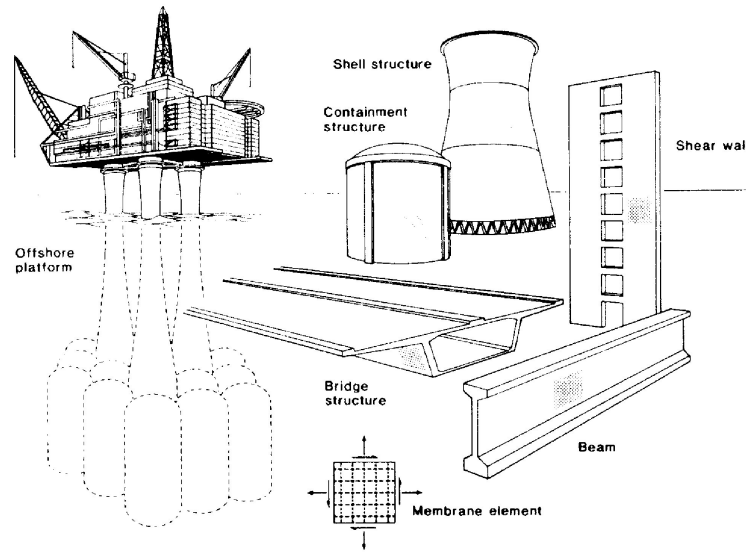


Figure 3.5: Structures include membrane elements[63]

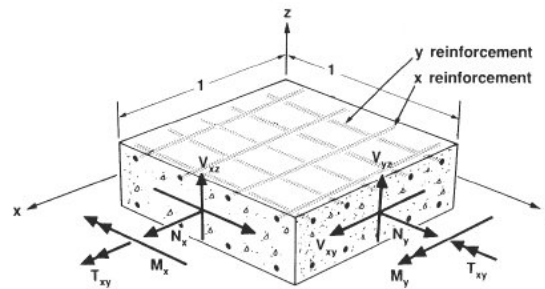


Figure 3.6: Reinforced concrete panel with complete loading scenario[16]

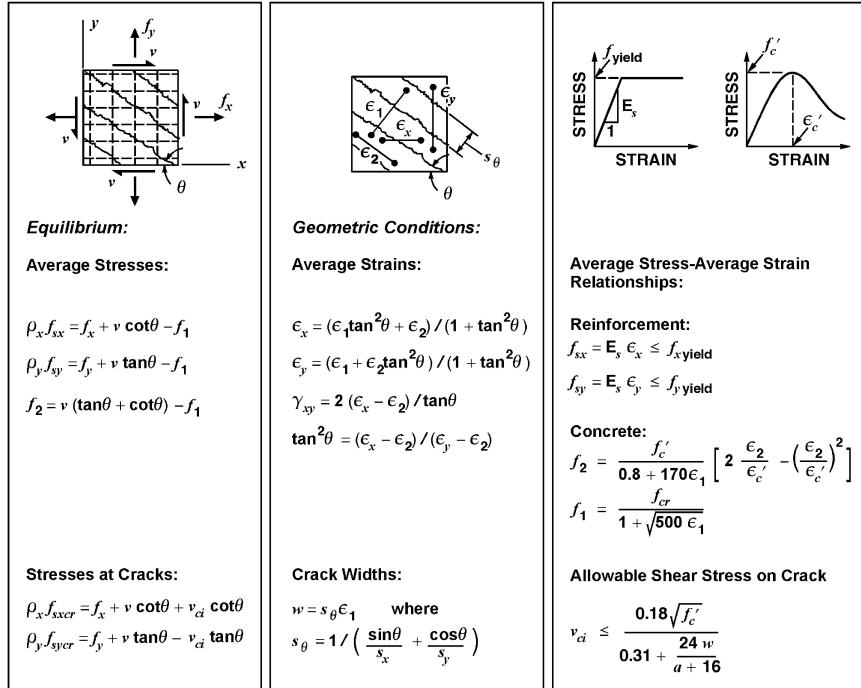


Figure 3.7: Constitutive equations of the MCFT[63]

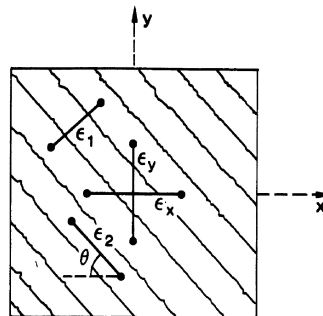


Figure 3.8: Average strain in a cracked membrane element[63]

## Theoretical Part

Compatibility and equilibrium conditions of the elements are studied the elements in theoretical part to build average-principal strain and average-principal stress relationships respectively in this part.

The first important assumption regarding to compatibility is having the same strain for concrete, reinforcing steel and reinforced concrete ( $\epsilon_{sx} = \epsilon_{cx} = \epsilon_x$  and  $\epsilon_{sy} = \epsilon_{cy} = \epsilon_y$ ). In this stage, relationship between average strains ( $\epsilon_x, \epsilon_y$  and  $\gamma_{xy}$ ) and principal strains ( $\epsilon_1$  and  $\epsilon_2$ ) are built by strain Mohr's circle. Equations 3.1, 3.2, and 3.3 are used later for calculating principal strain of the elements from experimentally measured average strain.

$$\gamma_{xy} = \frac{2(\epsilon_x - \epsilon_2)}{\tan \theta} \quad (3.1)$$

$$\epsilon_x + \epsilon_y = \epsilon_1 + \epsilon_2 \quad (3.2)$$

$$\tan^2 \theta = \frac{\epsilon_x - \epsilon_2}{\epsilon_y - \epsilon_2} = \frac{\epsilon_1 - \epsilon_y}{\epsilon_1 - \epsilon_x} = \frac{\epsilon_1 - \epsilon_y}{\epsilon_y - \epsilon_2} = \frac{\epsilon_x - \epsilon_2}{\epsilon_1 - \epsilon_x} \quad (3.3)$$

Stresses in the element should follow equilibrium conditions for all sections as well. Figure 3.9 shows equilibrium conditions for stresses for a section on a membrane element in y direction and the same formula cab be derived for x direction. There are two basic assumptions to get Equations 3.5, 3.6 and 3.7; continuous concrete cross section by ignoring the area of bars and no shear resistance by reinforcing steel in Equation 3.4 ( $\nu_{sx} = \nu_{sy} = 0$ ).

$$\nu_{xy} = \nu_{cx} + \rho_{sx} \cdot \nu_{sx} = \nu_{cy} + \rho_{sy} \nu_{sy} \quad (3.4)$$

$$f_x = f_{cx} + \rho_{sx} \cdot f_{sx} \quad (3.5)$$

$$f_y = f_{cy} + \rho_{sy} \cdot f_{sy} \quad (3.6)$$

$$\nu_{xy} = \nu_{cx} = \nu_{cy} \quad (3.7)$$

Average and principal stress relationship is computed by Equations 3.8, 3.9 and 3.10 Using Mohr's circle for concrete stress that is shown in Figure 3.10

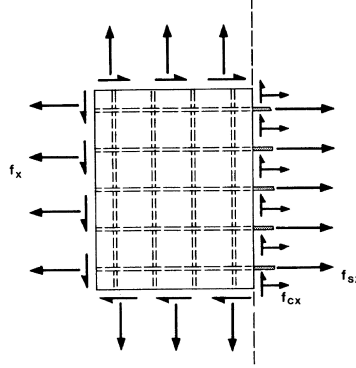


Figure 3.9: Equilibrium conditions in  $x$  direction [63]

$$f_{cx} = f_{c1} - \frac{\nu_{cxy}}{\tan \theta_c} \quad (3.8)$$

$$f_{cy} = f_{c1} - \nu_{cxy} \cdot \tan \theta_c \quad (3.9)$$

$$f_{c2} = f_{c1} - \nu_{cxy} \cdot \left( \tan \theta_c + \frac{1}{\tan \theta_c} \right) \quad (3.10)$$

### Experimental Part

There are three assumptions that are numerated bellow in this part:

1.  $f_{sx} = E_s \cdot \epsilon_x \lesssim f_{yx}$
2.  $f_{sy} = E_s \cdot \epsilon_y \lesssim f_{xy}$
3.  $\theta_c = \theta$

Assumptions number 1 and 2 are because of assuming the bilinear uniaxial stress-strain relationship for the reinforcing steel. Assumption 3 means the principal stress and principal strain direction is coincided.

Thirty RC panels subjected to pure shear, shear and biaxial compression or tension and shear with uniaxial compression and tension were examined by Vecchio in 1982 to derive tensile and compressive stress-strain relationship of concrete for completing MCFT.



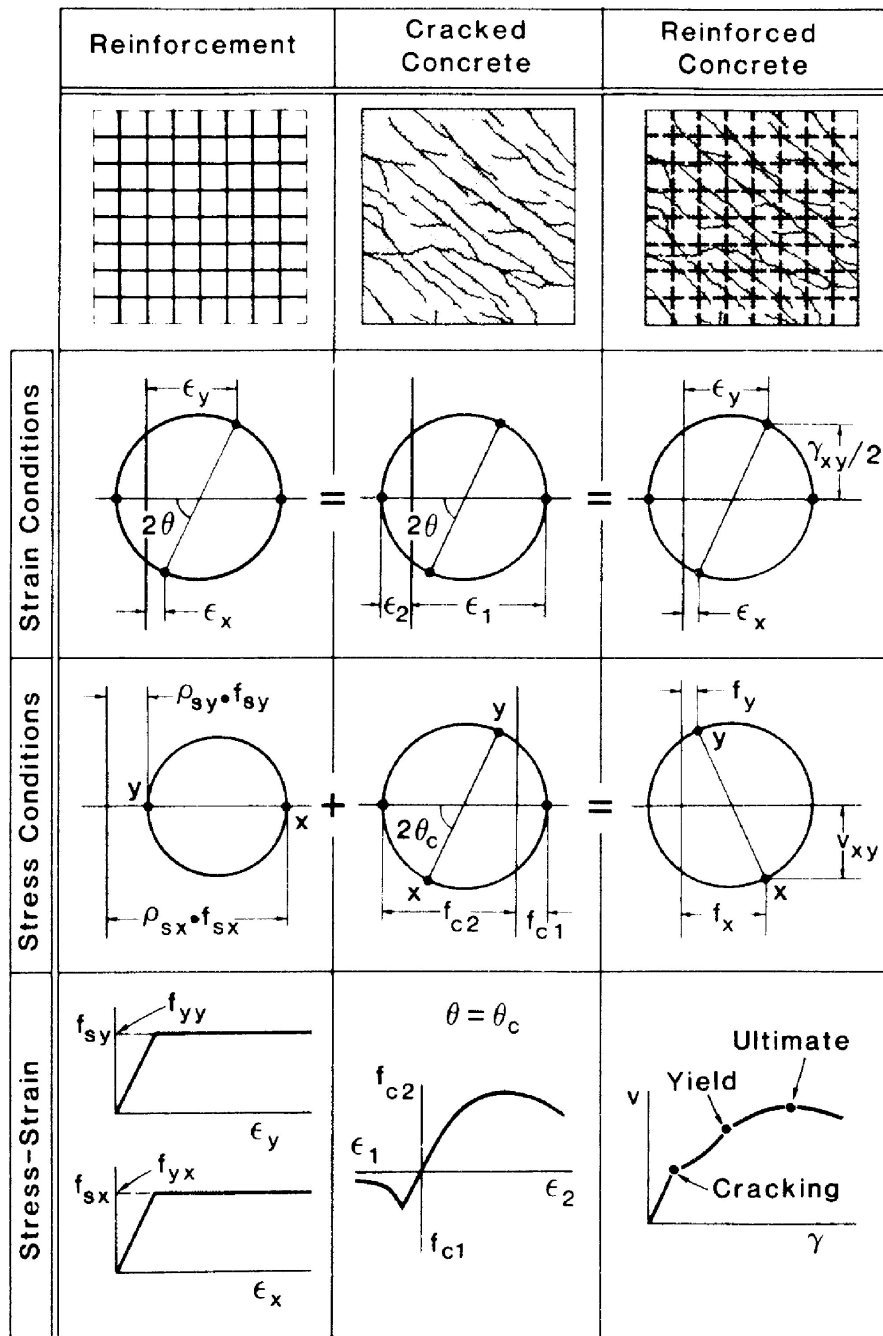


Figure 3.10: Stress and strain condition for the modified compression field theory for membrane elements [63]

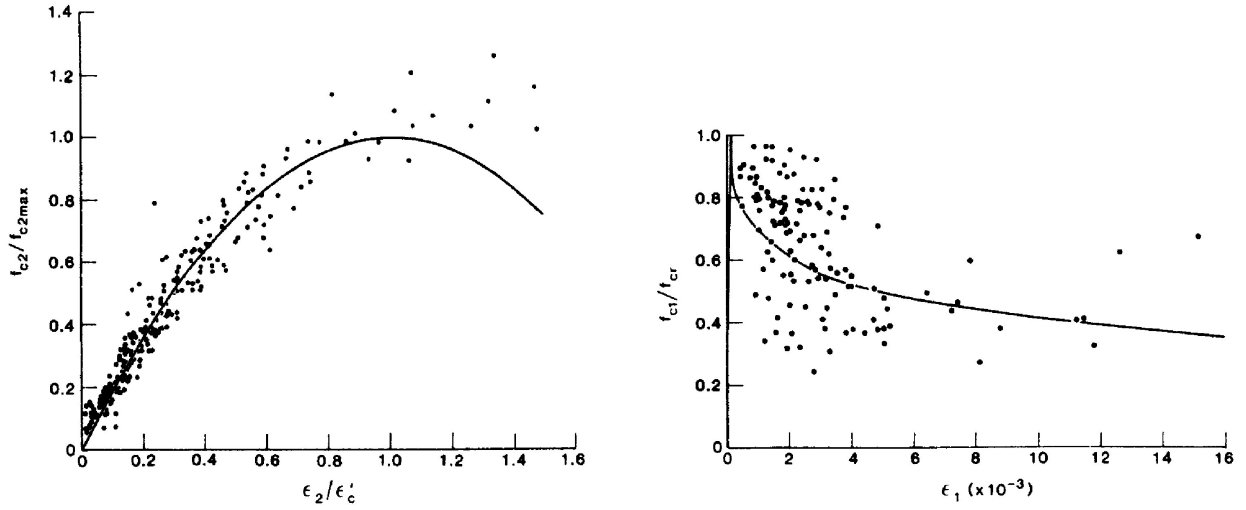


Figure 3.11: Empirical stress-strain relationship[63]

Experimental details are available in reference [62]. Stresses applied to the elements ( $f_x$ ,  $f_y$  and  $v_{xy}$ ) and strains due to stresses ( $\epsilon_x$ ,  $\epsilon_y$  and  $\gamma_{xy}$ ) are measured by equipments.

$f_{c1}$ , and  $f_{c2}$  are calculating from  $\epsilon_x$ ,  $\epsilon_y$  and  $\gamma_{xy}$  by the steps numerated bellow:

1. Known  $\epsilon_x$ ,  $\epsilon_y$  and  $\gamma_{xy}$   $\rightarrow$  using standard reinforcement stress-strain relationship  $\rightarrow f_{sx}$  and  $f_{sy}$  are known
2. Using Equations 3.5 and 3.6  $\rightarrow f_{cx}$  and  $f_{cy}$  are known
3. using Equations 3.8 and 3.9  $\rightarrow f_{c1}$  is known
4. Using Equation 3.10  $\rightarrow f_{c2}$  is known

In this step,  $\epsilon_1$ ,  $\epsilon_2$ ,  $\epsilon_x$ , and  $\epsilon_y$  are known. Next step is finding relationship between stress and strain from the correlating data shown in Figure 3.11.

Vecchio suggested Equations 3.11 and 3.12 for concrete compressive and Equation 3.13 for tensile stress-strain relationships before cracking ( $\epsilon_1 \lesssim \epsilon_{cr}$ ) and Equation 3.15 for after cracking (tension stiffening). Coefficient 200 for the tension stiffening changed to 500 in 1987 by examining of larger elements that is done by Collins and Mitchel [16]. Bentz also introduced Equations 3.16 and 3.17 by replacing coefficient with term  $3.6m$  in 1998

to show the importance of considering the effect of bond between steel and concrete for tension stiffening [7].

$$f_{c2} = \left( \frac{1}{.8 - .34 \frac{\epsilon_1}{\epsilon_c}} \right) \cdot \left( 2 \frac{\epsilon_2}{\epsilon_c} - \left( \frac{\epsilon_2}{\epsilon_c} \right)^2 \right) \quad (3.11)$$

$$\frac{f_{c2max}}{f'_c} = \frac{1}{.8 - .34 \frac{\epsilon_1}{\epsilon_c}} \lesssim 1.0 \quad (3.12)$$

$$f_{c1} = E_c \cdot \epsilon_1 \quad (3.13)$$

$$f_{cr} = 0.33 \sqrt{f'_c} \quad (3.14)$$

$$f_{c1} = \frac{f_{cr}}{1 + \sqrt{500 \epsilon_1}} \quad (3.15)$$

$$f_{c1} = \frac{f_{cr}}{1 + \sqrt{3.6 m \epsilon_1}} \quad (3.16)$$

$$m = \frac{A_c}{\Sigma d_b \pi} \quad (3.17)$$

## Crack Check

The most important part of the theory is checking the concrete tensile stress ( $f_2$ ) to be sure that equilibrium conditions are satisfied at a crack and the tensile stress is transferred by concrete between cracks. MCFT is using the bare-bar stress strain relationship for reinforcing steel. So, the tensile stress transmission should be check at crack location. Neglecting crack check included in MCFT showed more than 30 % non conservative results [29]. Crack check provided by MCFT in 1986 is explained in a simple example by Collins in 1998 [15] and illustrated with details for 1D, 2D, and 3D nodes by Bentz [5]. We are going to briefly explain 2D crack check that is used in Membrane-2000.

Two checks should be done for a membrane element (an orthogonally RC panel subjected to biaxial and shear loading). First check is for ensuring that the steel stress of bare bars at the crack in  $x$  and  $y$  directions ( $f_{sxcr}$  and  $f_{sy cr}$ ) never exceed yield stresses of bare bars ( $f_{yx}$  and  $f_{yy}$ ). Second check is provided to be ensure that the shear stress on crack for yielding in both directions is not more than the allowable shear stress based on the crack width ( $v_{ci} = \text{minimum}(v_{cimax1} \text{ and } v_{cimax2})$ ). These checks will be provided by

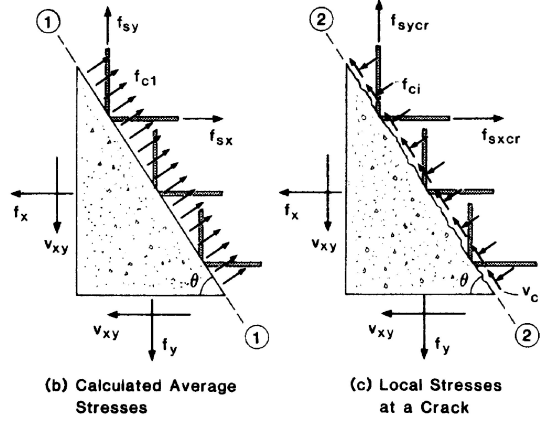


Figure 3.12: Comparison of local stresses at a crack with calculated average stresses[63]

minimizing the value of principal tension of the element by getting the minimum value of four different tensions calculating from tensile stress due to material properties ( $f_{1a}$ ), the maximum allowed tensile stress without shear on the crack ( $f_{1b}$ ) and the maximum allowed tensile stress from  $x$  and  $y$  directions with shear on crack ( $f_{1c}$  and  $f_{1d}$ ).

$f_{1a}$  could be calculated by Equations 3.15 or 3.16 or other tension stiffening allowed in Membrane-2000 like Izumo, Tamai and elasto-plastic [59] and [33].  $f_{1b}$  is calculated by considering no shear force on the crack by using the following equation:

$f_{1b} = f_{1cx} \cos^2 \theta + f_{1cy} \sin^2 \theta$  where,  $f_{1cx} = \rho_x (f_{yx} - f_{sx})$   $f_{1cy} = \rho_y (f_{yy} - f_{sy})$  The last two checking is provided to be sure that elements are in equilibrium conditions on crack. Figure 3.12 shows stresses in a cracked plane and uncracked plane in a cracked RC panel. Regarding to equilibrium conditions, Equations 3.18 and 3.19 can be derived for  $x$  and  $y$  directions respectively when  $f'_{ci}$  assumed to be zero.

$$f_{sx} \rho_x \sin \theta + f_{c1} \cos(90 - \theta) = v_{ci} \cos \theta + f_{sxcr} \rho_x \sin \theta \quad (3.18)$$

$$f_{sy} \rho_x \cos \theta + f_{c1} \sin(90 - \theta) = v_{ci} \sin \theta + f_{sxcr} \rho_x \cos \theta \quad (3.19)$$

$f_{1c}$  and  $f_{1d}$  are calculated from equations above in the form of Equations 3.20 and 3.21

$$f_{1c} = f_{1cx} + \frac{\min(v_{cimax1}, v_{cimax2})}{\tan \theta} \quad (3.20)$$

$$f_{1d} = f_{1cy} + \min(v_{cimax1}, v_{cimax2}) \cdot \tan \theta \quad (3.21)$$

$v_{cimax1}$  is shear resistance of the concrete at the crack due to the aggregate interlock. It is calculated from an empirical equation obtained from Walravens experimental work by Equation 3.22.

$$v_{cimax1} = \frac{\sqrt{-f'_c}}{0.31 + 24\frac{w}{a+16}} \quad (3.22)$$

Where,  $w$  (crack width) is calculated from the equation bellow and  $a$  is the maximum aggregate size.  $w = \epsilon_1 \cdot S_\theta$   $S_\theta$  calculated from the equation bellow, where  $S_{mx}$  and  $S_{my}$  are the crack spacing limitation by codes in  $x$  and  $y$  direction respectively.

$S_\theta = \frac{1}{\frac{\sin \theta}{S_{mx}} + \frac{\cos \theta}{S_{my}}} v_{cimax2}$  is the shear stress due to the equilibrium available in Equation 3.12. It is calculated by adding Equations 3.20 and 3.21 and considering equal values for  $f_{1c}$  and  $f_{1d}$ .

$$v_{cimax2} = \frac{|f_{1cx} - f_{1cy}|}{\tan \theta + \frac{1}{\tan \theta}} \quad (3.23)$$

Finally, the crack check is done by taking the minimum value of  $f_{1a}$ ,  $f_{1b}$ ,  $f_{1c}$ , and  $f_{1d}$ .

### 3.2.2 Membrane-2000

Membrane-2000 is one of the four nonlinear finite element programs; Membrane-2000, Response-2000, Triax-2000, and Shell-2000 that Dr. Evan Bentz developed based on MCFT in 2000. Response-2000 measures the load-deformation response of RC structural elements like; beams and columns by using MCFT. Triax-2000 is used to understand behavior of a general 3D RC box. Shell-2000 is a complete version of membrane that could analyze plates and shells that are subjected in-plane and out-plane loading that are shown in Figure 3.26.

Membrane-2000 analyzes RC membrane elements subjected to in-plane stresses;  $N_x$ ,  $N_y$ , and  $v_{xy}$ . It is a free program found on the University of Toronto web site [5]. A manual for all the programs is also available online [6].

#### Input Data

Membrane elements define general by quick define tool box that is shown in Figure 3.13. It is divided into three categories; concrete, reinforcing detail in  $x$ , and  $y$  directions. Table 3.5 is an example of one element properties in the quick define. Figure 3.14 is the basic cross section produced by the quick define.

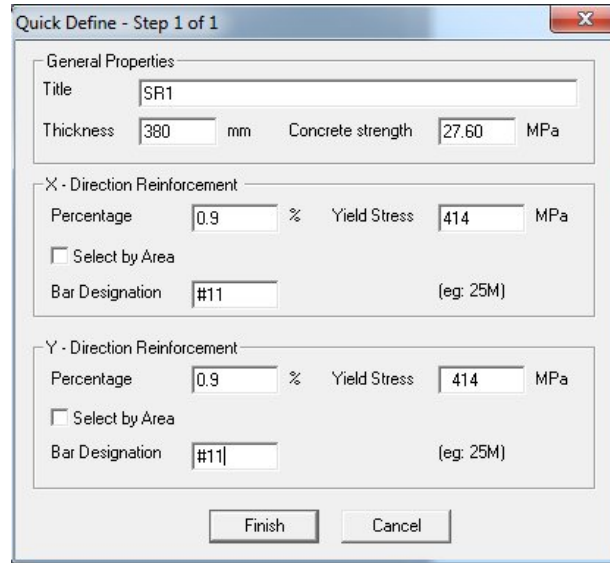


Figure 3.13: Quick define window in Membrane-2000

Table 3.5: Element R1 details

Element	Thickness mm	Compressive Strength <i>MPa</i>	$\rho_x = \rho_y$	$f_{xy} = f_{yy}$ <i>MPa</i>	Bar	Reinforcing Steel
R1	380	27.6	0.9	414	<i>JD 29</i>	<i>ASTM A615 grade 60</i>

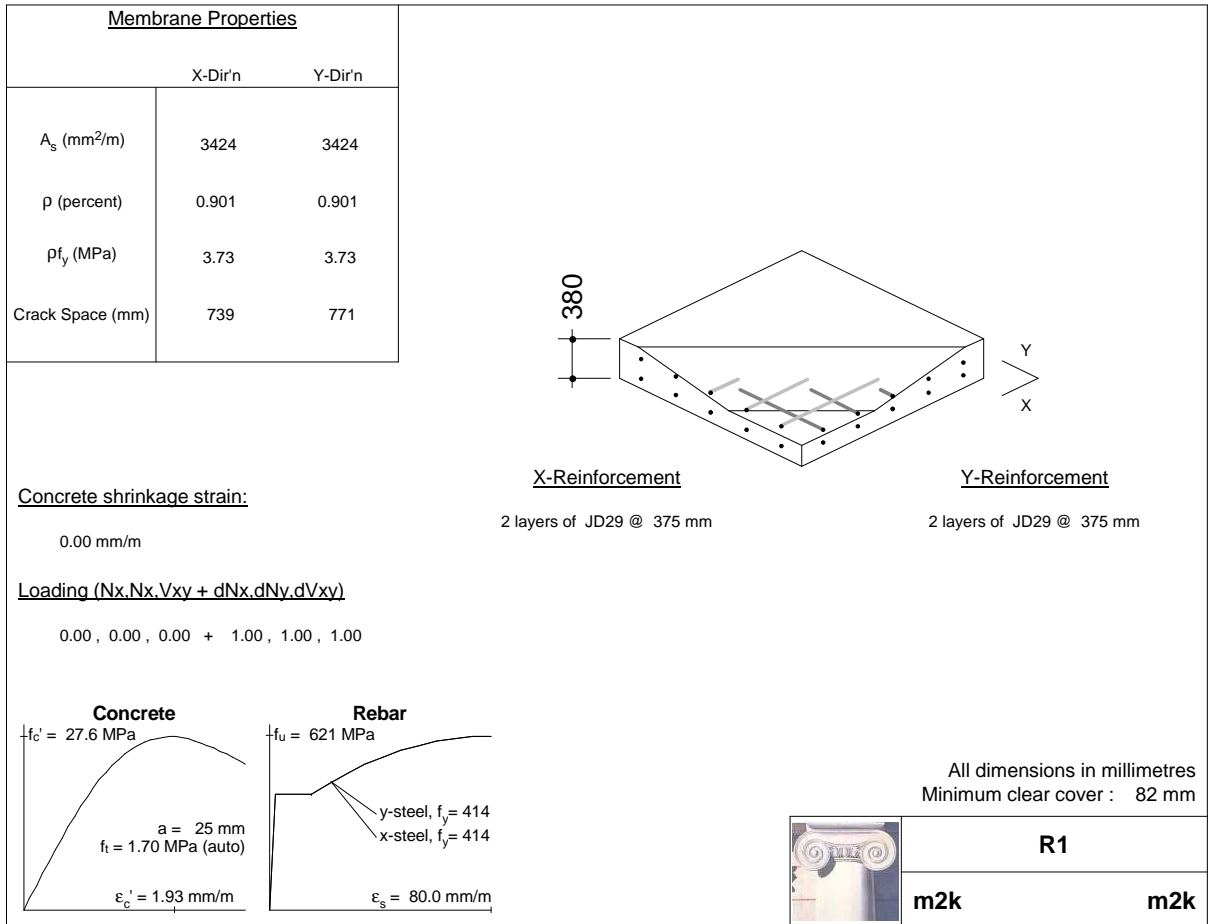


Figure 3.14: Membrane section built by quick define

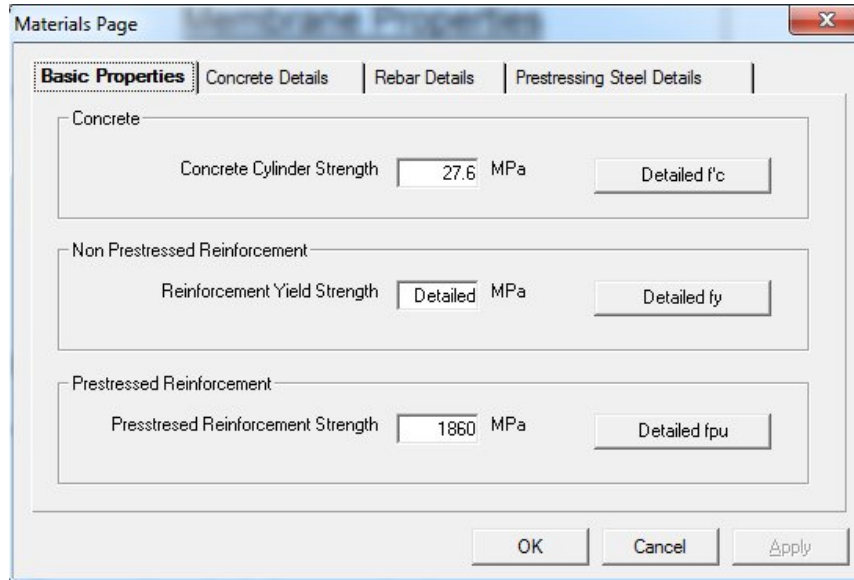


Figure 3.15: Material properties can be defined in Membrane-2000

Material properties of the cross section can be modified in details by using define option in tool box or double clicking in the cross section. Changes are done for the example element in the following sections. By double clicking on the concrete stress-strain curve, Figure 3.15 appears. Then, Concrete, non-prestress steel, and prestressed steel properties in details are available to change.

**Concrete Properties:** Five types of concrete can be defined for sections in Response-2000 and it could be done in the part type list. However, this box does not work for Membrane-2000 and it can get only one type of concrete. So, we had to modify every time when the degradation factor is going to be entered.

Concrete compressive strength is obtained from ABWR design and it is the same as what was in the quick define. The main changes are done for the stress-strain relationship of concrete that are shown in Figures 3.16.

Material properties of concrete can be defined as follow:

1. Cylinder strength ( $f'_c$ ): Compressive strength of cylinder tests during the construction is 27.6 MPa (4000 PSI) in ABWR design.
2. Tension strength ( $f_t$ ): Tension strength is a function of  $f'_c$  that is automatically calculated by default Equation 3.24. It could be also manually entered by users calculated from different equations like ACI shear cracking model that is calculated by Equation 3.25 or other values.



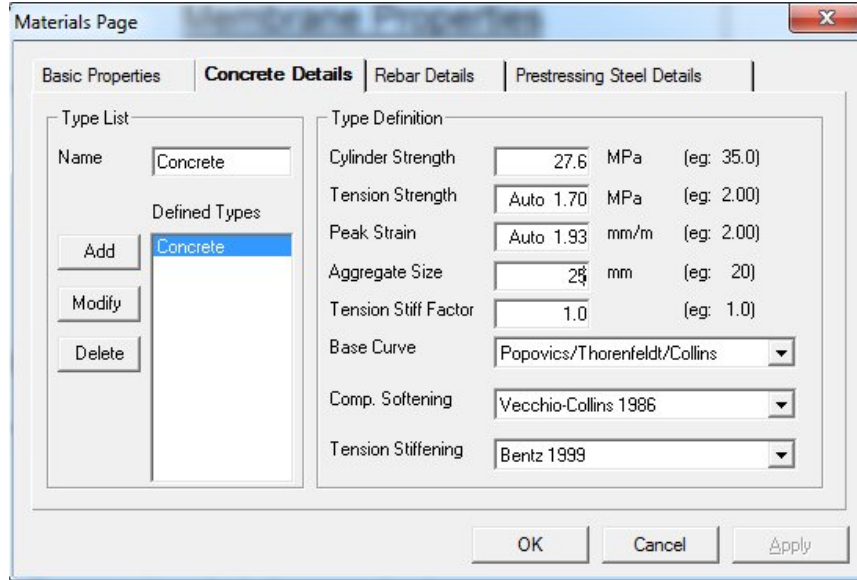


Figure 3.16: Concrete properties can be defined in Membrane-2000

Table 3.6: Peak strain for varieties of  $f'_c$  [16]

$f'_c$ MPa	20.7	24.1	27.6	34.5	41.4	55.2	69.0	82.7	110.0
$\epsilon'_c \times 1000$	1.88	1.91	1.94	2.03	2.13	2.33	2.53	2.71	3.07

$$f_t = 0.45 \times f'_c{}^4 \quad (3.24)$$

$$f_t = 0.33 \times \sqrt{f'_c} \quad (3.25)$$

3. Peak strain ( $\epsilon'_c$ ):  $\epsilon'_c$  is also calculated automatically based on default values available in Table 3.6
4. Aggregate size (a): Maximum aggregate size is 19 mm by default, but 25 mm is chosen according to the Japanese concrete mix design and Standard Specification for Concrete Aggregates (ASTM C33).
5. Tension stiff factor: tension stiff factor ( $ts_{factor}$ ) is related to the tension stiffening and its default value is 1.0 for Membrane-2000.
6. Base curve: There are different empirical stress-strain relationships for concrete in compression: linear, parabolic, Popovics-thorenfeldt-collins, elasto-plastic,

and segmental(user defined curve). Base curve for concrete in NPPs can be linear elastic or bilinear [52]. Popovics-thorenfeldt-collins is the base curve chosen for the elements in this thesis.

7. Compression softening: Post peak behavior of the concrete in compression is called compression softening. It could be calculated by different empirical equations shown in Table 3.7.  $\beta$  in the equation below is the parameter changes for different models.

$$f_{2max} = \beta \cdot f'_c$$

8. Tension stiffening: Tensile stress-strain curve of concrete after cracking is known as tension stiffening part. Usually this part is ignored for RC structures in NPPs. However, MCFT counts tensile strength of concrete between cracks and has a crack check for this contribution. Empirical equations for tension stiffening that Membrane-2000 can consider is available in Table 3.8.

**Reinforcing Steel Properties:** Reinforcing steel properties are modified in the window that is shown in Figure 3.17. Rebar details can be entered by the custom type of the reinforcing steel or standard groups of reinforcement in Membrane-2000 that are available in Table 3.9.  $E_s$  has default value  $2 \times 10^5$  MPa for all types of steel and it is very close to the limit of ACI-349 available in Section 3.3.2. As mentioned in Section 3.3.2, the reinforcing steel used in the safety related structures in ABWRs is from ASTM A615 Grade 60 Ksi standard group. All changes in this step should be done for steel in the both  $x$  and  $y$  directions.

**Reinforcing Steel Layout:** is modified in details by double clicking on X-Reinforcement and Y-Reinforcement part of the Figure 3.14. As shown in Figure 3.18, reinforcements can be individual or distributed layers. There is an ability to define more than one type of reinforcement for an element.

Information changes for individual and distributed layers are available in Table 3.10. Reinforcement layout of all elements analyzed are distributed. Layout details of the example element is available in Table 3.10. These values are suggested by the program when reinforcement ratio and bar diameter is defined by the quick define.

Some considerations should be provide here for elements such as the controlling minimum concrete cover by ACI-349 and ASME codes. The minimum clear cover available in ACI-349 is 80 mm. This condition is not satisfied for the elements by suggested 22 minimum clear cover n Membrane-2000. Hence, the reinforcing cover is changed here based on R series elements of Korean experiments that is shown in Figure 3.2.

**Crack Spacing:** in Membrane-2000 can be defined manually or automatically by the software. Crack spaces automatically calculated based on Collins and Mitchell suggestion

Table 3.7: Compression softening models available in Membrane-2000

Compression softening model	Softening parameter
Vecchio-Collins 1982	$\beta = \frac{1}{0.85 - 0.27 \frac{\epsilon_1}{\epsilon_2}}$
Vecchio-Collins 1986	$\beta = \frac{1}{0.8 + 0.34 \frac{\epsilon_1}{\epsilon_o}}$
Vecchio-Collins 1992-A	$\beta = \frac{1}{1.0 + K_c K_f}$ $K_c = 0.35(-\frac{\epsilon_1}{\epsilon_2} - 0.28)^{0.8}$ $K_f = 0.1825 \sqrt{f'_c} \geq 1$
Vecchio-Collins 1992-B	$\beta = \frac{1}{1.0 + K_c}$ $K_c = 0.27(\frac{\epsilon_1}{\epsilon_o} - 0.37)$
Maekawa et al	$\epsilon_1 < 1.2 \times 10^{-3} \quad \beta = 1.0$ $1.2 \times 10^{-3} < \epsilon_1 < 4.4 \times 10^{-3} \quad \beta = 1.15 - 125\epsilon_1$ $\epsilon_1 > 4.4 \times 10^{-3} \quad \beta = 0.6$
Noguchi et al	$\beta = \frac{1}{0.27 + 0.96(\frac{\epsilon_1}{\epsilon_o})^{0.167}}$
Belarbi-Hsu proportional	$\beta_\sigma = \frac{1}{\sqrt{1 + K_\sigma \epsilon_1}}$ $\beta_\epsilon = \frac{1}{\sqrt{1 + K_\epsilon \epsilon_1}}$ $\theta = 45, 90 \quad K_\sigma = 400$ $\theta = 45 \quad K_\epsilon = 550$ $\theta = 90 \quad K_\epsilon = 160$
CAN CSA S474	$\beta = \frac{1}{0.85 + 170\epsilon_1}$
Kaufmann-Marti 1998	$\frac{f_c}{f'_c} = \frac{1}{0.4 + 30\epsilon_1}$
Porasz-Collins 1988	$\beta = \frac{n \frac{\epsilon_2}{\epsilon_c}}{n - 1 + (\frac{\epsilon_2}{\epsilon_c})^{nk}}$ $n = 0.8 + \frac{f'_c}{17}$ $k = 0.67 + \frac{f'_c}{62}$
Hsu-Zhang 1998	$\beta = \frac{1}{0.8 + 170\epsilon_1} \cdot \frac{1}{0.9 + 0.0045 f'_c}$

Table 3.8: Tension stiffening models available in Membrane-2000

Tension stiffening model	Equation
None	No tension stiffening
Vecchio-Collins 1982	$f_1 = \frac{f_t}{1 + \sqrt{200\epsilon_1}}$
Collins-Mitchell 1986	$f_1 = \frac{f_t}{1 + \sqrt{500\epsilon_1}}$
Izumo et al	$f_1 = f_{cr} \quad \epsilon_{cr} < \epsilon_1 < 2\epsilon_{cr}$ $f_1 = f_{cr} \cdot \left(\frac{2\epsilon_{cr}}{\epsilon_1}\right)^{0.4} \quad \epsilon_1 > 2\epsilon_{cr}$
Tamai et al	$f_1 = \frac{f_{cr}}{\left(\frac{\epsilon_1}{8 \times 10^{-5}}\right)^{0.4}}$
Elasto-Plastic	$f_t = E_c \times \epsilon_{cr} \quad \epsilon_2 < \epsilon_{cr}$ $f_t = f_{cr} \quad \epsilon_2 > \epsilon_{cr}$
Bentz 1999	$f_1 = \frac{f_t}{1 + \sqrt{3.6 \cdot m \cdot \epsilon_1}}, m = \frac{A_c}{\Sigma d_b \pi}$

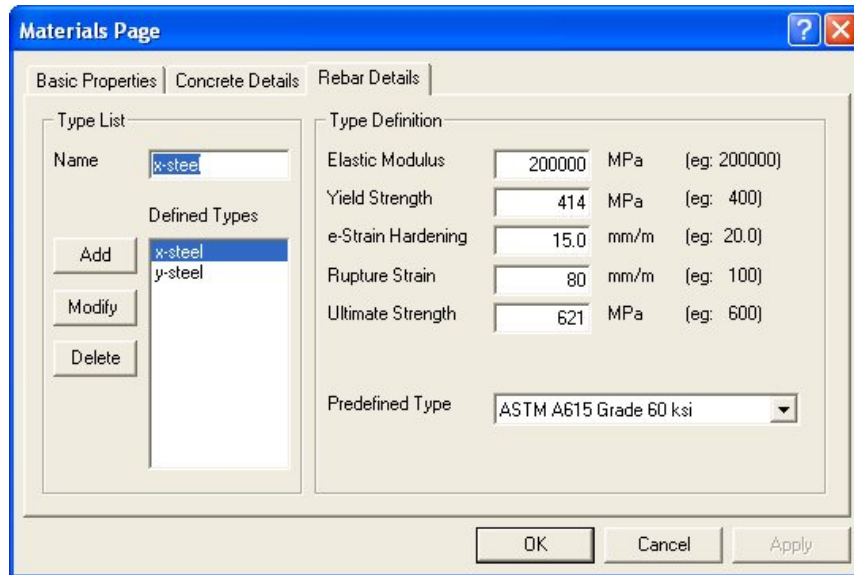


Figure 3.17: Reinforcing steel properties of the element R1 can be defined in Membrane-2000

Table 3.9: Standard reinforcing steel available in Membrane-2000

ASTM standard reinforcement	$f_y$ MPa	$\epsilon_H$ $\frac{mm}{m}$	$\epsilon_r$ $\frac{mm}{m}$	$f_u$ MPa
ASTM A615 Grade 40 Ksi	276	20	120	483
ASTM A615 Grade 60 Ksi	414	15	80	621
ASTM A706 Grade 60 Ksi	414	15	120	552
CSA G30.12 300 MPa	300	20	110	450
CSA G30.12 400 MPa	400	15	80	600
CSA G30.16 400 MPa Weldable	400	15	130	550
1030 MPa Dywidag Bars	800	10	40	1030
1080 MPa Dywidag Bars	820	10	40	1080

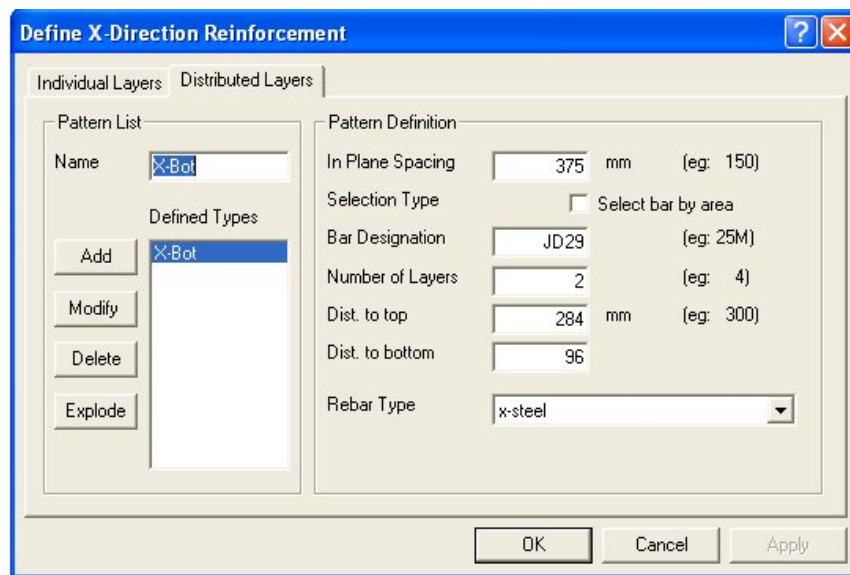


Figure 3.18: Reinforcing steel layout details of the element R1

Table 3.10: Reinforcing steel layout

Individual Reinforcement	Distributed reinforcement	reinforcement layout of SR1
In-Plane Spacing	In-Plane Spacing	589
Bar Designation	Bar Designation	<i>JD29</i>
-	Number of Layers	2
-	Distance to Top	340
Distance from Bottom	Distance to Bottom	40
Prestrain	-	-
Rebar Type	Rebar Type	X steel and Y steel

by equation below:

$$S_{mx} = 2c + 0.1 \frac{d_b}{\rho_x} \quad (3.26)$$

Where,  $c$  is the largest diagonal distance between a bar and any point in the concrete,  $d_b$  is the diameter of the nearest bar, and  $\rho_x$  is percentage of reinforcing steel in  $x$  direction. Crack spacing in  $y$  direction  $S_{my}$  will be calculated same as  $x$  direction [16].

## Degradation Factor

Radiation deterioration on the mechanical properties of the safety class RC structures and radiation thresholds available in different codes are reviewed in Section 2.5.

As shown in Figure 2.13 and Table 2.14, compressive strength of the concrete reduces by 95%, 72.5% and 40% for  $2 \times 10^{19}$ ,  $2 \times 10^{20}$ , and  $2 \times 10^{21}$  n/cm<sup>2</sup> levels of radiation, respectively. As can be seen from experimental results, another factor for radiation deterioration is tensile reduction factor. Tensile strength of concrete is even more affected by high level of radiation. As explained in Section 2.5.2, tensile strength of concrete is reduced by an amount between 20 and 82 % for  $5 \times 10^{19}$  n/cm<sup>2</sup> fluence. Average of this interval (51% tensile reduction) is considered as degradation factor for the first level of degradation. There is no information available about tensile reduction in higher levels of degradation. So, it is assumed that 51% is the minimum tensile reduction for other levels of radiation that can be chosen for degradation levels 2 and 3.

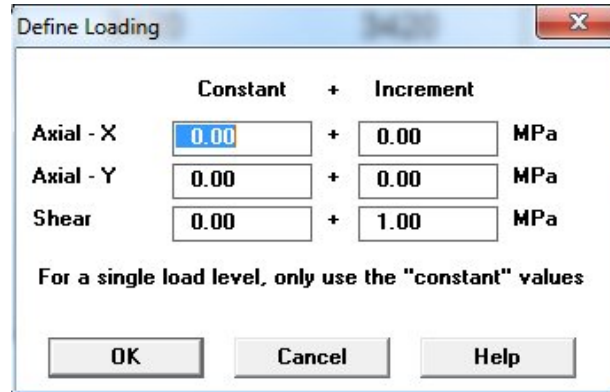


Figure 3.19: Load definition in Membrane-2000

## Load Applied

Membrane element loads are in-plane loadings;  $N_x, N_y$ , and  $v_{xy}$ . Magnitude of loads are not important because the solution method explained in the following section is working with the ratio of loads. It should be noticed that the sign of the load ratios is important for program to recognize tension and compression. Tension load ratio is positive and compression is negative. As shown in Figure 3.19, loads that are applied to the elements can be constant or monotonic or combination of them. If concrete is shrunk, shrinkage will be considered when load patterns are defined by entering thermal and the shrinkage strain of concrete.

Shrinkage of steel is considered as prestrain in the reinforcement properties. The shrinkage effect is ignored in this thesis, however, it is suggested for further research to count contribution of shrinkage in damaged RC panels in NPPs.

Monotonic loads starts from zero and increase incrementally till ultimate capacity of the elements and value in the right column represent load increments for monotonically loading condition. When axial increments in  $x$  and  $y$  direction are zero, loading scenario is pure shear. Obviously, shear increments must be non zero since the MCFT is for elements subjected to shear. Left column shows the value of constant loads and they could be zero for axial and shear loads. If combination of constant and increments are applied, constant value is the value that analysis starts and increments are applicable after that level. All elements analyzed in this thesis are assumed under monotonic loading and the constant values are zero for axial and shear loads. As explained in Section 3.3.4,  $\frac{f_x}{f_y}$  and  $\frac{v_{xy}}{f_x}$  are loading variables for the RC panels. All load cases considering two variables for each element are available in Table 3.4. Biaxial compression increments are same as biaxial tension ones, but with the negative sign for the axial increments.

## 3.3 Discussion on the Selection of Membrane Elements

The geometrical and material properties of the RC panels and the loading scenarios for the analysis are chosen based on the study of existing NPPs. The experimental studies that are done for analyzing the shear mechanism in the RC structures in NPPs is also reviewed. Discussions on the selection of details of the RC panels, are available in the following section. First, different RC structural systems in NPPs, which are susceptible to the radiation deterioration, are studied. Then, the critical parts of the structures that are exposed to the critical levels of radiation are studied to select appropriate element details. Finally, the loading scenarios that are applicable for the RC panels in NPPs are chosen for the analysis.

### 3.3.1 RC Panels from Containment

As mentioned in Chapter 2, containment is a cylindrical wall that could be analyzed by the conventional shell theory. Reinforced concrete panels extracted from these structures are analyzed by researchers to explain the exact behavior of whole structure under different possible load conditions during their life time. Variables for RC panels in experimental work are: concrete compressive strength, reinforcement ratio in  $x$  direction, reinforcement ratio in  $y$  direction, thickness, load applied, ratio of axial and shear loads, etc. RC panels are chosen from experiments performed by researchers who are working on structural behavior of RC structures in NPPs to have the reasonable geometry, material properties, and load applied to analyze.

Elements S, R1, R2, and R3, called RC panels, have been reviewed by Korean researchers in Korean atomic institutes to find their cracking behavior when they are subjected to biaxial tension [11], [12], [40]. Some studies use the volume control technique to analyze RC shells failure [25].

Reinforcement ratios of R1, R2, and R3, based on Korea existing RC containment structures, are shown in Figure 3.20. It is noticed that the reinforcement ratio should be chosen beyond the appropriate value to avoid cracking due to reinforcement yielding. This is considered by choosing a limit as 0.8 % for R series of elements. Minimum reinforcement ratio is also calculated for RC walls of an ABWR based on equation 3.27 [18]. Since  $f_y$  is equal to 414 MPa,  $\rho_{min}$  is equal to 0.33%, our elements reinforcement ratio satisfies the ACI-349 code limit.

$$\rho_{min} = \frac{200}{f_y} \quad (3.27)$$

We add one more higher reinforced element from a solved example in manual of ASME code [52]. Element R4 is from the bottom portion of the wall close to the base. As can



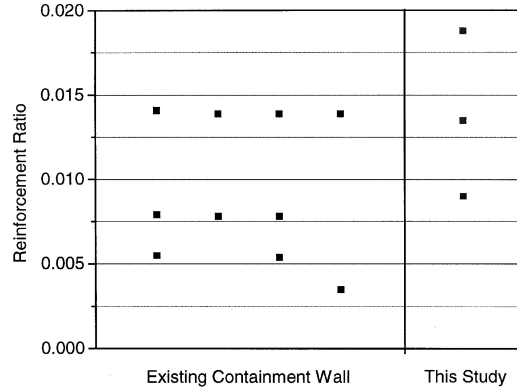


Figure 3.20: Reinforcement ratios of existing containment[12]

Table 3.11: RC panels details

Elements	$\rho_x\%$	$\rho_y\%$	$\Phi$	t mm	$f'_c$ MPa	$f_y$ MPa
S	0.85	0.85	D35	600	40.5	400
R1	0.9	0.9	D29	380	44	400
R2	1.35	1.35	D29	380	36.6	400
R3	1.88	1.88	D29	380	43.4	400
ASME-bottom (R4)	3.01	3.01	# 18	600	40	400
ASME-top	1.51	1.51	# 18	600	40	400

be seen from design details available in Figure 3.21,  $\rho_x$  and  $\rho_y$  are equal and around 3 % at bottom of the cylinder. The reason for this reinforcement ratio is to cover parts of the primary containment structures and internal RC walls that are located in highly reinforced areas like connections and hatches. Table 3.11 represents panels S, R1, R2, R3, R4 and elements from ASME manual example.

### 3.3.2 RC Panels from Safety Class Structures in NPP

RC Structures might be exposed to high level of radiation are located in safety class structure category in NPPs. Concrete can be high level of radiation. Our definition for radiation in the degradation mechanism is described in Section 2.5. Radiation sources in

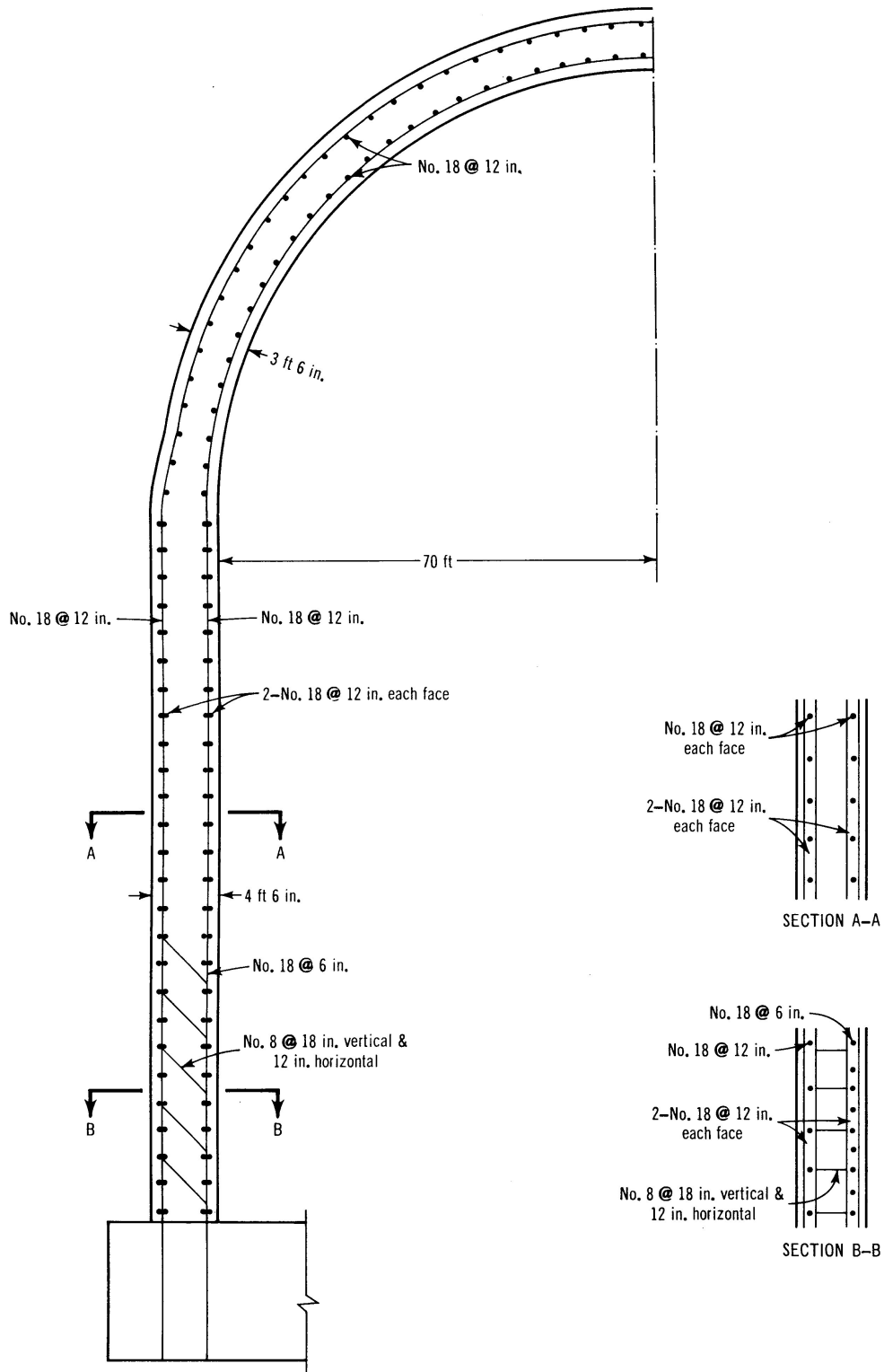


Figure 3.21: ASME manual example of RC containment[52]

NPPs can be internal like, the reactor core and fuel storage, or external like, external waste casks. RC structures that are closer to these sources are more susceptible to irradiation. However, it is very difficult to find design properties of these structures in the literature.

The only document found, which has fairly good information, and used is Advanced Boiler Water Reactors (ABWR) design [21]. An ABWR is a single-cycle, force-circulation that has a boiling-water reactor, with a rated power of 3926 MWt, designed by General Electric Nuclear Energy. All design certifications should be evaluated every several years by Nuclear Regularity Commission (NRC). Final safety evaluation of this kind of NPP was performed in 1994 [17] and was approved by NRC in 1997.

The ABWR design document helps us to find RC elements that are exposed to high levels of radiation. These structures location is obtained from a chapter focusing on the threshold in different environmental conditions such as radiation, temperature, etc. Radiation zones are detected and explained in the following section.

## **Radiation Zones in Containment**

The ABWR design document (Appendix I chapter 3) has specified requirements for qualifying environmental condition of safety related systems and equipments. Environmental parameters considered in this evaluation are: pressure, temperature, relative humidity, radiation, and chemical conditions. Hence, plant zones that are subject to the radiation are clarified in this part. ABWR is divided into two parts: inside primary containment and out side primary containment (reactor, control, and turbine buildings), as shown in Figure 3.22. Each part is going to be limited for two level of conditions: plant normal operating condition (including test and abnormal environment conditions) and plant accident condition.

Inside primary containment is the only location that structures and systems are exposed to neutron fluxes [21]. Neutron fluences are important during long period of time, so for accident condition only gamma and beta fluxes are important and are considered not neutron fluxes. As shown in Figure 3.23, areas exposed to neutron inside primary containment are upper drywell area, upper area of lower drywell, lower area of lower drywell, and Wetwell area (suppression pool and airspace)[21].

## **Structures Exposed to Radiation**

As mentioned in Section 2.1.2, shields and SNF are the most critical areas that may contribute to the radiation damage. Appendix H, Chapter 3 of The ABWR design documents includes design details of seismic category *I* structures, as shown in Tables 3.12 and 3.13. RC walls in reactor and radwaste building are mostly under consideration for this study.

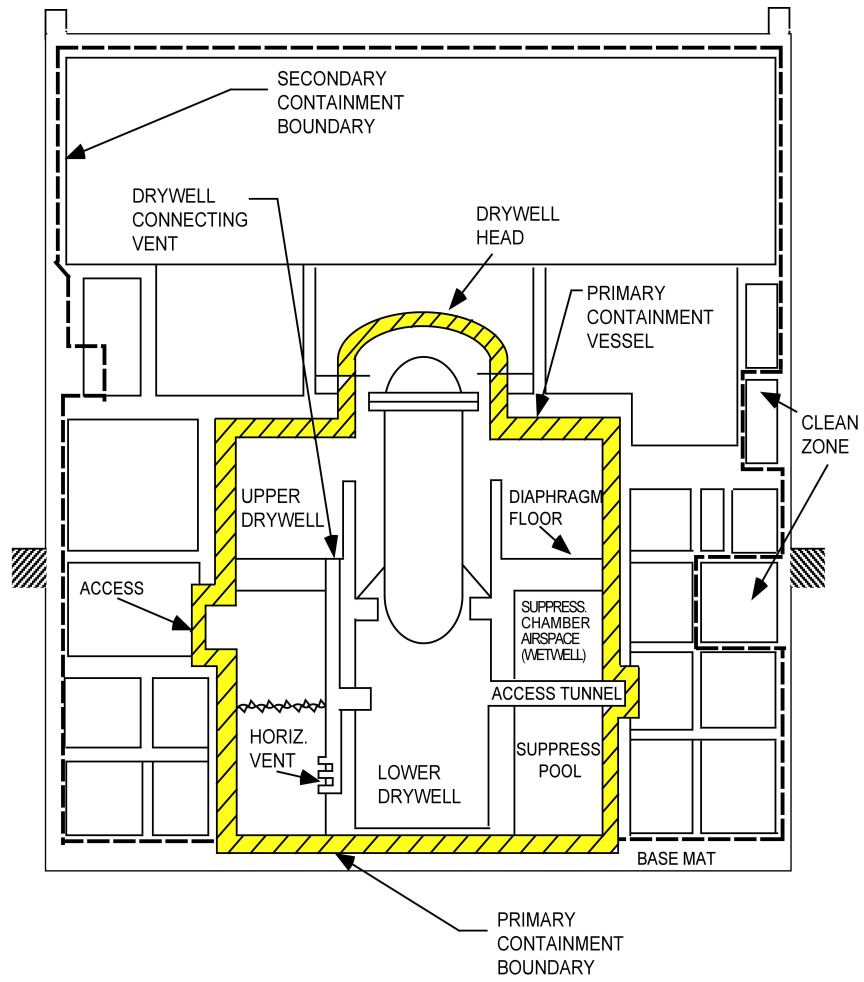


Figure 3.22: Inside and outside of primary containment (ABWR)[21]

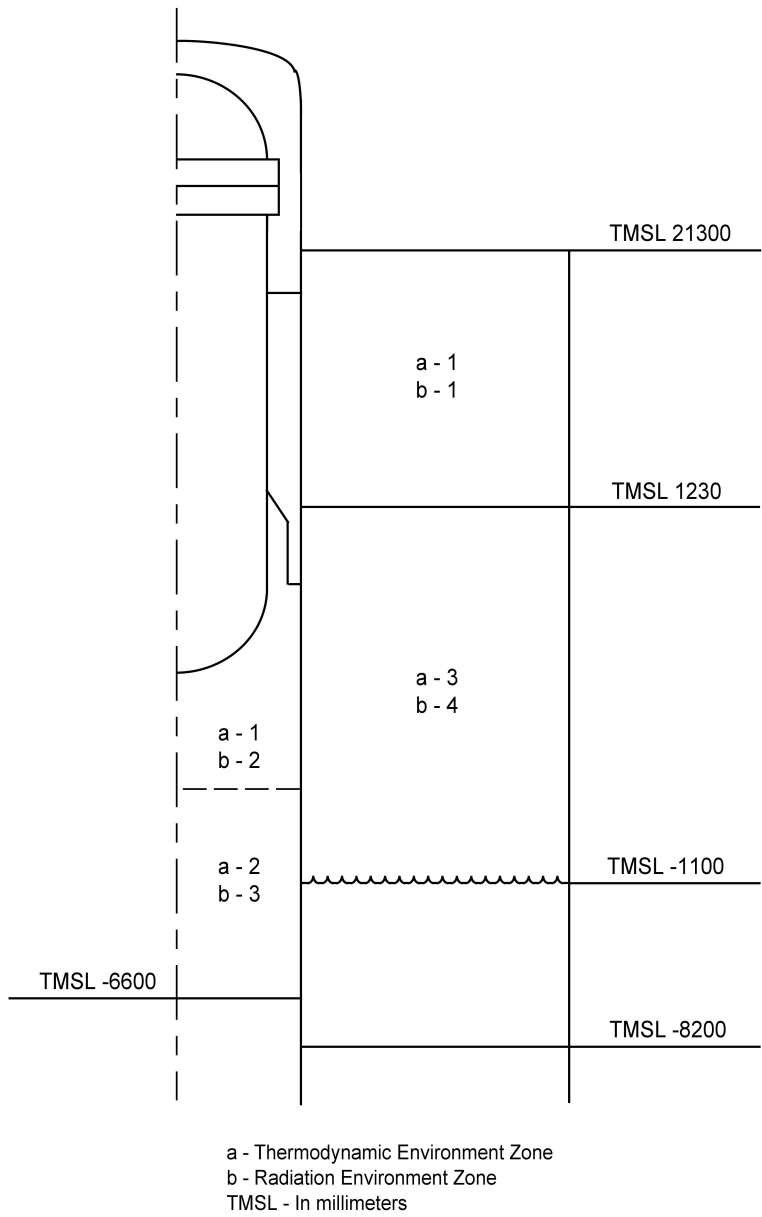


Figure 3.23: Radiation zones in primary containment vessel (ABWR)[21]

Reinforcement ratio, axial load, and shear load ratios of RC walls are calculated from Tables 3.12 and 3.13 and are available in Table 3.14.

RC walls subjected to high levels of radiation are interior walls. Their location can be detected by the number of the element available in Tables 3.12 and 3.13. However, it is not possible to find exact location of the elements, because the drawings of the ABWR design document are not accessible due to the security considerations by NRC. Collection of pieces of information could guide us to see the location of elements that were more likely to be exposed to high level of radiation. For instance, it is known that evaluation of compartment walls that are usually used for radwaste are located between elevations -8200 and 12300 mm. Considering these points, elements located between elevation 17150 and roof are eliminated.

### 3.3.3 Element Details

Design details from the ABWR design show that elements chosen from Korean and Japanese experiments could be applicable for safety related elements with some changes. Similarities are the close reinforcement ratio range, the steel yield strength, and the element thickness.

Two series of RC wall details are available from the ABWR design document: general RC wall details, which are shown in Tables 3.12 and 3.13 and also detail providing for shear checking of RC walls subjected to High Energy Line Break (HELB). HELB evaluation is necessary to provide shear reinforcement [21] required for shear and non shear RC walls in reactor buildings. Tables 3.15 and 3.16 show results of this evaluation for an ABWR.

ABWR RC wall information available in Tables 3.14, 3.15, and 3.16, show that the wall thickness varies between 250 mm to 1600mm. Limit of 380 mm for the thickness is considered in the ABWR design code to minimize the harmful effect of tornado like: penetration, perforation, or spalling. Element thickness (380 mm) is chosen half of the real wall thickness(720) to have an appropriate prediction of the wall behavior form element response in Korean research [11]. Hence, Korean element thickness satisfies the ABWR limitation.

Another consideration for choosing thickness comes from dependency of radiation exposure to concrete thickness, as mentioned by Hilsdorf, according to data from biological shield of ORNL done by Blosser (see Figure 3.24). It is shown that first 305 mm of the shield is the most affected area by radiation. Reviewing all conditions shows that 380 mm thickness used by Korean experiments is good for RC panels are subjected to the critical levels of radiation.

Another experiments proved the effect of the concrete thickness on strength reduction in shields is an experimental test on a shielding wall of a 20-year-old NPP in Ontario, Canada. the Shielding wall is a cylinder with 2.14 meter thickness. Specimens of Ontario

Table 3.12: Reinforced concrete wall design forces and reinforcement in ABWR design(continues)[21]

Element No.	Load Combination	Thickness mm (in)	Design Loads (See Notes 1 and 2)						Reinforcement						
			Axial		Shear		Flexure		Vertical ea face, (cm <sup>2</sup> /m)		Horizontal ea face, (cm <sup>2</sup> /m)		Shear Ties (cm <sup>2</sup> /m)		Remarks
			Horizontal	Vertical	In-Plane	Out-of-Plane	About Horizontal Axis	About Vertical Axis	Required	Actual	Required	Actual	Required	Actual	
2809	D+L <sub>0</sub> +H $\phi$ +P <sub>a</sub> +E $\phi$ +T <sub>a</sub>	600 (24)	1.39E+06 (95,021)	1.70E+06 (116,256)	1.28E+06 (87,830)	9.20E+04 (6,302)	4.39E+05 (98,657)	3.49E+05 (78,551)	<83.7	84.8	55.0	56.8	None	None	
2781	D+L <sub>0</sub> +H $\phi$ +P <sub>a</sub> +E $\phi$ +T <sub>a</sub>	600 (24)	1.17E+06 (80,438)	2.38E+06 (163,363)	1.09E+06 (74,995)	6.25E+04 (4,280)	6.25E+05 (140,611)	3.78E+05 (84,878)	83.7	84.8	<55.0	56.8	None	None	
2730	D+L <sub>0</sub> +H $\phi$ +P <sub>a</sub> +E $\phi$ +T <sub>a</sub>	1000 (39)	5.71E+06 (391,238)	-3.29E+05 (-22,559)	1.04E+06 (71,232)	3.87E+05 (26,510)	1.29E+06 (289,467)	1.02E+06 (229,060)	<119.1	127.2	122.7	127.2	<19.9	21.2	Walls on grid lines A and D — portion between basement (El. -8200) and El. 17150
3448	D+L <sub>0</sub> +H $\phi$ +P <sub>a</sub> +E $\phi$ +T <sub>a</sub>	1000 (39)	3.85E+06 (263,693)	-1.82E+06 (-124,454)	3.45E+06 (236,275)	4.39E+05 (30,092)	1.31E+06 (295,419)	1.10E+06 (248,020)	119.1	127.2	<122.7	127.2	<19.9	21.2	Walls on grid lines A and D — portion between basement (El. -8200) and El. 17150
2474	D+L <sub>0</sub> +H $\phi$ +P <sub>a</sub> +E $\phi$ +T <sub>a</sub>	1000 (39)	-8.49E+05 (-58,188)	1.17E+06 (80,237)	2.32E+06 (158,928)	1.97E+06 (134,669)	8.31E+05 (186,864)	2.33E+05 (52,426)	<119.1	127.2	<43.0	56.8	19.9	21.2	*Between finished grade and El. 17150 only.
2437	D+L <sub>0</sub> +H $\phi$ +P <sub>a</sub> +E $\phi$ +T <sub>a</sub>	1000 (39)	-1.95E+06 (-133,728)	-1.66E+05 (-11,370)	2.38E+06 (163,094)	1.27E+06 (86,688)	6.90E+04 (15,505)	9.27E+05 (208,403)	<123.4	127.2	43.0	56.8	<19.9	21.2	
3133	D+L <sub>0</sub> +H $\phi$ +P <sub>a</sub> +E $\phi$ +T <sub>a</sub>	1000 (39)	-9.28E+05 (-63,356)	2.24E+06 (153,821)	2.65E+06 (181,507)	3.41E+05 (23,392)	1.83E+06 (410,942)	4.26E+05 (95,659)	123.4	127.2	<43.0	56.8	<19.9	21.2	
3757	D+L <sub>0</sub> +H $\phi$ +F <sub>a</sub> +E $\phi$ +T <sub>a</sub>	600 (24)	8.12E+05 (55,608)	1.05E+06 (71,702)	1.11E+06 (76,070)	2.25E+05 (15,429)	5.09E+05 (114,398)	3.07E+05 (68,961)	58.7	66.1	49.2	49.6	None	None	Walls on grid lines 1 and 7 — portion between El. 17150 and roof
3751	D+L <sub>0</sub> +H $\phi$ +F <sub>a</sub> +E $\phi$ +T <sub>a</sub>	1000 (39)	2.24E+06 (153,283)	3.52E+05 (24,098)	1.44E+06 (98,582)	1.04E+06 (7,116)	9.97E+05 (224,210)	9.97E+05 (223,990)	95.4	101.8	71.2	84.7	<18.0	21.2	Walls on grid lines 1 and 7 — portion between basement (El. -8200) and El. 17150
3605	D+L <sub>0</sub> +H $\phi$ +F <sub>a</sub> +E $\phi$ +T <sub>a</sub>	1000 (39)	-1.49E+06 (-102,211)	1.28E+06 (87,965)	2.69E+06 (184,195)	2.22E+05 (15,221)	1.44E+06 (323,639)	3.25E+05 (73,149)	95.4	101.8	<71.2	84.7	<18.0	21.2	
3632	D+L <sub>0</sub> +H $\phi$ +F <sub>a</sub> +E $\phi$ +T <sub>a</sub>	1000 (39)	-2.80E+06 (-191,587)	1.17E+06 (80,237)	1.96E+06 (134,198)	1.82E+06 (124,723)	6.66E+05 (149,606)	2.40E+04 (5,401)	<95.4	101.8	<71.2	84.7	18.0	21.2	

Notes: 1. The values of axial forces and shears are shown in N/mm and those for flexure are shown in N•m/m. The corresponding values in lb/ft and lb-ft/ft are shown in parenthesis.  
 2. Positive axial forces are tensile; negative axial forces are compressive.

Table 3.13: Reinforced concrete wall design forces and reinforcement in ABWR design[21]

Element No.	Load Combination	Thickness mm (in)	Design Loads (See Notes 1 and 2)						Reinforcement						
			Axial		Shear		Flexure		Vertical sea face, (cm <sup>2</sup> /m)		Horizontal sea face, (cm <sup>2</sup> /m)		Shear Ties (cm <sup>2</sup> /m)		Remarks
			Horizontal	Vertical	In-Plane	Out-of-Plane	About Horizontal Axis	About Vertical Axis	Required	Actual	Required	Actual	Required	Actual	
3912	D+L <sub>0</sub> +H $\phi$ +P <sub>a</sub> +E $\phi$ +T <sub>a</sub>	1600 (63)	5.98E+06 (409,450)	1.05E+07 (721,728)	6.08E+06 (416,774)	7.36E+05 (50,427)	2.18E+06 (490,749)	3.25E+05 (73,149)	249.7	254.4	<189.7	203.5	<10.6	12.7	
3912	D+L <sub>0</sub> +H $\phi$ +P <sub>a</sub> +E $\phi$ +T <sub>a</sub>	1600 (63)	5.98E+06 (409,450)	1.05E+07 (721,728)	6.08E+06 (416,774)	7.36E+05 (50,427)	2.18E+06 (490,749)	3.25E+05 (73,149)	249.7	254.4	189.7	203.5	<10.6	12.7	
3948	D+L+H+1.5P <sub>a</sub> +E $\phi$ +T <sub>a</sub>	1600 (63)	-3.06E+06 (-209,462)	-2.29E+06 (-157,114)	2.42E+06 (165,715)	1.99E+06 (136,349)	204,262 (101,236)	3.81E+05 (85,738)	<249.7	254.4	<189.7	203.5	10.6	12.7	

Notes: 1. The values of axial forces and shears are shown in N/m and those for flexure are shown in N•m/m. The corresponding values in lb/ft and lb-ft/ft are shown in parenthesis.  
 2. Positive axial forces are tensile; negative axial forces are compressive.



Table 3.14: Reinforcement ratios and loading ratios of RC walls in ABWR

Wall Element Number	$\frac{f_x}{f_y}$	$\frac{f_x}{v_{xy}}$	$\rho_x$	$\rho_y$
2809	0.8176	1.0859	0.95	1.41
2781	0.4916	1.0734	0.95	1.41
2730	-17.3556	5.4904	2.12	2.12
3448	-2.1154	1.1159	2.12	2.12
2474	-0.7256	-0.3659	2.12	0.95
2437	11.7470	-0.8193	2.12	0.95
3133	-0.4129	-0.3491	2.12	0.95
3757	0.7733	0.7315	1.10	0.83
3751	6.3636	1.5556	1.70	1.41
3605	-1.1641	-0.5539	1.70	1.41
3632	-2.3932	-1.4286	1.70	1.41
3912	0.5695	0.9836	4.24	3.39
3912	0.5695	0.9836	4.24	3.39
3948	1.3362	-1.2645	4.24	3.39

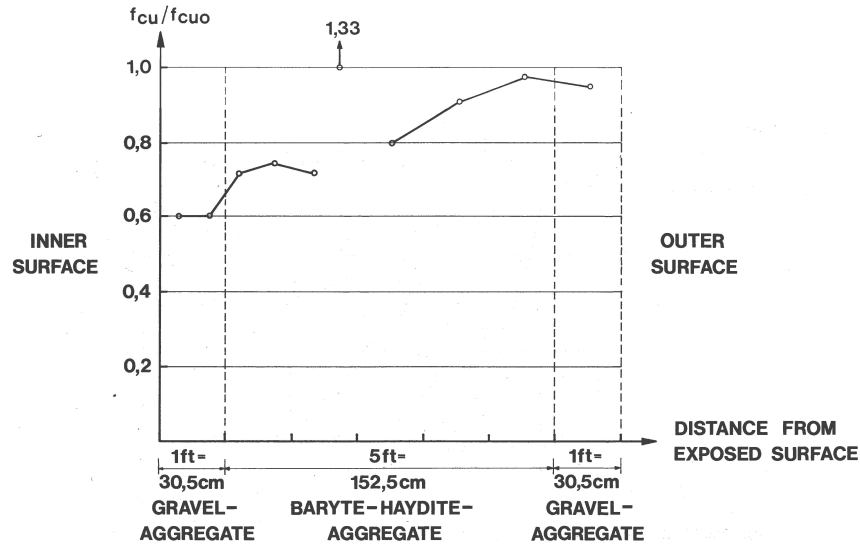


Figure 3.24: Distribution of concrete compressive strength over thickness of biological shield of ORNL-Graphite reactor[27]

Hydro investigation were not selected from the inner 300 mm thickness of the shield due to safety provision of the reactor. However, they also found the different strength reduction between 10 to 20 % based on the distance of drilled core to the reactor core in the remain 1.84 meter thickness of the shield. The cores closer to the reactor had higher strength reduction compared to the further cores. This confirms Hilsdorf curves in the sense that first 300 mm thickness of the shield has higher than 20 % strength reduction[45].

The main difference of these elements with containment elements is lower compressive strength. The property  $f'_c$  of concrete is considered as 27.6 MPa (4000 PSI) for safety related elements of NPPs.

Reinforcing steel is deformed billet steel ASTM A-615 grade 60 with the minimum yield strength of  $F_y = 414$  MPa. It can be seen that the yield strength of the elements satisfies the condition of ACI-349 for being less than 415 MPa.

From information available in the ABWR design code, maximum reinforcing number for RC walls as shields is #11. Since area of reinforcing steel in R series of elements is around half of #11 bar, JD29 is appropriate for RC panels analyzing in this thesis. Young modulus of reinforcing steel and concrete are chosen based on standards in Membrane-2000 and are checked with American codes.  $E_s$  is 200000 MPa for standard reinforcing steel ASTM A-615 grade 60 in Membrane-2000 .  $E_c$  follows Vecchio 1986 stress-strain relationship and ACI-349 uses the following equation for calculating  $E_c$  ( $f'_c$  in MPa) :

$$E_c = 393\sqrt{f'_c}$$

Table 3.15: ABWR details of shear walls exposed to high energy line break[21]

Wall #	Thickness (m)	Height (m)	Length (m)	Main Reinforcing (E.W. & E.F.)		Shear Reinforcing			
				AsREQ (cm <sup>2</sup> /m)	AsPROV (cm <sup>2</sup> /m)	AvREQ (cm <sup>2</sup> /cm <sup>2</sup> )	AsPROV (cm <sup>2</sup> /cm <sup>2</sup> )		
S1a	0.90	3.00	5.60	83.6	84.7	#18 @ 0.305 m	0.0008	0.0031	#6 @ 0.305 m x 0.305 m
S1b	0.90	1.90	5.60	81.9	84.7	#18 @ 0.305 m	0.0008	0.0031	#6 @ 0.305 m x 0.305 m
S2	0.60	5.70	8.50	70.1	72.6	#18 @ 0.356 m	None	None	None
S3	0.80	5.70	5.90	55.0	56.5	#18 @ 0.457 m	None	None	None
S4	0.60	5.70	8.50	76.2	84.7	#18 @ 0.305 m	None	None	None
S5	0.80	5.70	6.70	72.4	72.6	#18 @ 0.357 m	0.0008	0.0022	#6 @ 0.357 m x 0.357 m

Table 3.16: ABWR details of non-shear walls exposed to high energy line break[21]

Thickness (m)	Max. Height (m)	Area of Main Reinforcing Steel (E.W. & E.F.)				Shear Reinforcing	
		Calculated (cm <sup>2</sup> /m)	Code Min (cm <sup>2</sup> /m)	Required (cm <sup>2</sup> /m)	Provided (cm <sup>2</sup> /m)	AvREQ (cm <sup>2</sup> /cm <sup>2</sup> )	AsPROV
0.25	3.00	20.1	7.0	20.1	25.2 #8 @ 0.203 m	None	None
0.40	3.20	12.7	11.4	12.7	16.7 #8 @ 0.305 m	None	None
0.50	5.80	33.4	14.8	33.4	49.5 #11 @ 0.203 m	None	None
0.55	6.50	38.5	16.5	38.5	49.5 #11 @ 0.203 m	0.000	None
0.60	7.50	47.2	18.2	47.2	49.5 #11 @ 0.203 m	0.000	None
0.70	6.50	31.1	21.4	31.1	33.0 #11 @ 0.305 m	None	None
0.80	5.80	22.9	24.8	24.8	25.2 #8 @ 0.203 m	None	None
0.90	5.80	21.4	27.9	27.9	33.0 #11 @ 0.305 m	None	None
1.00	6.50	24.8	31.3	31.3	33.0 #11 @ 0.305 m	None	None
1.10	3.30	7.8	34.7	34.7	49.5 #11 @ 0.203 m	None	None
1.20	5.80	19.0	37.9	37.9	49.5 #11 @ 0.203 m	None	None
1.30	6.50	22.4	41.3	41.3	49.5 #11 @ 0.203 m	None	None

Notes:  
 1. AsCODE MIN is based on  $\rho_{MIN} = 200/f_y$  from ACI 349-90 Section 10.5.1.

### 3.3.4 Loading Scenarios for RC Panels

The conventional shell theory (membrane theory) for cylinders can be used for containment and internal vessels like drywell walls. As shown in Figure 3.25, a membrane element is extracted from a cylinder by the coordinate  $x$  and the angle  $\varphi$  [60]. Axial loads  $N_\varphi$  and  $N_x$  are the tensile stress caused by the internal pressure.  $N_{x\varphi}$ , which is applied in the tangential direction, is tangential shear and  $N_{\varphi x}$ , which is applied in the axial direction of the cylinder, is called axial shear. The shear stress is produced by lateral loads like earthquake. If the element is chosen small enough, it is an appropriate assumption that  $d\varphi$  and  $dx$  are close to zero, so terms  $\frac{\partial N_{\varphi x}}{\partial \varphi} d\varphi$ ,  $\frac{\partial N_\varphi}{\partial \varphi} d\varphi$ ,  $\frac{\partial N_x}{\partial x} dx$  and  $\frac{\partial N_{x\varphi}}{\partial x} dx$  are zero.

A concrete cylindrical shell containment with vessel diameter 10 times greater than vessel thickness does not require the triaxial stress state. Hence, containment structures are designed for the hoop and meridian stresses 2.2. Equations 3.28 and 3.29 are used to show the relationship between pressure  $P$ , hoop stress  $N_{\varphi x}$ , and meridian stress  $N_x$  in pressure vessels. These equations show that the ratio of axial loading for hoop and meridional direction is 2 to 1 for the elements from vessels.

$$N_{\varphi x} = \frac{P \times r}{t} \quad (3.28)$$

$$N_x = \frac{P \times r}{2 \times t} \quad (3.29)$$

where  $P$ : Internal pressure,  $t$ : the cylinder thickness, and  $r$ : the inside radius of cylinder.

Since all the elements in this thesis are membrane elements, so radial or any other out of plane load conditions like the twisting moment ( $T_{xy}$  shown in Figure 3.6) or the bending moment ( $M_x$  and  $M_\varphi$  shown in Figure 3.26) are ignored.

#### Elements Loading

RC elements in this study are analyzed under six types of loading enumerated below:

1. Pure shear
2. Shear-biaxial tension
3. Shear-biaxial compression
4. Shear-biaxial tension-compression
5. Shear-uniaxial tension

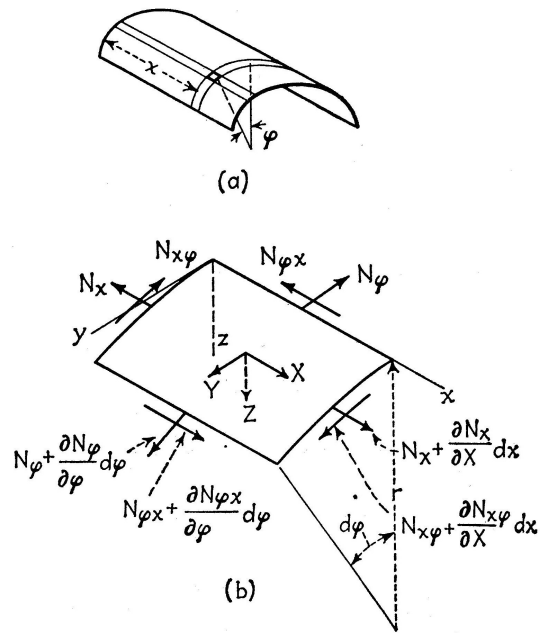


Figure 3.25: Membrane element with in plane loading[60]

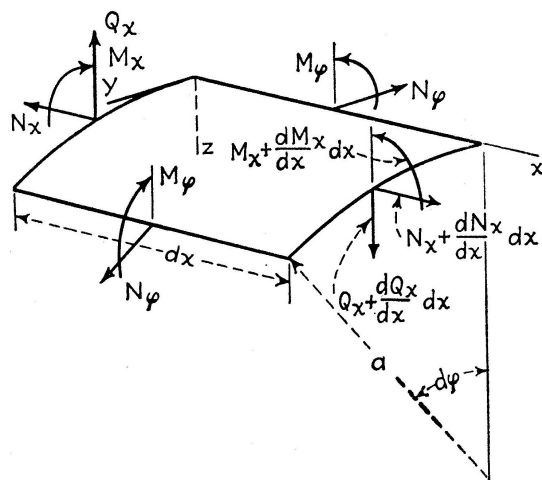


Figure 3.26: Membrane element with out of plane loading [60]

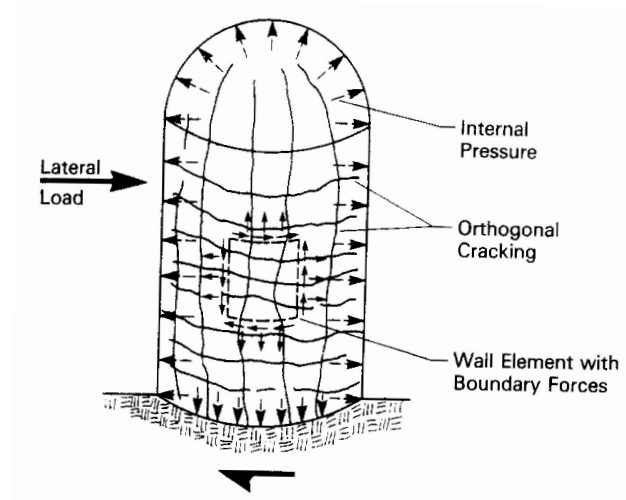


Figure 3.27: Combined pressurization and tangential shear[54]

## 6. Shear-uniaxial compression

These load combinations are chosen since they show critical loading cases in NPPs. Applicability of the elements under these load combinations depends on their location in the structure. Figure 3.27 shows an element under the shear-biaxial tension loading condition. When vessels under internal pressure loading are subjected to lateral load like earthquake, RC walls are under shear-biaxial tension loading condition.

As can be seen from Figure 3.28, RC elements in connection of cylinder with base or roof are under biaxial compression. Another location that biaxial and uniaxial loadings are likely to happen in close to openings is shown in Figure 3.28. Numerical methods using finite element analysis are applied to find complex stress distribution of locations close to connections.

Load ratios should be close to the real load scenarios that structures are going to face. So, an appropriate understanding of the structure behavior is provided by the elements responses. Hence, there are two variables for choosing loading ratios: ratio of axial-shear loading which is  $\frac{v_{xy}}{f_x}$  and ratio of axial load in  $x$  and  $y$  directions which is  $\frac{f_x}{f_y}$ .

The first variable is based on experimental works and existing NPPs [8, 62, 42]. Table 3.17 shows values used for axial tension and compression of the elements. Since experiments work mostly with the ratio  $\frac{f_x}{v_{xy}}$  we will discuss about this ratio and then invert it to the ratio chosen for this study, which is  $\frac{v_{xy}}{f_x}$ . Experimental values show the loading ratios that RC elements with the different reinforcement ratio and compressive strength can have. The ratio recorded in experimental is  $\frac{f_x}{v_{xy}}$ , which is inverted of our ratio  $\frac{v_{xy}}{f_x}$ . The

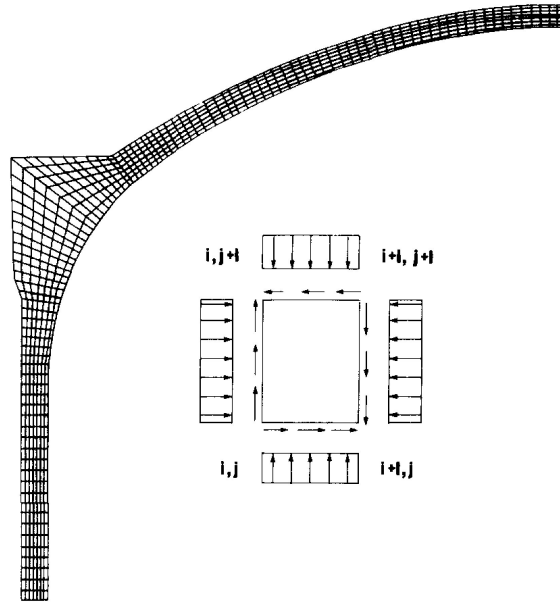


Figure 3.28: Location of elements under biaxial compression in vessels [65]

experimental loading ratio  $\frac{f_x}{v_{xy}}$  is between -0.3 to -0.83 for compression and 0.3 for tension. A group called "ABWR" is provided from RC walls existed in an ABWR explained in Section 3.3.2 and it has value of -0.82 and -1.26 for compression and 0.98 and 1.56 for tension loading. Another important data considering the axial-shear ratio is provided by Habasaki et al, shown in Figure 3.29. It shows that range of axial-shear load ratio for box wall elements is mostly below 1 for box type wall and it arrives at 1.5 for shell wall elements. Our overall understanding is that higher ratio from experiments are not likely to be experienced in reactor buildings. By drawing a line with slope 1 on Figure 3.29, it can be seen that the usual range of loading ratio  $\frac{f_x}{v_{xy}}$  is between 0.25 to 1.

At the end, loading values that cover high number of RC wall elements in NPPs are selected. Hence, 0.25, 0.5 and 1.0 are chosen for the ratio of axial load to shear in the analysis of panels in this thesis. These ratio will be inverted for simplicity and also considering increasing shear load compare to axial load. So, ratio  $\frac{f_x}{v_{xy}}$  equals to 0.25, 0.5 and 1.0 will be enter in the analysis by ratio  $\frac{v_{xy}}{f_x}$  equals to 4, 2, and 1.

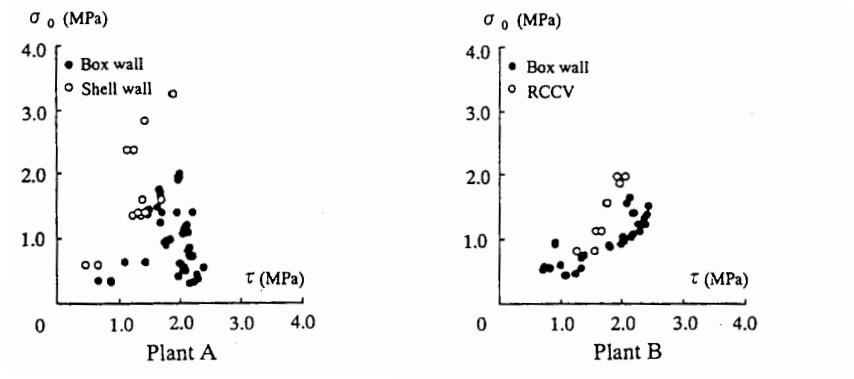


Figure 3.29: Relationship of axial load and shear load in actual reactor buildings[26]

Table 3.17: Shear-axial load ratios of experiments and existing NPPs

Axial load	Source of Elements	Researcher	$f'_c$	$\rho_x$	$\rho_y$	$\frac{f_x}{v_{xy}}$
Compression	Experiments	Vecchio and Collins 1982	23.8	1.785	1.785	-0.39
			20.5	1.785	1.785	-0.69
		Mart and Mayboon	28.1	1.59	1.59	-0.38
			27.7	1.24	1.24	-0.8
	Exiting NPPs	ABWR	27.6	2.12	0.95	-0.82
			27.6	4.24	3.39	-1.26
Tension	Experiments	Vecchio and Collins 1982	19	1.785	1.785	0.32
			27.6	1.70	1.44	1.56
	Exiting NPPs	ABWR	27.6	4.24	3.39	0.98
			27.6	4.24	3.39	0.98



Table 3.18: Element's name based on the variables of the element properties

Element Name	Degradation level	Loading pattern	Reinforcement ratio %	Loading ratios ( $f_x:f_y:v_{xy}$ )
U-PR1-L001	undegraded	pure shear	0.9	L001(0:0:1)

### 3.3.5 Element Definition

Elements are named based on the geometrical, material, and loading variables. U, D1, D2, and D3 show the level of radiation for the elements. P and BT are the two loading scenarios explained in Section 3.3.4. R1, R2, R3, and R4 show the different amount of reinforcement ratio in the elements. The last notation shows different loading variables  $\frac{f'_x}{f'_y}$ , and  $\frac{f'_x}{v_{xy}}$ . The first number after capital alphabet L is 1 for  $\frac{f'_x}{f'_y}$  equal to 1 and 2 for  $\frac{f'_x}{f'_y}$  equals to 2. Second number is 1, 2, and 3 for  $\frac{f'_x}{v_{xy}}$  equals to 1, 0.5, and 0.25 respectively. For instance, L001 and L111 are for the pure shear and Shear-Uniaxial loading. Table 3.18 show an elements with its variables for an example.

# Chapter 4

## Analysis of Results

This chapter discusses the analyze of the shear stress-strain curves for the undegraded and degraded elements. First, load-deformation curves of the elements are compared to find significant changes due to degradation. Then, the factors that influence the shear capacity of the elements are studied considering degradation levels 1, 2, and 3. Finally, the effects of degradation on the ultimate shear strength of the elements, failure mode, and ductility index of the elements are studied.

### 4.1 Load-Deformation Curve

Reinforced Concrete (RC) panels R1, R2, R3, and R4 are analyzed in this section under six loading scenarios (pure shear, shear-biaxial tension, shear-biaxial compression, shear-biaxial tension-compression, shear-uniaxial tension, and shear-uniaxial compression loading) in four levels of radiation (zero radiation and radiation levels 1, 2 and 3 ). As can be seen from Table 4.1, 288 elements are analyzed under different loading conditions with different material and geometrical properties.

Hence, 288 element responses are obtained and should be stored. Shear stress and strain values of each element are stored in a  $m \times 2$  matrix. The first column of the matrix represents shear strain  $\gamma_{xy}$  and the second column represents shear stress  $v_{xy}$ . Number of rows  $m$  represents number of shear strain increments used to build a stress strain curve. Stress and strain information of each element are stored in a matrix named after the element's variables. For example, element D2-UCR1-L104 represents the element exposed to fast neutron radiation  $2 \times 10^{20}$ n/cm<sup>2</sup> (D2) under shear-uniaxial compression loading ( $f_x : f_y : v_{xy}$  equals to -1:0:4) with the reinforcement ratio equal to 0.9 % (R1). More information about the Matlab code, which include all elements responses and comparisons, is available in Appendix B.

Table 4.1: Different elements analyzed in this study with respect to the variables considered in the analysis

Degradation level	Loading pattern <sup>a</sup>	Reinforcement ratio %	Loading ratios ( $f_x:f_y:v_{xy}$ )	Number of elements <sup>b</sup>
U (zero radiation)	P	R1 ( $\rho = 0.9$ )	L001 (0:0:1)	48
D1 ( $2 \times 10^{19}$ )		R2 ( $\rho = 1.35$ )	L002 (0:0:2)	
D2 ( $2 \times 10^{20}$ )		R3 ( $\rho = 1.88$ )	L004 (0:0:4)	
D3 ( $2 \times 10^{21}$ )		R4 ( $\rho = 3$ )		
U (zero radiation)	BT	R1 ( $\rho = 0.9$ )	L111(1:1:1)	144
D1 ( $2 \times 10^{19}$ )	BC	R2 ( $\rho = 1.35$ )	L112(1:1:2)	
D2 ( $2 \times 10^{20}$ )	BTC	R3 ( $\rho = 1.88$ )	L114(1:1:4)	
D3 ( $2 \times 10^{21}$ )		R4 ( $\rho = 3$ )		
U (zero radiation)	UT	R1 ( $\rho = 1.35$ )	L101(1:0:1)	96
D1 ( $2 \times 10^{19}$ )	UC	R2 ( $\rho = 1.35$ )	L102(1:0:2)	
D2 ( $2 \times 10^{20}$ )		R3 ( $\rho = 1.88$ )	L104(1:0:4)	
D3 ( $2 \times 10^{21}$ )		R4 ( $\rho = 3$ )		

<sup>a</sup> P, BT, BC, BTC, UT, and UC represents pure shear, shear-biaxial tension, shear-biaxial compression, shear-biaxial tension-compression, shear-uniaxial tension, and shear-uniaxial compression loading

<sup>b</sup> The Number of elements are equal to multiplication of the number of variables(48 elements  $4 \times 1 \times 4 \times 3$  are loaded under the pure shear loading condition)

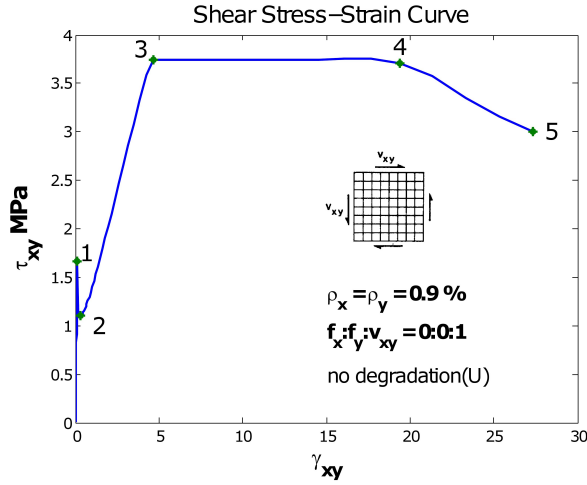


Figure 4.1: Typical load deformation diagram for a membrane element

Figure 4.1 shows a typical stress-strain curve for an integrated point of one of the 64 elements studied in this thesis. Five important points of the curve are numerated from cracking point to crushing point. These points separate five parts of an element response that illustrate behavior of the RC panels under monotonic loading.

The first part starts from zero to the cracking point and is called precracking part, where only concrete is responsible for shear. Crack will happen in concrete when tension applied to the element becomes greater than tensile capacity of concrete. Cracking shear stress is usually very small compared to the ultimate shear strength. Initial stage shear modulus  $G_I$  is the slope of the line between origin and cracking shear stress (point number one).

The second part starts with a sharp decrease in the element response immediately after cracking. This reduction is due to transferring shear stress from concrete to the reinforcing steel. Reinforcing steel is added to the concrete members to avoid concrete cracking failure. Hence, yielding of reinforcing steel can control member failure, which is studied in the following parts of the curve. When steel becomes effective, third stage starts with a gradual increase to the point where reinforcing steel yields. According to MCFT, steel and concrete between cracks are responsible for shear stress in this stage [26].

The fourth part is located between yielding point and ultimate point. Strain length of this part represents ductility index of the elements. Ductility index of the elements is computed by dividing ultimate strain to yield strain. The last part of the curve represents post failure behavior of the elements. Generally, it is quite difficult and some times impossible to measure this part of load deformation curves in experimentals, so it is mostly predicted

by theories.

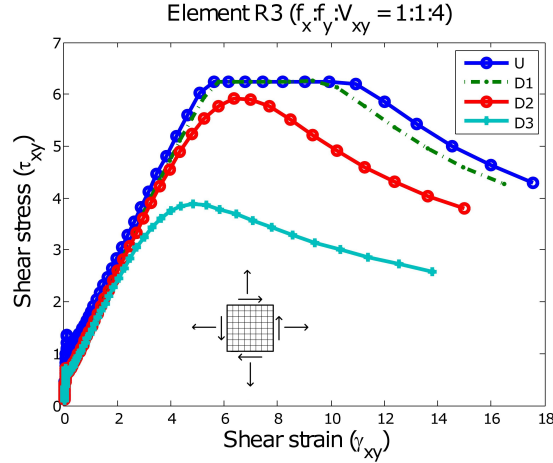


Figure 4.2: Comparison of element R3 ( $\rho = 3\%$ ) under shear and biaxial tension loading in different levels of degradation

Three most affected characteristic of the load-deformation curves, which are cracking shear stress  $V_{cr}$ , ultimate strength capacity  $V_u$ , and ductility index  $\mu_u$ , are recognized by comparing the results of the elements. Figure 4.2 is an example of comparing elements U-BTR3-L114, D1-BTR3-L114, D2-BTR3-L114, and D3-BTR3-L114, which represent element R3 under shear-biaxial loading in different levels of degradation.

## 4.2 Ultimate strength Capacity Reduction

Ultimate strength capacity of a RC panel is the maximum shear stress that an element can face before failure happens. Shear capacity of RC walls is affected by different variables. Compressive strength, tensile strength, and reinforcement ratio are most well known parameters that affect the shear capacity of RC panels [62]. This thesis considers increasing shear loading compared to axial loading as another factor that influence the shear capacity. Shear-axial loading ratio is important for RC walls subjected to earthquake loading in NPPs [26].

Here we study the effect of degradation on shear capacity of the RC panels, for each of the four different reinforcement ratios. Moreover, the ultimate strength capacity reduction of the elements with respect to degradation increase and increasing of shear-axial loading

ratio is analyzed. In other words, three variables of reinforcement ratio  $\rho$ , loading scenario  $\frac{v_{xy}}{f_x}$ , and degradation levels (U, D1, D2, and D3) are considered.

Results of the elements subjected to shear-axial loading are represented in two categories. The categories are distinguished by having or not having tension loading. The first group of analysis are the elements under shear-biaxial tension (BT), shear-biaxial tension-compression (BTC), and shear-uniaxial tension (UT). The second group includes elements under shear-biaxial and shear-uniaxial compression.

### 4.2.1 Elements Subjected to Tension

The general trend observed from the elements under BT, BTC, and UT loading show that by increasing radiation deterioration, the shear capacity of the elements for highly reinforced concrete, which has 3 % reinforcement ratio  $\rho$ , is decreased significantly. The values in Table 4.2 show that elements with  $\rho = 3\%$  are the most significantly affected by different levels of degradation. In addition, low reinforced elements ( $\rho = 0.9\%$ ) is not significantly affected by radiation.

As can be seen in Table 4.2, elements show same patterns under shear-biaxial tension, shear-biaxial tension-compression and shear-uniaxial tension loading conditions. Figure 4.3 is an example of the shear strength reduction pattern of the elements under shear-biaxial tension loading. As can be shown in Figure 4.3, the degradation level 3 affects the elements with reinforcement ratio  $\rho$  above 1.88 %. The effect of the critical levels of radiation (between  $2 \times 10^{19}$  and  $2 \times 10^{21}$ ) on the elements with the reinforcement ratio 0.9 % is not significant. Elements R2, R3, and R4 show different amounts of strength reduction for same levels of radiation described in Table 4.2. The element R4 with reinforcement ratio 3% is the most affected elements by high levels of radiation. The element R4 experience 52% ultimate strength reduction in degradation level 3 and 22% reduction in degradation level 2. Ultimate strength capacity reduction is increased for elements with reinforcement ratios between 1.35 and 1.88 by increasing loading ratio  $\frac{v_{xy}}{f_x}$ . However, there is no change in shear capacity reduction for the highly reinforced element ( $\rho = 3\%$ ) when the ratio of shear to axial loading is increased.

The results are interpreted as follows: for each specific loading scenario in different levels of degradation,  $V_u$  changes more significantly for elements with higher reinforcement ratio. This kind of behavior can be explained by a curve obtained from experiments [62]. As shown in Figure 4.4, the relationship between ultimate strength capacity reduction and compressive strength is changed by increasing reinforcement ratio. Studying dependency of the elements with different reinforcement ratios to  $f'_c$  show that our results follow the same pattern. Significant reductions are for higher reinforcement ratios in all levels of degradation since they become more dependent on  $f'_c$ .

Table 4.2: Ultimate strength capacity reduction of elements R1, R2, R3, and R4 in different levels of degradation when shear loading increases

Loading Scenario <sup>b</sup>	Degradation Level	Radiation n/cm <sup>2</sup>	Strength Reduction %			
			Element R1 <sup>a</sup> $\left  \frac{v_{xy}}{f_x} \right $	Element R2 $\left  \frac{v_{xy}}{f_x} \right $	Element R3 $\left  \frac{v_{xy}}{f_x} \right $	Element R4 $\left  \frac{v_{xy}}{f_x} \right $
			1 2 4	1 2 4	1 2 4	1 2 4
BT	D1	$2 \times 10^{19}$	0 0 0	0 0 0	0 0 0	0 4 4
	D2	$2 \times 10^{20}$	0 0 0	0 0 0	0 0 5	5 21 22
	D3	$2 \times 10^{21}$	0 0 0	0 11 22	13 40 39	39 51 51
BTC	D1	$2 \times 10^{19}$	2 1 0	2 1 0	1 2 2	2 4 4
	D2	$2 \times 10^{20}$	6 1 1	0 4 0	4 7 10	8 17 17
	D3	$2 \times 10^{21}$	10 10 9	9 28 33	27 41 47	47 52 52
UT	D1	$2 \times 10^{19}$	2 0 0	0 0 0	1 0 0	1 4 4
	D2	$2 \times 10^{20}$	6 0 0	0 1 1	1 3 6	6 16 17
	D3	$2 \times 10^{21}$	3 2 14	9 21 28	25 38 44	45 51 52

<sup>a</sup> Elements R1, R2, R3, and R4 have reinforcement ratios equal to 0.9, 1.35, 1.88, 3 % respectively.

<sup>b</sup> BT, BTC, and UT represents shear-biaxial tension, shear-biaxial tension-compression, and shear-uniaxial tension loading conditions.

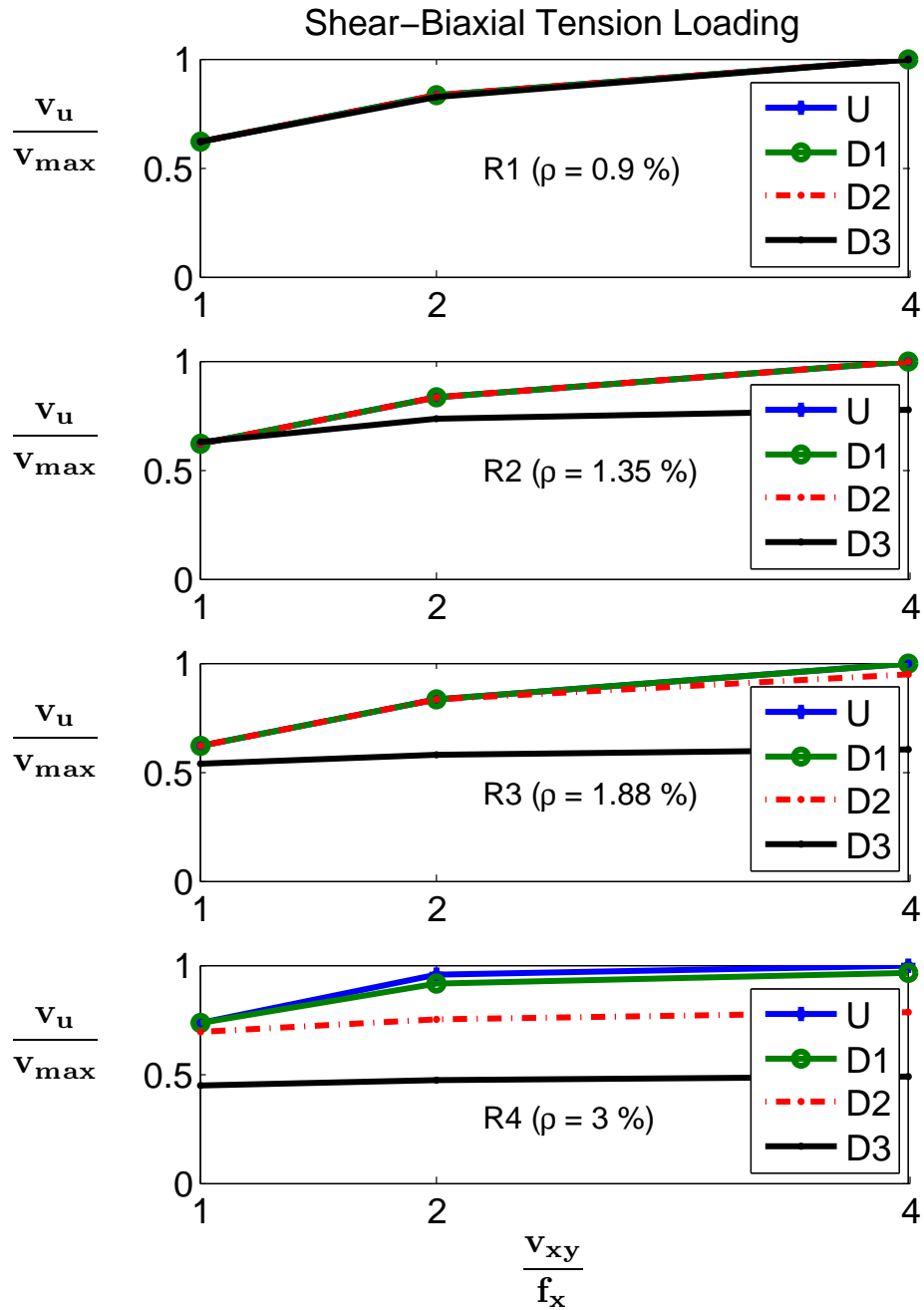


Figure 4.3: Effect of reinforcement ratio and shear-biaxial tension loading ratio in different levels of radiation (normalized)



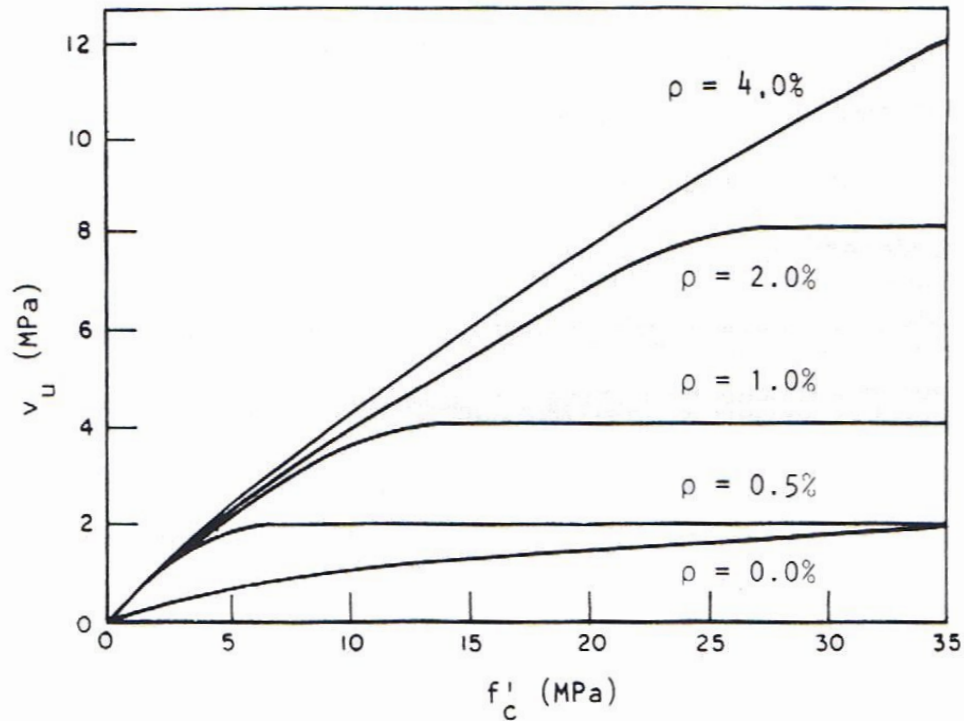


Figure 4.4: Ultimate shear stress changes with reinforcement ratio and compressive strength[62]

As Figure 4.5 shows, ultimate strength capacity of low reinforced members are not affected by low levels of degradation since  $f'_c$  is around 26 and 20 MPa for degradation levels 1 and 2. In this range of  $f'_c$ , elements R1 and R2 still have a constant shear capacity, which is not dependent on compressive strength value.

#### 4.2.2 Elements Not Subjected to Tension

Shear capacity reduction of RC panels subjected to shear-biaxial and shear-uniaxial compression are shown in Figures A.4 and A.3 available in Appendix A, respectively. As shown in Table 4.3, maximum reduction values of 29 and 62 % are available for degradation levels 2 and 3, respectively. RC panels under uniaxial compression loading conditions show the same pattern as the elements under shear-biaxial compression with the maximum reduction values of 18 and 52 % on degradation levels 2 and 3, respectively.

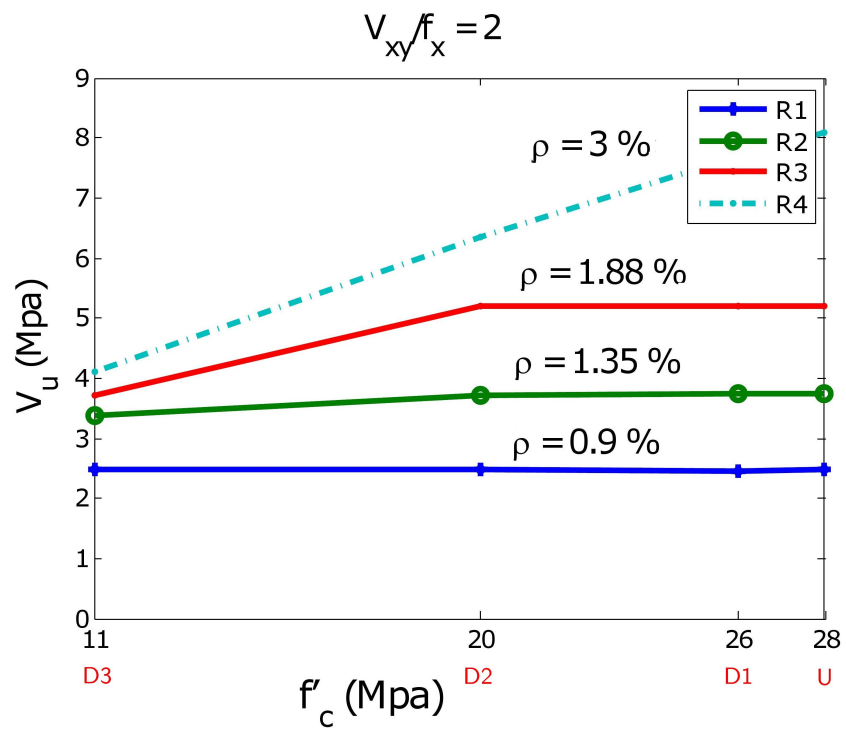


Figure 4.5: Ultimate shear stress changes with reinforcement ratio and compressive strength for the elements under biaxial tension loading with loading 1:1:2

Table 4.3: Ultimate strength capacity reduction of elements R1, R2, R3, and R4 in different levels of degradation when shear loading increases

Loading Scenario <sup>b</sup>	Degradation Level	Radiation n/cm <sup>2</sup>	Element R1 <sup>a</sup>	Element R2	Element R3	Element R4
			$\left  \frac{v_{xy}}{f_x} \right $	$\left  \frac{v_{xy}}{f_x} \right $	$\left  \frac{v_{xy}}{f_x} \right $	$\left  \frac{v_{xy}}{f_x} \right $
			1 2 4	1 2 4	1 2 4	1 2 4
Strength Reduction %						
BC	D1	$2 \times 10^{19}$	6 0 0	6 4 0	6 5 4	6 5 4
	D2	$2 \times 10^{20}$	29 17 0	29 22 17	29 23 22	29 24 23
	D3	$2 \times 10^{21}$	62 48 28	62 52 48	62 54 52	61 55 54
UC	D1	$2 \times 10^{19}$	1 0 0	2 3 0	4 4 4	5 4 4
	D2	$2 \times 10^{20}$	6 0 0	12 9 2	17 16 16	18 17 18
	D3	$2 \times 10^{21}$	36 26 19	49 46 40	53 52 51	55 53 53

<sup>a</sup> Elements R1, R2, R3, and R4 have reinforcement ratios equal to 0.9, 1.35, 1.88, 3 % respectively.

<sup>b</sup> BC and UC represents shear-biaxial compression and shear-uniaxial compression loading conditions.

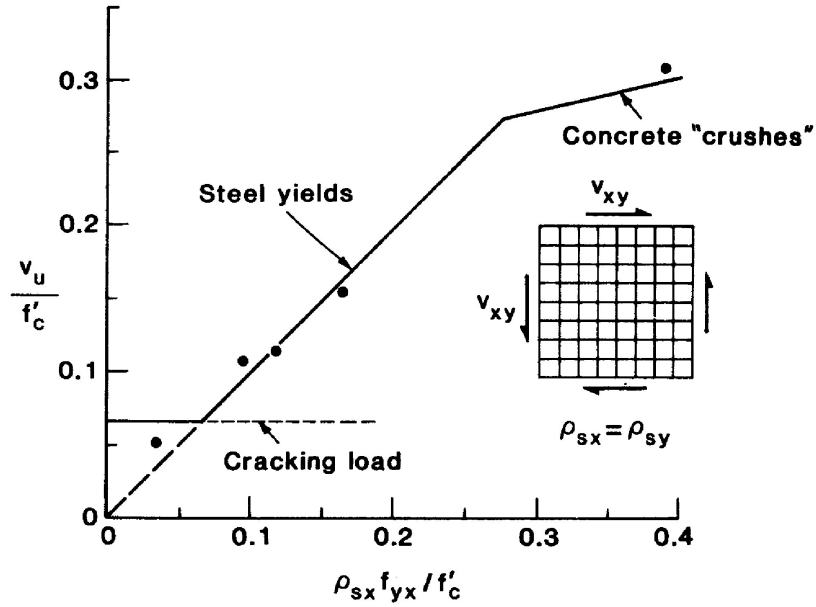


Figure 4.6: Shear strength variation when reinforcement increases in  $x$  and  $y$  directions[63]

### 4.3 Failure Mode Changes

Failure mode of RC panels subjected to pure shear loading can be divided into three areas based on reinforcement ratio [63]. The first area is related to the elements with very low amount of reinforcement in which cracking load is responsible for failure. When tension becomes greater than the tensile strength of concrete, crack happens. Cracking shear stress is the location when the crack starts propagating in the RC panels. The value of  $V_{cr}$  of concrete is not affected by reinforcement ratio since it is more related to aggregate interlock in concrete. Reinforcement becomes effective after cracking for controlling crack propagation in the RC members. Magnitude of cracking shear stress of the elements is not significant compared to that of the ultimate shear stress.

The second area covers a large interval of reinforcing steel ratio where yielding of steel governs the failure ( $\frac{V_u}{f'_c} = \frac{\rho_{sx} f_{yx}}{f'_c}$ ). The third area is for highly reinforced members that experience concrete crushing because of shear. Figure 4.6 shows experimental results from panels tested by Vecchio et al [63].

Failure mode of RC panels are changed from yielding steel to concrete crushing when they are exposed to critical levels of radiation. In order to study the failure mode of undegraded and degraded elements, the elements under pure shear loading are compared in Figure 4.7. Figure 4.7 shows that slope of the curve decreases when level of degradation

Table 4.4: Slope of the line between different reinforcement ratios

Degradation level	m1 <sup>a</sup>	m2	m3
U	1	1	<b><u>0.25</u></b>
D1	1	<b><u>0.93</u></b>	<b><u>0.21</u></b>
D2	1	<b><u>0.30</u></b>	<b><u>0.16</u></b>
D3	<b><u>0.19</u></b>	<b><u>0.12</u></b>	<b><u>0.08</u></b>

<sup>a</sup> m1, m2, and m3 represent slope of the line between elements R1-R2, R2-R3, and R3-R4 respectively.

increases. Yielding of steel governs failure of the elements as long as slope of the line in Figure 4.7 is equal to one. Table 4.4 provides information on the change in the slope for each level of degradation for different reinforcement ratio. Degradation level 3 changes failure mode of all elements with reinforcement ratios between 0.9 and 3% considerably. Degradation level 2 affects failure mode of elements with reinforcement ratios between 1.35 and 3 % significantly. Failure mode of elements with reinforcement ratio between 1.88 and 3 % is not affected significantly in degradation level 1 ( $2 \times 10^{19}$  fast neutron radiation).

It can be concluded that failure mode of elements with high reinforcement ratios ( $\rho = 3\%$ ) are more affected by lower levels of degradation than elements with lower reinforcement ratios. In other words, less reinforcement ratio is required in high levels of degradation to cause the element to be over-reinforced.

## 4.4 Ductility Index Reduction

Ductility is a factor that shows the capability of material, section, structural element, or structural system to have large deformation before failure happens. There are two types of ductility: material or structural ductility. Structural ductility can be categorized to curvature, rotation, and deflection ductility. In this section, we discuss structural deflection ductility.

Structural deflection ductility is computed by dividing the ultimate strain by the yield strain ( $\mu_u = \frac{\epsilon_u}{\epsilon_y}$ ). Members with low ductility index have brittle failure; so it is always desirable for designer to control this factor by an appropriate limit. For example, val-

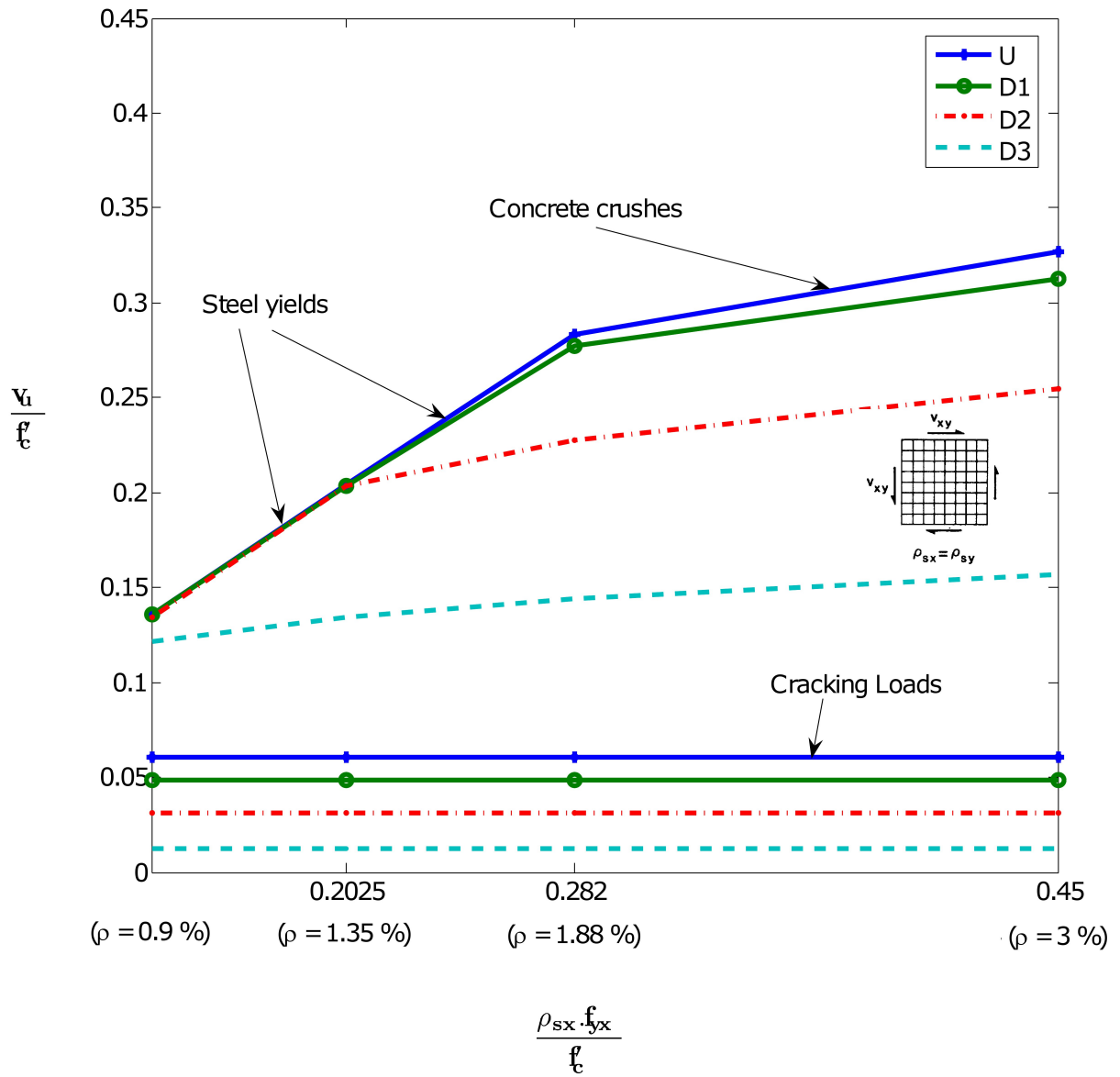


Figure 4.7: Failure mode changes when reinforcement ratio increases in different levels of degradation

ues between 1.5 and 2.5 are suggested by Newmark [50]. Since the range suggested by Newmark is not conservative enough for NPPs codes, Applied Technology Council(ATC) recommends a ductility factor between 3 and 4 [19]. Factors influence structural ductility in RC members are numerated bellow [46]:

1. Reinforcement ratio
2. Compressive strength
3. Compressive stress-strain relationship
4. Tensile stress-strain relationship
5. Ratio of axial load in combined loading
6. Geometry of the section

Effect of radiation on ductility index for elements with different reinforcement ratios when shear loading increases is studied in this section. Yielding and ultimate points of the analysis results are retrieved from the stress-strain curves to compute ductility index of the elements. Figure 4.8 shows that the ductility index reduction is decreased significantly by increasing the level of degradation for elements R1, R2, and R3. However, the rate of reduction is decreased for element R4. The results coincide with the fact that there is no yielding of steel before failure for highly reinforced elements; so ductility index of the elements is actually the ultimate strain over a point close to ultimate. It makes the value of ductility index of these elements around 1. However, it is not possible physically to have ductility index around one and it is theoretically achieved by the theory.

Ductility reduction rate is decreased by increasing ratio  $\frac{v_{xy}}{f_x}$  and there is no ductility reduction for highly reinforced members by increasing the level of degradation when shear loading is 2 or 4 times greater than the the axial loading.

Table 4.5 shows non-normalized values of the ductility index for elements R1, R2, R3, and R4 in different levels of degradation. As shown in Table 4.5, the ductility index of the elements decrease to the values below ATC range when degradation increases. Ductility reduction reaches at the critical values below 3 when shear loading increases. Ductility index values below allowable values are highlighted in Table 4.5.

Ductility of RC panels that are highly reinforced ( $\rho > 1.88$ ) do not affected by radiation since they have low ductility. Ductility of the elements with reinforcement ratio between 0.9 and 1.35 % reduced to the values below than allowable ductility of RC structures in NPPs. It can be concluded that radiation may affects design considerations of ductility of the RC structures exposed to high levels of radiation considerably.

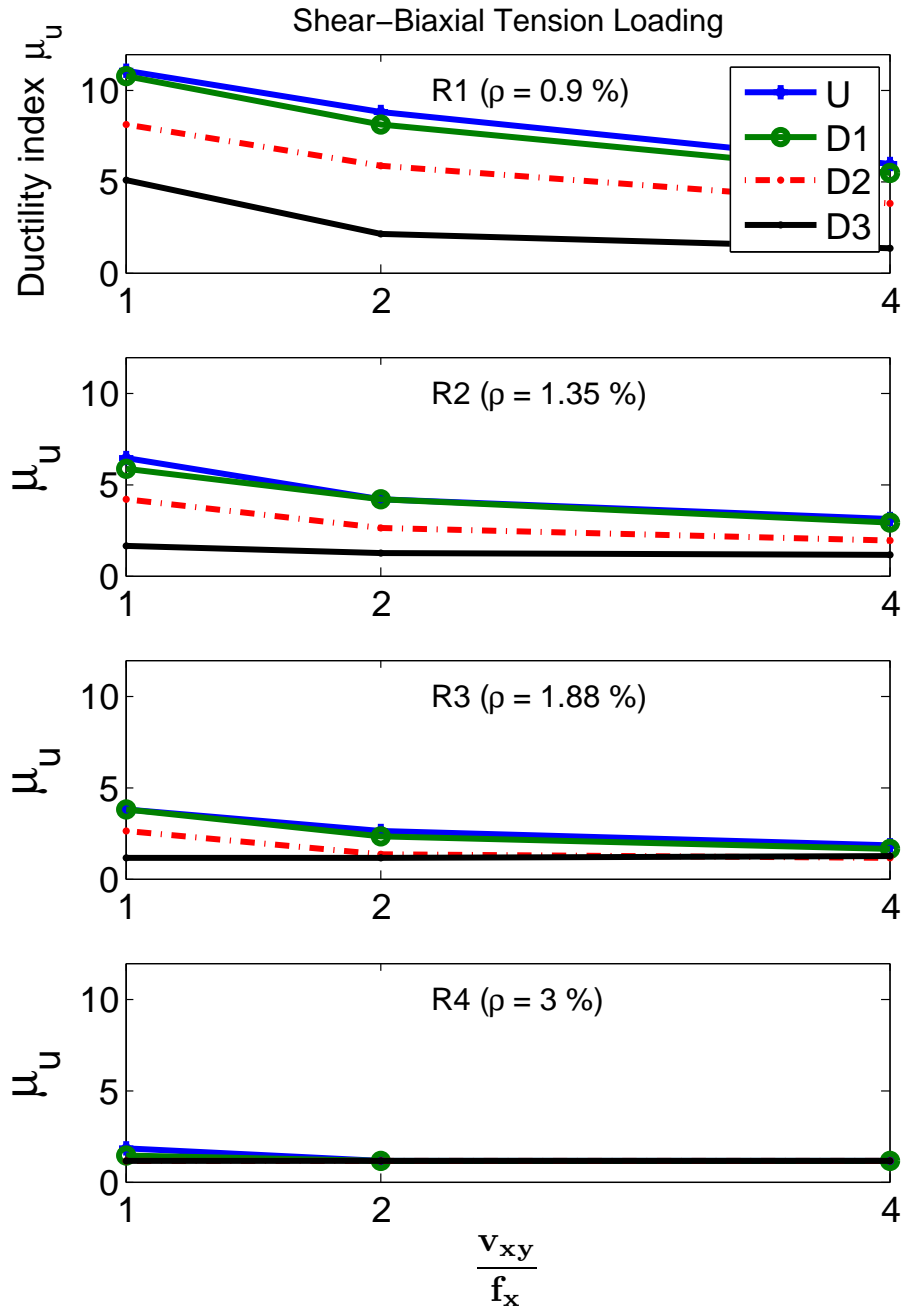


Figure 4.8: Ductility index for elements with different reinforcement ratio as degradation level and  $\frac{v_{xy}}{f_x}$  increases



Table 4.5: Ductility index of elements R1, R2, R3, and R4 in different levels of degradation when shear loading increases

Load <sup>d</sup>	Degradation Level	$\mu_u$											
		Element R1 <sup>a</sup>		Element R2		Element R3		Element R4					
BT	U	L111 <sup>b</sup>	L112	L114	L111	L112	L114	L111	L112	L114	L111	L112	L114
	D1	11.04	8.84	5.91	6.44	4.18	3.14	3.8	<b>2.59</b> <sup>c</sup>	<b>1.77</b>	<b>1.77</b>	<b>1.1</b>	<b>1</b>
	D2	10.73	8.08	5.48	5.87	4.18	<b>2.85</b>	3.8	<b>2.36</b>	<b>1.61</b>	<b>1.46</b>	<b>1.1</b>	<b>1.1</b>
	D3	8.15	5.85	3.8	4.18	<b>2.59</b>	<b>1.95</b>	<b>2.6</b>	<b>1.33</b>	<b>1.1</b>	<b>1.1</b>	<b>1.1</b>	<b>1.1</b>
BTC	U	5.04	<b>2.14</b>	<b>1.33</b>	<b>1.61</b>	<b>1.21</b>	<b>1.1</b>	<b>1.1</b>	<b>1</b>	<b>1.21</b>	<b>1.1</b>	<b>1.1</b>	<b>1.2</b>
	D1	8.03	4.18	4.18	4.59	<b>1.77</b>	<b>1.95</b>	<b>2.59</b>	<b>1.33</b>	<b>1.21</b>	<b>1.33</b>	<b>1.1</b>	<b>1.1</b>
	D2	8.03	3.45	3.8	3.8	<b>1.77</b>	<b>1.77</b>	<b>2.36</b>	<b>1.33</b>	<b>1.1</b>	<b>1.33</b>	<b>1.1</b>	<b>1.1</b>
	D3	7.4	<b>2.59</b>	<b>2.85</b>	3.14	<b>1.46</b>	<b>1.21</b>	<b>2.14</b>	<b>1.21</b>	<b>1.1</b>	<b>1.1</b>	<b>1.1</b>	<b>1.1</b>
UT	U	3.14	<b>1.61</b>	<b>1.1</b>	<b>1.33</b>	<b>1.21</b>	<b>1.1</b>	<b>1.21</b>	<b>1.1</b>	<b>1.1</b>	<b>1.21</b>	<b>1.1</b>	<b>1.1</b>
	D1	8.6	5.93	5.03	4.18	3.14	<b>2.85</b>	<b>2.14</b>	<b>1.61</b>	<b>1.46</b>	<b>1.33</b>	<b>1.1</b>	<b>1.1</b>
	D2	8.63	5.48	4.6	3.45	<b>2.59</b>	<b>2.59</b>	<b>1.77</b>	<b>1.33</b>	<b>1.33</b>	<b>1.21</b>	<b>1.1</b>	<b>1.1</b>
	D3	7.66	3.8	3.45	<b>2.59</b>	<b>1.95</b>	<b>1.95</b>	<b>1.46</b>	<b>1.21</b>	<b>1.1</b>	<b>1.1</b>	<b>1.1</b>	<b>1.1</b>

<sup>a</sup> Elements R1, R2, R3, and R4 have reinforcement ratios equal to 0.9, 1.35, 1.88, 3 % respectively.

<sup>b</sup> L111, L112, and L114 are loading condition with the value  $\frac{v_{xy}}{f_x}$  equals to 1, 2, and 4 respectively.

<sup>c</sup> Highlighted values are values below limitation of 3 for ductility index

<sup>d</sup> BT, BTC, and UT represent shear-biaxial tension, shear-biaxial tension-compression, and shear-uni-axial tension loading conditions

# Chapter 5

## Conclusion and Further Research Recommendations

### 5.1 Conclusion

In this thesis we investigated the behavior of Reinforced Concrete (RC) structures exposed to the critical levels of radiation in Nuclear Power Plants (NPPs). An RC panel with in-plane stresses was found to be the most representative scale element for RC structures in NPPs. 288 RC panels were analyzed under pure shear and combination of shear-axial loading conditions. RC panels were selected by choosing appropriate geometrical, material, and loading properties in NPPs. The elements were analyzed with a nonlinear finite element program Membrane-2000, developed in the University of Toronto based on the Modified Compression Field Theory. We divided the elements responses into three categories:

1. RC panels subjected to pure shear loading (p)
2. The elements subjected to tension: RC panels subjected to shear-biaxial tension (BT), shear-biaxial tension-compression (BTC), and shear-uniaxial tension(UT) loading conditions
3. The elements not subjected to tension: RC panels subjected to shear-biaxial compression (BC) and shear-uniaxial compression (UC) loading conditions

We analyzed three significant effects of radiation on RC panels in this study: ultimate strength capacity reduction, changing failure mode from yielding steel to concrete crushing, and ductility reduction. Ultimate strength reduction was calculated for the elements in categories 2 and 3. Failure modes of the 48 RC panels under pure shear loading, which were

in category 1, were analyzed. We also reviewed the ductility reduction of the elements in the category 2. The following conclusions have been made regarding the effects of critical levels of radiation on RC structures in NPPs:

- Ultimate strength capacity reduction for the elements subjected to tension:
  - The low reinforced elements ( $\rho = 0.9\%$ ) were not affected by the critical levels of radiation between  $2 \times 10^{19}$  and  $2 \times 10^{21}$ .
  - Shear strength capacity reduction of RC the panels was increased by increasing reinforcement ratio from 1.35 % to 3 %.
  - Ultimate strength capacity was reduced by 51 %, which is significant, for highly reinforced concrete elements ( $\rho > 1.88\%$ ) when radiation was equal to  $2 \times 10^{21}$
  - Elements with reinforcement ratio of 1.35 % had ultimate strength reduction values from 11 % to 22 % by radiation degradation when shear-axial loading ratio  $\frac{V_{xy}}{f_x}$  had values from 2 to 4.
  - Ultimate strength reduction values of the elements with reinforcement ratios of 1.88 and 3 % did not change when the loading ratio  $\frac{V_{xy}}{f_x}$  varied from 1 to 4.
  
- Ultimate strength capacity reduction for the elements not subjected to tension:
  - Ultimate strength capacity of the elements with reinforcement ratio between 0.9 and 3 % were noticeably reduced by 29% when radiation was equal to  $2 \times 10^{20}$ n/cm<sup>2</sup>
  - The elements with reinforcement ratio between 0.9 and 3 % were significantly affected in radiation  $2 \times 10^{21}$ n/cm<sup>2</sup> by 62 % ultimate strength capacity reduction.
  - The elements under uniaxial compression had strength reduction values of half the values for the elements under biaxial compression loading conditions.
  
- Failure mode changing from yielding steel to concrete crushing:

- When radiation was equal to  $2 \times 10^{21} \text{n/cm}^2$ , failure modes of the RC panels with reinforcement ratio from 0.9 to 1.88% was changed from yielding steel to concrete crushing.
- For the elements with reinforcement ratios between 1.35 and 1.88 % that were exposed to radiation more than  $2 \times 10^{20} \text{n/cm}^2$ , failure was governed by concrete crushing instead of steel yielding.
- Ductility reduction of elements subjected to tension:
  - Ductility index reduced significantly by increasing level of degradation for the elements with reinforcement ratios of 0.9, 1.35, and 1.88 %.
  - By increasing the level of radiation, ductility of the RC panels reduced to the values bellow the allowable ductility of RC structures in NPPs, which was equal to 3 based on Applied Technology Council criteria.
  - The rate of ductility reduction decreased by increasing shear-axial loading ratio.

## 5.2 Further Research Recommendations

Additional opportunities for future studies are listed bellow:

- There are a number of loading conditions assumed in this study that could change for further research. One of the most important of them is having plane stresses for the element. This assumption comes from the fact that concrete cylindrical shell containments with vessel diameter 10 times greater than vessel thickness do not require triaxial stress state. However, this might not be the case for biological shields, whose diameter is smaller than containment structures. Hence, radial shear stresses can be added to the stress term to have a result closer to the actual situation in NPPs.
- It was assumed in this study that the reinforcement ratios in  $x$  and  $y$  directions have equal values. However, the elements from the locations close to the basement of the RC walls in NPPs have different reinforcement ratios in  $x$  and  $y$  directions. The RC panels from parts of the building with discontinuity in shear and moment may be considered with different values for  $\rho_x$  and  $\rho_y$ .

- As mentioned in Section 2.5.2, the critical levels of fast neutron radiation may deteriorate chemical process in the RC panels. The effect of fast neutron radiation on chemical process of concrete can be studied for further research.
- Degraded elements, which are analyzed in this study, are deteriorated only by radiation. Since radiation and temperature deteriorate concrete at the same time, the combined effect of radiation and temperature on shear capacity of the RC panels can be studied in the future.
- The radiation fluence that is considered in this research is only from fast neutron fluxes. As mentioned in literature, certain levels of gamma radiation also may deteriorate concrete significantly. The effects of gamma radiation combined with the effects of critical fast neutron radiation levels on the RC panels in NPPs can be the subject of a separate study.

# Appendices

# Appendix A

## Ultimate strength Capacity and Ductility Reduction

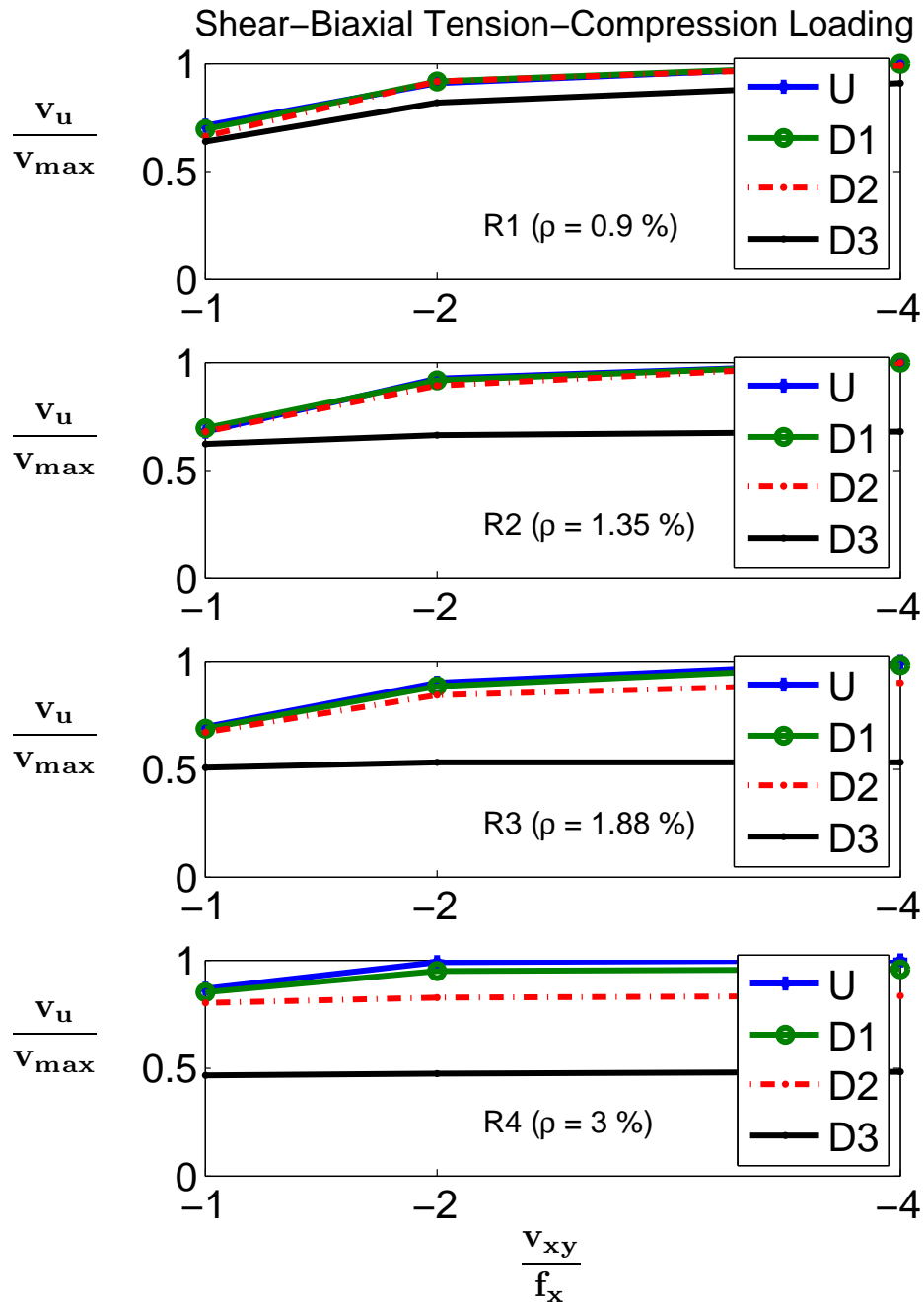


Figure A.1: Effect of reinforcement ratio and shear-biaxial tension-compression loading ratio in different levels of radiation (normalized)



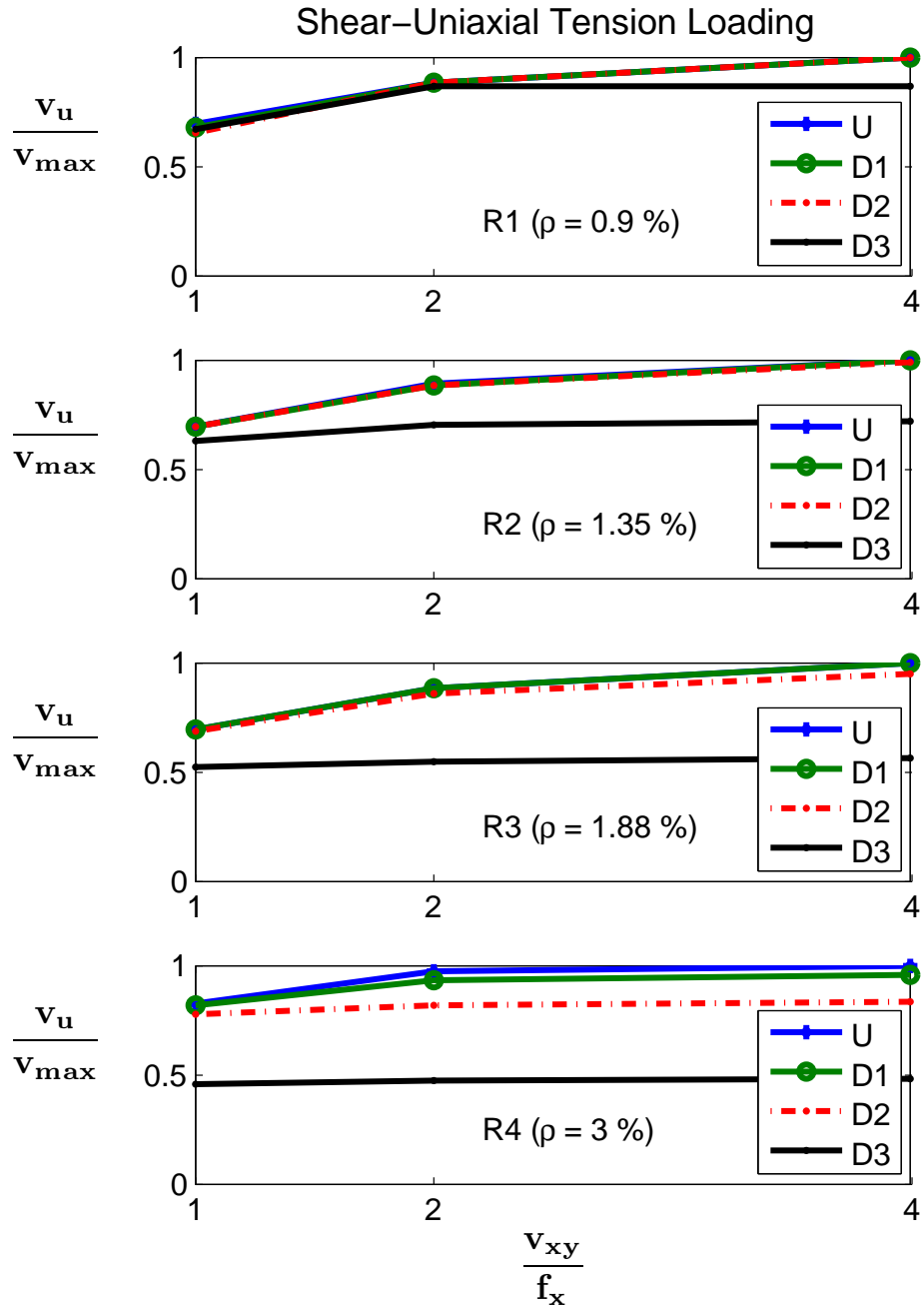


Figure A.2: Effect of reinforcement ratio and shear-uniaxial tension loading ratio in different levels of radiation (normalized)

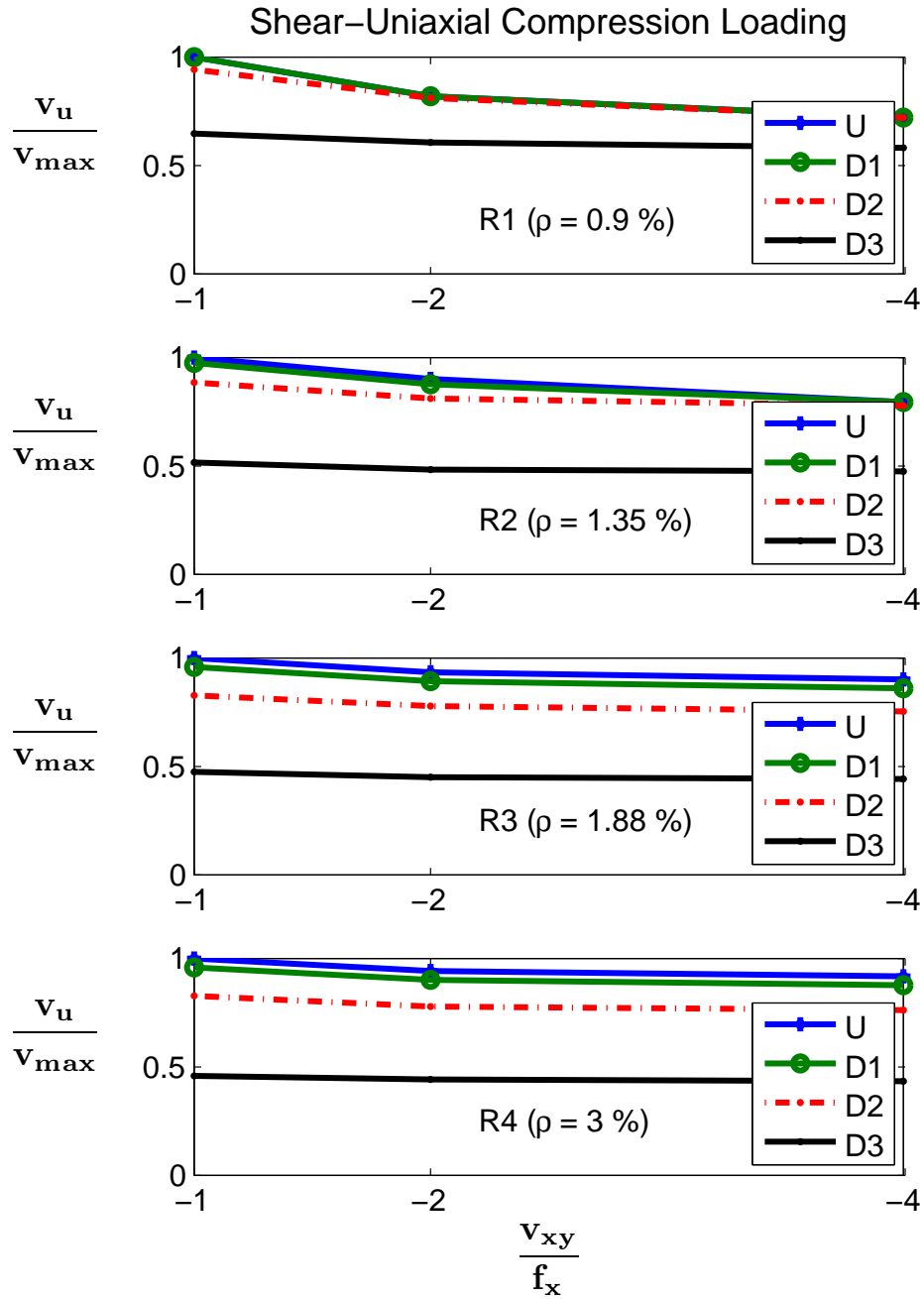


Figure A.3: Effect of reinforcement ratio and shear-uniaxial compression loading ratio in different levels of radiation (normalized)

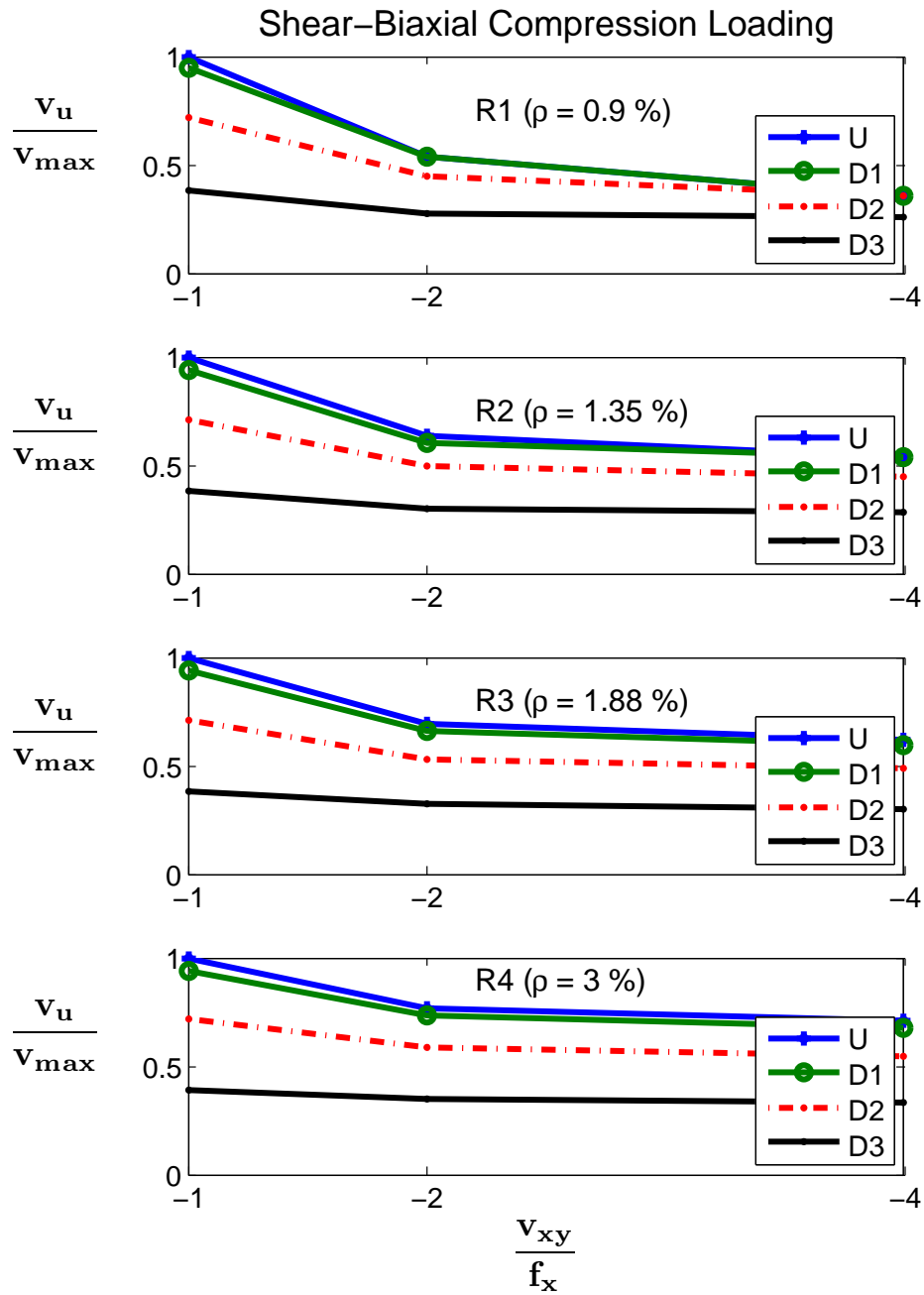


Figure A.4: Effect of reinforcement ratio and shear-biaxial compression loading ratio in different levels of radiation (normalized)

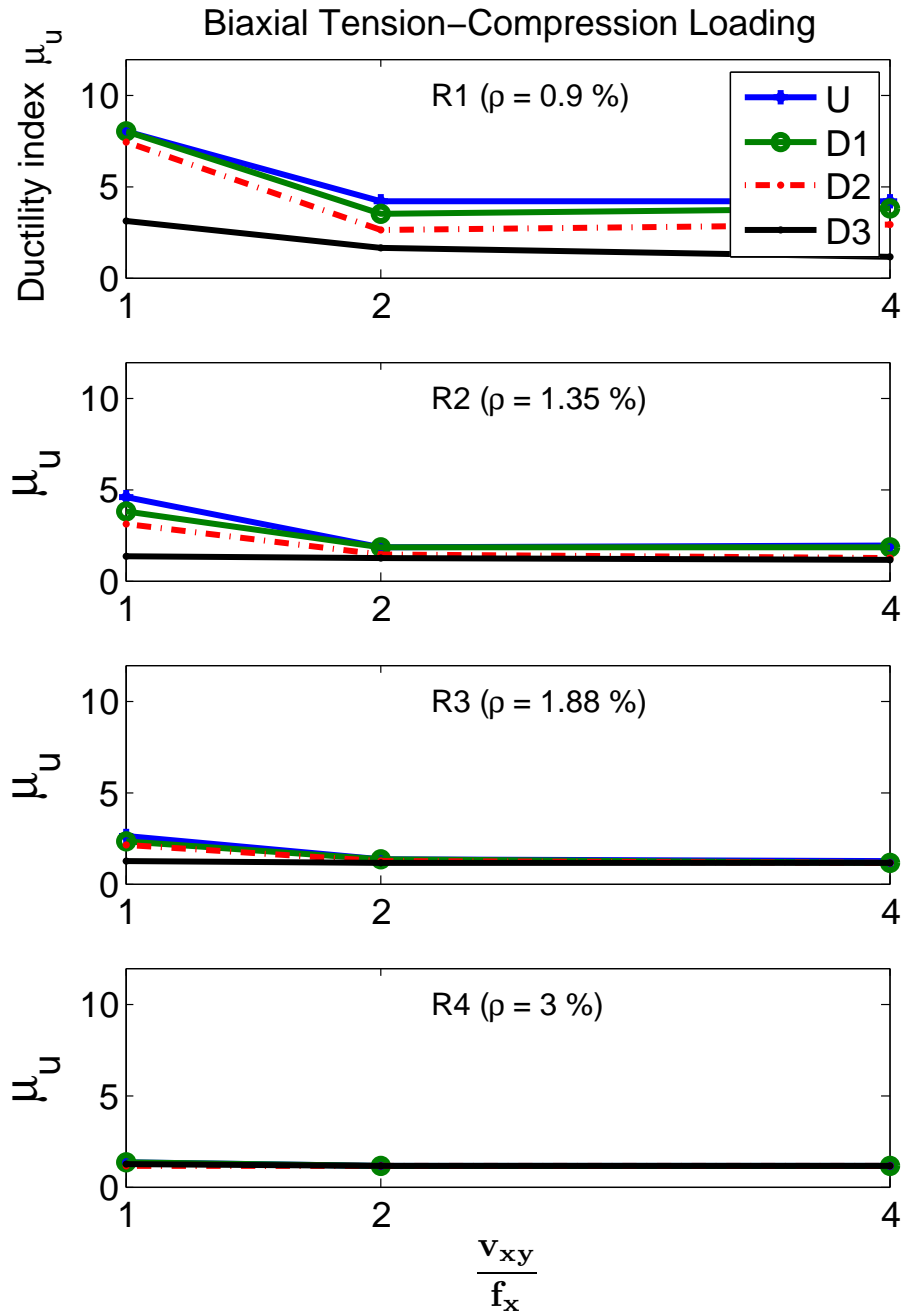


Figure A.5: Ductility reduction of the elements subjected to shear-biaxial tension-compression loading when radiation increases

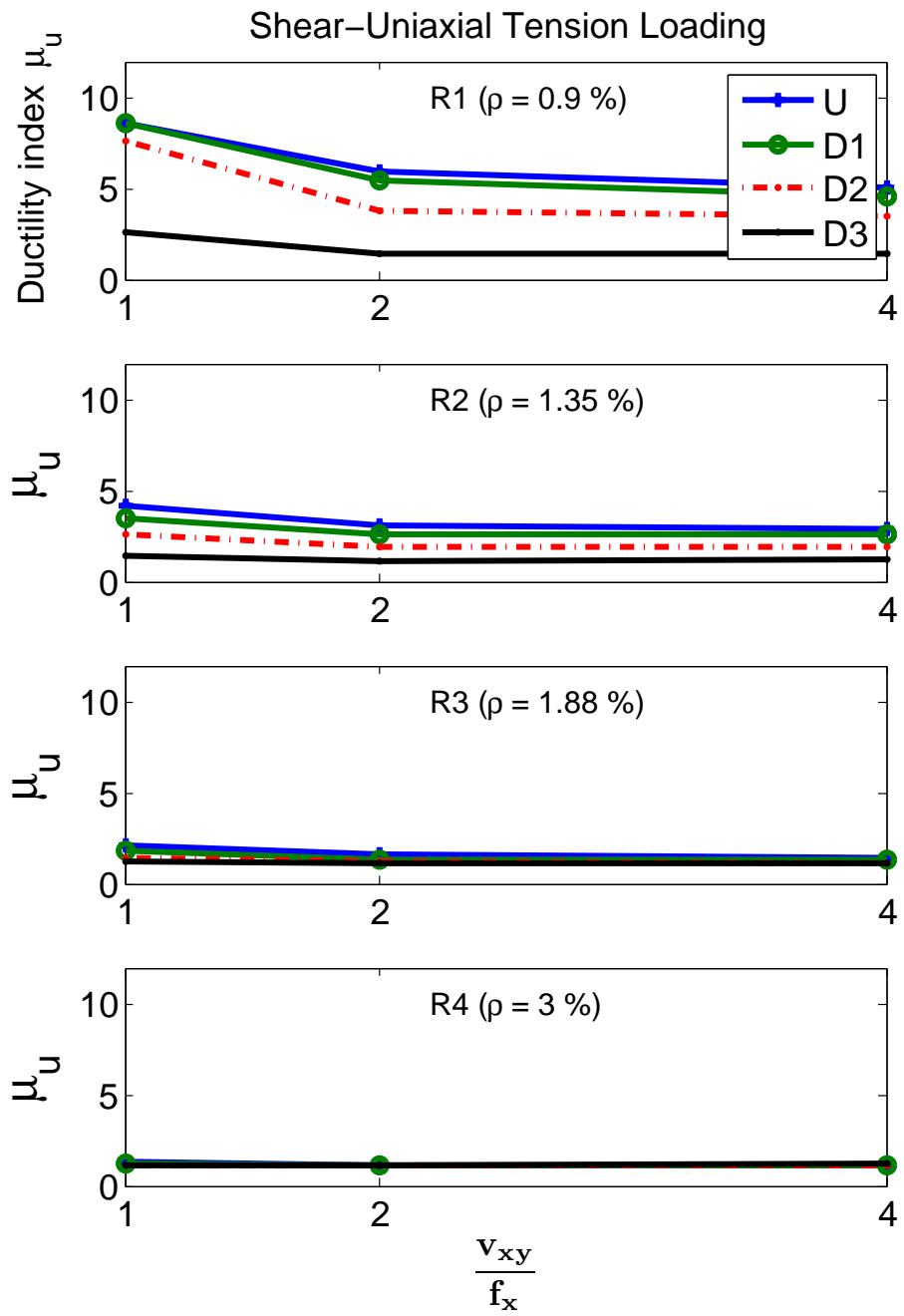


Figure A.6: Ductility reduction of the elements subjected to shear-uniaxial tension loading when radiation increases

# Appendix B

## Element Responses and Analysis

```

Total_P_BT_BC;

%-----
%-----
%-----Responses of Elements Subjected to P-BT-BTC-----
%-----
%-----

MuTT = zeros (4,28);
VcrTT = zeros (4,28);
VuTT = zeros (4,28);

e1_TT = zeros(4,28);
s1_TT = zeros(4,28);

e2_TT = zeros(4,28);
s2_TT = zeros(4,28);

e3_TT = zeros(4,28);
s3_TT = zeros(4,28);

e4_TT = zeros(4,28);
s4_TT = zeros(4,28);

e5_TT = zeros(4,28);
s5_TT = zeros(4,28);

for cc = 1:112

    switch cc
%-----
%-----          Element R1-----
%-----

        case 1
            DR=U_PR1_L001;
        case 2
            DR=D11_PR1_L001;
        case 3
            DR=D22_PR1_L001;
        case 4
            DR=D33_PR1_L001;
%-----Tension Loading-R1-----

        case 5
            DR=U_BTR1_L111;
        case 6
            DR=D11_BTR1_L111;
        case 7
            DR=D22_BTR1_L111;
        case 8
            DR=D33_BTR1_L111;

        case 9
            DR=U_BTR1_L112;
        case 10
            DR=D11_BTR1_L112;
        case 11
            DR=D22_BTR1_L112;
        case 12
            DR=D33_BTR1_L112;

        case 13
            DR=U_BTR1_L114;
        case 14
            DR=D11_BTR1_L114;
        case 15
            DR=D22_BTR1_L114;
    end
end

```

```

case 16
  DR=D33_BTR1_L114;

  %-----Compression Loading--R1-----

case 17
  DR=U_BCR1_L111;
case 18
  DR=D11_BCR1_L111;
case 19
  DR=D22_BCR1_L111;
case 20
  DR=D33_BCR1_L111;

case 21
  DR=U_BCR1_L112;
case 22
  DR=D11_BCR1_L112;
case 23
  DR=D22_BCR1_L112;
case 24
  DR=D33_BCR1_L112;

case 25
  DR=U_BCR1_L114;
case 26
  DR=D11_BCR1_L114;
case 27
  DR=D22_BCR1_L114;
case 28
  DR=D33_BCR1_L114;

%-----
%----- Element R2-----
%-----

case 29
  DR=U_PR2_L001;
case 30
  DR=D11_PR2_L001;
case 31
  DR=D22_PR2_L001;
case 32
  DR=D33_PR2_L001;

%-----Tension Loading--R2-----

case 33
  DR=U_BTR2_L111;
case 34
  DR=D11_BTR2_L111;
case 35
  DR=D22_BTR2_L111;
case 36
  DR=D33_BTR2_L111;

case 37
  DR=U_BTR2_L112;
case 38
  DR=D11_BTR2_L112;
case 39
  DR=D22_BTR2_L112;
case 40
  DR=D33_BTR2_L112;

case 41

```



```

DR=U_BTR2_L114;
case 42
DR=D11_BTR2_L114;
case 43
DR=D22_BTR2_L114;
case 44
DR=D33_BTR2_L114;

%-----Compression Loading--R2-----

case 45
DR=U_BCR2_L111;
case 46
DR=D11_BCR2_L111;
case 47
DR=D22_BCR2_L111;
case 48
DR=D33_BCR2_L111;

case 49
DR=U_BCR2_L112;
case 50
DR=D11_BCR2_L112;
case 51
DR=D22_BCR2_L112;
case 52
DR=D33_BCR2_L112;

case 53
DR=U_BCR2_L114;
case 54
DR=D11_BCR2_L114;
case 55
DR=D22_BCR2_L114;
case 56
DR=D33_BCR2_L114;

%-----
%----- Element R3-----
%-----

case 57
DR=U_PR3_L001;
case 58
DR=D11_PR3_L001;
case 59
DR=D22_PR3_L001;
case 60
DR=D33_PR3_L001;

%-----Tension Loading-----

case 61
DR=U_BTR3_L111;
case 62
DR=D11_BTR3_L111;
case 63
DR=D22_BTR3_L111;
case 64
DR=D33_BTR3_L111;

case 65
DR=U_BTR3_L112;
case 66
DR=D11_BTR3_L112;
case 67
DR=D22_BTR3_L112;
case 68

```

```

DR=D33_BTR3_L112;

case 69
DR=U_BTR3_L114;
case 70
DR=D11_BTR3_L114;
case 71
DR=D22_BTR3_L114;
case 72
DR=D33_BTR3_L114;

%-----Compression Loading--R3-----

case 73
DR=U_BCR3_L111;
case 74
DR=D11_BCR3_L111;
case 75
DR=D22_BCR3_L111;
case 76
DR=D33_BCR3_L111;

case 77
DR=U_BCR3_L112;
case 78
DR=D11_BCR3_L112;
case 79
DR=D22_BCR3_L112;
case 80
DR=D33_BCR3_L112;

case 81
DR=U_BCR3_L114;
case 82
DR=D11_BCR3_L114;
case 83
DR=D22_BCR3_L114;
case 84
DR=D33_BCR3_L114;

%-----
%----- Element R4-----
%-----

case 85
DR=U_PR4_L001;
case 86
DR=D11_PR4_L001;
case 87
DR=D22_PR4_L001;
case 88
DR=D33_PR4_L001;

%-----Tension Loading--R4-----

case 89
DR=U_BTR4_L111;
case 90
DR=D11_BTR4_L111;
case 91
DR=D22_BTR4_L111;
case 92
DR=D33_BTR4_L111;

case 93
DR=U_BTR4_L112;

```

```

    case 94
        DR=D11_BTR4_L112;
    case 95
        DR=D22_BTR4_L112;
    case 96
        DR=D33_BTR4_L112;

    case 97
        DR=U_BTR4_L114;
    case 98
        DR=D11_BTR4_L114;
    case 99
        DR=D22_BTR4_L114;
    case 100
        DR=D33_BTR4_L114;

%-----Compression Loading--R4-----
    case 101
        DR=U_BCR4_L111;
    case 102
        DR=D11_BCR4_L111;
    case 103
        DR=D22_BCR4_L111;
    case 104
        DR=D33_BCR4_L111;

    case 105
        DR=U_BCR4_L112;
    case 106
        DR=D11_BCR4_L112;
    case 107
        DR=D22_BCR4_L112;
    case 108
        DR=D33_BCR4_L112;

    case 109
        DR=U_BCR4_L114;
    case 110
        DR=D11_BCR4_L114;
    case 111
        DR=D22_BCR4_L114;
    case 112
        DR=D33_BCR4_L114;

    end

m = size(DR);
for n = (1:m(:,1))
    if DR(n+1,2) < DR(n,2)
        P1 = n;
        e1 = DR(n,1);
        s1 = DR(n,2);
        break;
    end
end

m = size(DR);
strange=0;
for n = (P1+1:m(:,1))
    if (n==m(:,1))
        strange=1;
        break
    end
    if DR(n+1,2) > DR(n,2)
        P2 = n;

```

```

        e2 = DR(n,1);
        s2 = DR(n,2);
        break;
    end
end

if (strange)
    e2 = e1;
    s2 = s1;
    P2 = P1;
    e3 = DR(m(:,1),1);
    s3 = DR(m(:,1),2);
    e4 = e3;
    s4 = s3;

    for n=10:P2
        slope1 = (DR(n+1,2)- DR(n,2))/(DR(n+1,1)- DR(n,1));
        slope2 = (DR(n+2,2)- DR(n+1,2))/(DR(n+2,1)- DR(n+1,1));
        if (slope2/slope1<0.7)
            P1= n;
            e1= DR(n,1);
            s1= DR(n,2);
            break;
        end
    end

end

else

    t = 0;
    for n = (P2+1:m(:,1))
        slope1 = (DR(n+1,2)- DR(n,2))/(DR(n+1,1)- DR(n,1));
        if slope1 > .2
            t = 1;
        end
        if slope1 < .1 && t == 1

            P3 = n;
            e3 = DR(n,1);
            s3 = DR(n,2);
            break;
        end
    end

end

e4 = DR(m(:,1),1);
s4 = DR(m(:,1),2);

for n = (P3+1:m(:,1)-2)
    slope1 = (DR(n+1,2)- DR(n,2))/(DR(n+1,1)- DR(n,1));
    slope2 = (DR(n+2,2)- DR(n+1,2))/(DR(n+2,1)- DR(n+1,1));

    if slope1 <-.05 && slope2 <-.05

        P4 = n;
        e4 = DR(n,1);
        s4 = DR(n,2);
        break;
    end
end

end

end

e5 = DR(m(:,1),1);
s5 = DR(m(:,1),2);

Vcr = s1;
Cn = floor((cc-1)/4)+1;
VcrTT((4-(4*Cn-cc)),Cn) = Vcr;

```

```

vu1 = max(s1,s2);
vu2 = max(s3,s4);

Vu = max(vu1,vu2);
Cn = floor((cc-1)/4)+1;
VuTT((4-(4*Cn-cc)),Cn) = Vu;

Cn = floor((cc-1)/4)+1;
e1_TT((4-(4*Cn-cc)),Cn) = e1;

Cn = floor((cc-1)/4)+1;
s1_TT((4-(4*Cn-cc)),Cn) = s1;

Cn = floor((cc-1)/4)+1;
e2_TT((4-(4*Cn-cc)),Cn) = e2;

Cn = floor((cc-1)/4)+1;
s2_TT((4-(4*Cn-cc)),Cn) = s2;

Cn = floor((cc-1)/4)+1;
e3_TT((4-(4*Cn-cc)),Cn) = e3;

Cn = floor((cc-1)/4)+1;
s3_TT((4-(4*Cn-cc)),Cn) = s3;

Cn = floor((cc-1)/4)+1;
e4_TT((4-(4*Cn-cc)),Cn) = e4;

Cn = floor((cc-1)/4)+1;
s4_TT((4-(4*Cn-cc)),Cn) = s4;

Cn = floor((cc-1)/4)+1;
e5_TT((4-(4*Cn-cc)),Cn) = e5;

Cn = floor((cc-1)/4)+1;
s5_TT((4-(4*Cn-cc)),Cn) = s5;

if e3 == e5
    Mu = e2/e1;
else
    Mu = e4/e3;
end

Cn = floor((cc-1)/4)+1;
MuTT((4-(4*Cn-cc)),Cn) = Mu;

end

```

```

Cases_P_BT_BC;

%-----
%-----
%-----Normalized Strength Reduction -----
%-----
%-----

VuTT_R1_BT123 = [VuTT(:,2) VuTT(:,3) VuTT(:,4)];
VuTT_R2_BT123 = [VuTT(:,9) VuTT(:,10) VuTT(:,11)];
VuTT_R3_BT123 = [VuTT(:,16) VuTT(:,17) VuTT(:,18)];
VuTT_R4_BT123 = [VuTT(:,23) VuTT(:,24) VuTT(:,25)];

x = [1 2 4];

subplot(4,1,1)
a1 = max(max(VuTT_R1_BT123(1,:)),max(VuTT_R1_BT123(2,:)));
a2 = max(max(VuTT_R1_BT123(3,:)),max(VuTT_R1_BT123(4,:)));
a3 = max(a1,a2);
plot(x,VuTT_R1_BT123(1,:)/a3,'*-',x,VuTT_R1_BT123(2,:)/a3,'o-',x,VuTT_R1_BT123(3,:)/a3,'.-',x,VuTT_R1_BT123(4,:)/a3,'.-');
title('Shear-Biaxial Tension Loading ','fontsize',15)
ylabel('$$\mathbf{\frac{v_u}{v_{max}}}\hspace{1.5cm}$$','fontsize',15,'interpreter','latex','rotation',0)
legend('U','D1','D2','D3',4)
axis([1 4 0 1])
set(gca,'xtick',x,'fontsize',15)
text(2.2,.5, 'R1 (\rho = 0.9 %)','fontsize',13)

subplot(4,1,2)
b1 = max(max(VuTT_R2_BT123(1,:)),max(VuTT_R2_BT123(2,:)));
b2 = max(max(VuTT_R2_BT123(3,:)),max(VuTT_R2_BT123(4,:)));
b3 = max(b1,b2);
plot(x,VuTT_R2_BT123(1,:)/b3,'*-',x,VuTT_R2_BT123(2,:)/b3,'o-',x,VuTT_R2_BT123(3,:)/b3,'.-',x,VuTT_R2_BT123(4,:)/b3,'.-');
axis([1 4 0 1])
ylabel('$$\mathbf{\frac{v_u}{v_{max}}}\hspace{1.5cm}$$','fontsize',15,'interpreter','latex','rotation',0)
set(gca,'xtick',x,'fontsize',15)
legend('U','D1','D2','D3',4)
text(2.2,.5, 'R2 (\rho = 1.35 %)','fontsize',13)

subplot(4,1,3)
c1 = max(max(VuTT_R3_BT123(1,:)),max(VuTT_R3_BT123(2,:)));
c2 = max(max(VuTT_R3_BT123(3,:)),max(VuTT_R3_BT123(4,:)));
c3 = max(c1,c2);
plot(x,VuTT_R3_BT123(1,:)/c3,'*-',x,VuTT_R3_BT123(2,:)/c3,'o-',x,VuTT_R3_BT123(3,:)/c3,'.-',x,VuTT_R3_BT123(4,:)/c3,'.-');
axis([1 4 0 1])
ylabel('$$\mathbf{\frac{v_u}{v_{max}}}\hspace{1.5cm}$$','fontsize',15,'interpreter','latex','rotation',0)
set(gca,'xtick',x,'fontsize',15)
legend('U','D1','D2','D3',4)
text(2.2,.4, 'R3 (\rho = 1.88 %)','fontsize',13)

subplot(4,1,4)
d1 = max(max(VuTT_R4_BT123(1,:)),max(VuTT_R4_BT123(2,:)));
d2 = max(max(VuTT_R4_BT123(3,:)),max(VuTT_R4_BT123(4,:)));
d3 = max(d1,d2);
plot(x,VuTT_R4_BT123(1,:)/d3,'*-',x,VuTT_R4_BT123(2,:)/d3,'o-',x,VuTT_R4_BT123(3,:)/d3,'.-',x,VuTT_R4_BT123(4,:)/d3,'.-');
xlabel('$$\mathbf{\frac{v_{xy}}{f_x}}\hspace{1.5cm}$$','fontsize',15,'interpreter','latex')
axis([1 4 0 1])
ylabel('$$\mathbf{\frac{v_u}{v_{max}}}\hspace{1.5cm}$$','fontsize',15,'interpreter','latex','rotation',0)
set(gca,'xtick',x,'fontsize',15)
legend('U','D1','D2','D3',4)
text(2.2,.3, 'R4 (\rho = 3 %)','fontsize',13)

Vu1_R1_reduction = (VuTT_R1_BT123(2,:)-VuTT_R1_BT123(1,:))./VuTT_R1_BT123(1,:);
Vu2_R1_reduction = (VuTT_R1_BT123(3,:)-VuTT_R1_BT123(1,:))./VuTT_R1_BT123(1,:);
Vu3_R1_reduction = (VuTT_R1_BT123(4,:)-VuTT_R1_BT123(1,:))./VuTT_R1_BT123(1,:);
Vu_R1_reduction = abs(round([Vu1_R1_reduction;Vu2_R1_reduction;Vu3_R1_reduction].*100)./100).*100;

```

```

Vu1_R2_reduction = (VuTT_R2_BT123(2,:) - VuTT_R2_BT123(1,:)) ./ VuTT_R2_BT123(1,:);
Vu2_R2_reduction = (VuTT_R2_BT123(3,:) - VuTT_R2_BT123(1,:)) ./ VuTT_R2_BT123(1,:);
Vu3_R2_reduction = (VuTT_R2_BT123(4,:) - VuTT_R2_BT123(1,:)) ./ VuTT_R2_BT123(1,:);
Vu_R2_reduction = abs(round([Vu1_R2_reduction; Vu2_R2_reduction; Vu3_R2_reduction] .* 100) ./ 100) .* 100;

Vu1_R3_reduction = (VuTT_R3_BT123(2,:) - VuTT_R3_BT123(1,:)) ./ VuTT_R3_BT123(1,:);
Vu2_R3_reduction = (VuTT_R3_BT123(3,:) - VuTT_R3_BT123(1,:)) ./ VuTT_R3_BT123(1,:);
Vu3_R3_reduction = (VuTT_R3_BT123(4,:) - VuTT_R3_BT123(1,:)) ./ VuTT_R3_BT123(1,:);
Vu_R3_reduction = abs(round([Vu1_R3_reduction; Vu2_R3_reduction; Vu3_R3_reduction] .* 100) ./ 100) .* 100;

Vu1_R4_reduction = (VuTT_R4_BT123(2,:) - VuTT_R4_BT123(1,:)) ./ VuTT_R4_BT123(1,:);
Vu2_R4_reduction = (VuTT_R4_BT123(3,:) - VuTT_R4_BT123(1,:)) ./ VuTT_R4_BT123(1,:);
Vu3_R4_reduction = (VuTT_R4_BT123(4,:) - VuTT_R4_BT123(1,:)) ./ VuTT_R4_BT123(1,:);
Vu_R4_reduction = abs(round([Vu1_R4_reduction; Vu2_R4_reduction; Vu3_R4_reduction] .* 100) ./ 100) .* 100;

```

```

Cases_P_BT_BC;
%-----
%-----
%-----Changing Failure Mode-----
%-----
%-----
x = [0.009 .0135 .0188 .03].*(414);

VuTT_P = [VuTT(:,1) VuTT(:,8) VuTT(:,15) VuTT(:,22)];
VcrTT_P = [VcrTT(:,1) VcrTT(:,8) VcrTT(:,15) VcrTT(:,22)];

Vcr = [VcrTT_P(1,:)./27.6;VcrTT_P(2,:)./26.22;VcrTT_P(3,:)./20.01;VcrTT_P(4,:)./11.04];

U = VuTT_P(1,:)./27.6;
D1 =VuTT_P(2,:)./26.22;
D2 = VuTT_P(3,:)./20.01;
D3 = VuTT_P(4,:)./11.04;

UU = [(U(:,2)-U(:,1))./(U(:,1)) (U(:,3)-U(:,2))./(U(:,2)) (U(:,4)-U(:,3))./(U(:,3))].*100;
D11 = [(D1(:,2)-D1(:,1))./(D1(:,1)) (D1(:,3)-D1(:,2))./(D1(:,2)) (D1(:,4)-D1(:,3))./(D1(:,3))].*100;
D22 = [(D2(:,2)-D2(:,1))./(D2(:,1)) (D2(:,3)-D2(:,2))./(D2(:,2)) (D2(:,4)-D2(:,3))./(D2(:,3))].*100;
D33 = [(D3(:,2)-D3(:,1))./(D3(:,1)) (D3(:,3)-D3(:,2))./(D3(:,2)) (D3(:,4)-D3(:,3))./(D3(:,3))].*100;

h1=axes;
plot(h1,x./27.6,VuTT_P(1,:)./27.6,'*-',x./27.6,VuTT_P(2,:)./27.6,'o-',x./27.6,VuTT_P(3,:)./27.6,'.-',x./27.6,V
hold on
plot(h1,x./27.6,VcrTT_P(1,:)./27.6,'*-',x./27.6,VcrTT_P(2,:)./27.6,'o-',x./27.6,VcrTT_P(3,:)./27.6,'.-',x./27.
text(.35,.1, 'Cracking Loads','fontsize',20)
text(.15,.3, ' Steel yields','fontsize',20)
text(.25,.35, ' Concrete crushes','fontsize',20)
axis(h1,[0.1350 0.4500 0 0.45])
ylabel(h1,'$$\mathbf{\frac{v_u}{f'_c}}\hspace{1.5cm}$$','interpreter','latex','fontsize',25,'rotation',0)
xlabel(h1,'$$\mathbf{\frac{\rho_{sx}.f_{yx}}{f'_c}}\hspace{1.5cm}$$','interpreter','latex','fontsize',25)
legend('U','D1','D2','D3')
set(h1,'xtick',x./27.6,'fontsize',20)

xx = x./27.6;

yy1 = VuTT_P(1,:)./27.6;

yy2 = VuTT_P(2,:)./27.6;
yy3 = VuTT_P(3,:)./27.6;
yy4 = VuTT_P(4,:)./27.6;
yyt = [yy1;yy2;yy3;yy4];

m1 = (yyt(:,2) - yyt(:,1))./(xx(:,2)-xx(:,1));
m2 = (yyt(:,3) - yyt(:,2))./(xx(:,3)-xx(:,2));
m3 = (yyt(:,4) - yyt(:,3))./(xx(:,4)-xx(:,3));
m = [m1 m2 m3];

```



# References

- [1] Alkali-silica reaction in concrete. <http://www.understanding-cement.com/alkali-silica.html>. xi, 47, 48
- [2] Fact sheet on the three mile island accident. <http://www.nrc.gov/reading-rm/doc-collections/fact-sheets/3mile-isle.html>. 6
- [3] Mohammad Amin, A. Curt Eberhardt, and Bryan A. Erler. Design considerations for concrete containments under severe accident loads. *Nuclear Engineering and Design*, 1993. 19
- [4] H. Ashar and Bagchi. Assessment of inservice conditions of safety-related nuclear plant structures. Technical Report NUREG-1522, Nuclear Regulatory Commission, 1995. 33
- [5] Evan C. Bentz. *Sectional Analysis of Reinforced Concrete Members*. PhD thesis, University of Toronto, 2000. 66, 68
- [6] Evan C. Bentz. *Response-2000, Membrane-2000, Triax-2000, and Shell-2000 User Manual*, 2001. 68
- [7] Evan C. Bentz. Explaining the riddle of tension stiffening models for shear panel experiments. *Journal of Structural Engineering (ASCE)*, 2005. 66
- [8] Evan C. Bentz, Frank J. Vecchio, and Michael P. Collins. Simplified modified compression field theory for calculating shear strength of reinforced concrete elements. *ACI Structural Journal*, 103(4), 2006. 93
- [9] T. Blosser, G. Bond, and L. Lee. A study of the nuclear and physical properties of the ornl graphite. reactor shield. Technical Report ORNL-2195, Oak Ridge National Laboratory, 1958. 50
- [10] B. Chilton, J. Kenneth Shultis, and Richard E. Faw. *Principles of Radiation Shielding*. Prentice-Hall (Englewood Cliffs, NJ), 1984. ix, 22, 23, 26

- [11] Jae-Yeol Cho, Nam-Sik Kim, Nam-So Cho, and In-Kil Choi. Cracking behavior of reinforced concrete panel subjected to biaxial tension. *ACI Structural Journal*, 101(1), 2004. 79, 85
- [12] Jae-Yeol Cho, Nam-Sik Kim, Nam-So Cho, and Young-Sun Choun. Stress-strain relationship of reinforced concrete subjected to biaxial tension. *ACI Structural Journal*, 101(2), 2004. xii, 79, 80
- [13] M. P. Collins and D. Mitchell. *prestressed concrete basic*. canadian prestressed concrete institute, 1987. 59
- [14] Michael P. Collins. Towards a rational theory for rc members in shear. *Journal of the Structural Division*, 104:649–666, 1978. 59
- [15] M.P. Collins. Procedures for calculating the shear response of reinforced concrete elements: A discussion. *Journal of Structural Engineering (ASCE)*, 124(123):1485–1488, 1998. 66
- [16] MP. Collins and D. Mitchell. *prestressed concrete structures*. Prentice Halls Englewood Cliffs, 1991. x, xii, 60, 65, 72, 77
- [17] Nuclear Regularity Commision. Final safety evaluation report related to the certification of the advanced boiling water reactor design, main report,. Technical Report NUREG-1503, Nuclear Regularity Commision, 1994. 82
- [18] ACI committee 349. *Code Requirements for Nuclear Safety-Related Concrete Structures and Commentary*. American Concrete Institute, 2001. 3, 79
- [19] Applied Technology Council. *Tentative provisions for the developement of seismic regulations for buildings*. National Science Foundation Publication, 1978. 110
- [20] L.F. Elleuch, F. Dubois, J. Rappeneau, and C.E. Kesler. Effects of neutron radiation on special concretes and their components. Technical Report CEA-CONF-1584; CONF-701007-1, Commissariat a l’Energie Atomique, Saclay (France). Centre d’Etudes Nucleaires, 1970. 44
- [21] General Electric (GE) Nuclear Energy. Issued design certification - advanced boiling-water reactor (abwr). Technical report, Nuclear Regularity Commision, 1989. x, xi, xii, 6, 12, 13, 49, 82, 83, 84, 85, 86, 87, 90
- [22] S. Granta and A. Montagnini. Studies on behavior of concretes under irradiation. *ACI*, 34:1163–1172, 1972. 47

- [23] B. S. Gray. The effect of reactor radiation on cements and concrete. In *Conference on prestressed concrete reactor pressure vessels*, 1972. 44
- [24] NUMARC Maintenance Working Group. Industry guideline for monitoring the effectiveness of maintenance at nuclear power plants. Technical Report NUMARC 93-01, Nuclear Energy Institute, 2007. 33
- [25] Song Ha-Won, Nam Sang-Hyeok, Kim Sang-Hyo, and Lee June-Hee. Path-dependent failure analysis of rc shell structures using volume control technique. *Engineering Structures*, 2008. 79
- [26] A. Habasaki, Y. Kitada, T. Nishakawa, and K. Takiguchi. Shear transfer mechanism of rc plates after cracking. In *Proceedings of the Workshop on Finite Element Analysis of Degraded Concrete Structures*, pages 259–278, Brookhavan National Laboratory, October 1998. xiii, 95, 99, 100
- [27] H. K. Hilsdorf, J. Kropp, and H. J. Koch. The effects of nuclear radiation on the mechanical properties of concrete. *ACI*, 55:223–254, 1978. xi, xii, 2, 44, 45, 46, 49, 89
- [28] J.A. Houben. Radiation of mortar specimens. *Commission of the European Communities Brussel*, pages 170–183, 1969. 49
- [29] T.T.C Hsu. Stress and crack angels in concrete membrane elements. *Journal of Structural Engineering (ASCE)*, 124(12):1476–1484, 1998. 66
- [30] T. Ichikawa and H. Koizumi. Possibility of radiation-induced degradation of concrete by alkali-silica reaction of aggregates. *Nuclear Science and Technology*, 39:880–884, 2002. 47, 48, 49
- [31] American National Standard Institute. *Nuclear Analysis and Design of Concrete Radiation Shielding for Nuclear Power Plants*. American Nuclear Society, 1977. ix, 23, 24
- [32] British Standards Institution. *Specification for prestressed concrete pressure vessels for nuclear reactors*. British Standards Institution, 1973. 50
- [33] J. Izumo, H. Shin, K. Maekawa, and H. Okamura. An analytical model for rc panels subjected to in-plane stresses. *Concrete Shear in Earthquake*, 1992. 67
- [34] R G Jaeger. *Engineering Compendium on Radiation Shielding*. Springer- Verlag, New York, 1975. 50
- [35] R. G. Jaeger. *Engineering Compendium on Radiation Shielding: Volume 2 Shielding Materials*. Springer, 1975. ix, 25

- [36] R. Clifton James. Predicting remaining service life of concrete. Technical Report NISTIR-4712, National Institute of Standards and Technology, 1991. 38, 39
- [37] M. F Kaplan. *Concrete Radiation Shielding: Nuclear Physics, Concrete Properties, Design and Construction*. Lognman Sceintific and Thechnical, 1989. 2, 5, 14, 43, 45
- [38] B.T. Kelly, J.E. Brocklehurst, D. Mottershead, S. McNearney, and I Davidson. Effects of reactor radiation on concrete. Technical Report EUR-4531, United Kingdom Atomic Energy Authority, Culcheth (England). Reactor Group; United Kingdom Atomic Energy Authority, Risley (England). Reactor Group, 1971. 44
- [39] N. N Kondic. Nrc research program on plant aging. Technical Report NUREG-1377, Nuclear Regulatory Commission, 1991. 33
- [40] Hyo-Gyoung Kwak and Do-Yeon Kim. Cracking behavior of rc panels subject to biaxial tensile stresses. *Computers and Structures*, 84, 2006. 79
- [41] F. Lange, Dornier GmbH; G. Pretzsch, Gesellschaft f ur Anlagen-und Reaktorsicherheit (GRS) mbH; E. Hoermann, and Fraunhofer W. Koch. Experiments to quantify potential releases and consequences from sabotage attack on spent fuel casks. In *13th International Symposium on the Packaging and Transportation of Radioactive Material*, 2001. xi, 15, 16
- [42] Peter MartiI and JoostT Meyboom. Response of prestressed concrete elements to in-plane shear forces. *ACI Structural Journal*, 89(5), 1992. 93
- [43] Denis Mitchell and Michael P. Collins. Diagonal compression field theory-a rational model for structural concrete in pure torsion. *ACI*, 71:396-408, 1974. 59
- [44] Y. Mondet and U. Bumann. Pushover analysis for the assessment of seismic safety margins of auxiliary buildings. In *19th International Conference on Structural Mechanics in Reactor Technology (SMiRT)*, 2007. 1
- [45] P. K. Mukherjee. Properties of high density concrete. *Journal of High Testing and Evaluation*, 20(1), 1992. 89
- [46] A. E. Naaman, M. H. Harajli, and J. K. Wight. Analysis of ductility in partially prestressed concrete flexural members. *Journal of Precast/Prestressed Concrete Institute (PCI)*, 1986. 110
- [47] D. Naus. Concrete component aging and its significance relative to life extension of nuclear power plants. Technical Report NUREG/CR-4652, Neuclear Regulatory Commission, 1986. 49

- [48] D. Naus. Primer on durability of nuclear power plant reinforced concrete structures. Technical Report ORNL/TM-2006/529, Oak Ridge National Laboratory, 2007. ix, 37, 38
- [49] D. Naus, C. B. Oland, and B. R. Ellingwood. Report on aging of nuclear power plant reinforced concrete structures. Technical Report NUREG/CR-6424, ORNL/TM-13148, Oak Ridge National Laboratory, The Johns Hopkins University, 1996. ix, 9, 10, 33
- [50] N.M. Newmark. Smirt-3. In *3th International Conference on Structural Mechanics in Reactor Technology (SMiRT)*, 1977. 110
- [51] J. Nie, J. Braverman, Y-S. Choun, C. Hofmayer, M. K. Kim, and I-K. Choi. Identification and assesment of recent aging-related degradation occurrences in u.s, nuclear power plants. Technical Report BNL-81741, KAERI/RR-2931, Brookhaven National Laboratory and Korea Atomic Energy Research Institue, 2008. xi, 34, 35, 36
- [52] American Society of Civil Engineering. *Structural Analysis and Design of Nuclear Power Plant Facilities*. American Society of Civil Engineering, 1980. xi, xii, 8, 11, 14, 17, 22, 73, 79, 81
- [53] American Society of Mechanical Engineers. *ASME Section 3 Division 2 Code for Concrete Reactor Vessels and Containments Rules for Construction of Nuclear Facility Components*. American Society of Civil Engineering, 2007.
- [54] Ostrele. Tangential shear design in rc containments research results and applications. *Nuclear Engineering and Design*, 79, 1984. xii, 93
- [55] Y. Park. Effect of aging degradation on seismic performance of reinforced concrete structures: Summary of japanese literature in related areas. Technical report, Brookhaven National Laboratory, 1998. 33
- [56] B. T. Price, C. C. Horon, and K.T Spinney. *Radiation Shielding*. Pergamon, London, New York, Paris, 1957. 49
- [57] C. Regan. Nuclear power plant generic aging lessons learned. Technical Report NUREG/CR-6490, Neuclear Regulatory Commission, 1997. 33
- [58] J.F Sommers. Gamma radiation damage of structural concrete immersed in water. *Health Physics*, 16:503–508, 1969. 50
- [59] S. Tamai, H. Shima, J. Izumo, and H. Okamura. Average stress-strain relationship in post yield range of steel bar in concrete. *Concrete Library of JSCE*, 1988. 67

- [60] S. Timoshenko and S. Woinowsky-krieger. *Theory of Plates and Shells*. McGRAW-HILL, 1959. xii, 91, 92
- [61] Katsuhiko Umeki, Yoshio Kitada, Takao Nishikawa, and Mamoru Yamada Koichi Maekawa. Shear transfer constitutive model for pre-cracked rc plate subjected to combined axial and shear stress. *Nuclear Engineering and Design*, 105, 2003.
- [62] F. Vecchio and M. P. Collins. The response of reinforced concrete to in-plane shear and normal stresses. Technical Report 82-03, University of Toronto, 1982. xiii, 65, 93, 100, 101, 104
- [63] Frank J. Vecchio and Michael P. Collins. The modified compression-field theory for reinforced concrete elements subjected to shear. *ACI*, 83:219–231, 1986. xii, xiii, 4, 59, 60, 61, 63, 64, 65, 67, 107
- [64] J. Wall. Program on technology innovation: Concrete civil infrastructure in united states commercial nuclear power plants. Technical Report 1020932, Electric Power Research Institute (EPRI), 2010. 44
- [65] Adolf Walser. An overview of reactor containment structures. *Nuclear Engineering and Design*, 61, 1980. xiii, 94
- [66] P. D. Wilson. *The Nuclear Fuel Cycle: From Ore to Waste*. Oxford Science Publication, 1996. xi, 42